

Characterization of islet cells during development and after transplantation

Léon van Gorp

The research described in this thesis was performed at the Hubrecht Institute of the Royal Netherlands Academy of Arts and Sciences (KNAW) within the framework of the Cancer Stem cells and Developmental biology (CS&D) program in Utrecht, The Netherlands.

Printed by: Gildeprint

Cover: a graft of embryonic pancreatic tissue transplanted under the kidney capsule of an immune deficient mouse. Clusters of insulin positive cells (in red) can be seen forming from the ductal lining of the pancreatic epithelium (in green).

Copyright © 2017 by Léon van Gulp. All rights reserved. No parts of this book may be reproduced, stored in a retrieval system or transmitted in any form or by any means, without prior permission of the author. The copyright of the publications remains with the publishers.

Characterization of islet cells during development and after transplantation

Karakterisatie van cellen in de eilandjes van Langerhans tijdens de ontwikkeling en na transplantatie

(met een samenvatting in het Nederlands)

Proefschrift

Ter verkrijging van de graad van doctor aan de Universiteit Utrecht op gezag van de rector magnificus, prof. dr. G.J. van der Zwaan, ingevolge besluit van het college voor promoties in het openbaar te verdedigen op dinsdag 28 maart 2017 des middags te 12.45 uur

door

Léon van Gorp
geboren op 13 september 1978 te Gorinchem

Promotoren: Prof. Dr. J. van Rheenen
Prof. Dr. E. J. P. de Koning

Table of contents:

Chapter 1	7
General Introduction	
Chapter 2	23
Sequential intravital imaging reveals in vivo dynamics of pancreatic tissue transplanted under the kidney capsule in mice	
Chapter 3	37
In vivo assessment of the migratory capacity of endocrine pancreatic progenitors during development	
Chapter 4	49
Dynamics of pancreas development using single cell transcriptome sequencing	
Chapter 5	69
Fabrication of three-dimensional bioploted hydrogel scaffolds for islets of Langerhans transplantation	
Chapter 6	95
General Discussion	
Addenda	101
Nederlandse Samenvatting	
Dankwoord	
Publication List	
Curriculum Vitae	

General Introduction

L. van Gorp

1

Hubrecht Institute, Royal Netherlands Academy of Arts and Sciences and University Medical Centre
Utrecht, Utrecht, The Netherlands

The pancreas and diabetes mellitus

The pancreas is an organ with two main functions: production of digestive enzymes that help digest food in the intestines (exocrine pancreas) and regulation of blood sugar homeostasis (islets of Langerhans). In the exocrine pancreas, the production of digestive enzymes is performed by acinar cells. Proenzymes are released through granules into the ducts connected to the acini, and are then transported through the ductal network to the duodenum. Here, the proenzymes are cleaved to form activated enzymes with protease, lipase and peptidase activity. The exocrine pancreas makes up approximately 99% of the pancreas. The remaining 1-2% is organized in structures called the islets of Langerhans, which are cell clusters varying from just a few to thousands of cells and reaching over 400 μm in diameter [1, 2].

The islets of Langerhans consist of five cell types: alpha, beta, gamma, delta and epsilon cells, of which alpha and beta cells are most abundant. These two cell types produce the hormones glucagon and insulin, respectively, which are key factors in regulating glucose homeostasis [3]. The gamma, delta and epsilon cells have a more regulatory role and are involved in food intake, satiety and exocrine pancreas function [4-6]. Of late, single cell transcriptome approaches have given an even more detailed insight into the cellular composition of the pancreas [7-12]. For example, a cluster of Reg3a positive acinar cells was identified in the exocrine pancreas nearby the islets of Langerhans [7], and a subpopulation of alpha cells expressing high levels of proliferation markers was detected [10].

Under healthy conditions, blood glucose concentrations in humans range between 4 and 6 mmol/l, which is called normoglycemia. After food intake, blood glucose levels start to rise. The highly vascularized beta cells in the islets of Langerhans sense blood glucose levels through

a pathway involving glucokinase [13]. With increasing blood glucose levels, insulin is released in increasing amounts into the bloodstream from intracellular granules [14]. Insulin causes glycogenesis in hepatocytes in the liver, converting blood glucose to stored glycogen [15]. It also stimulates striated muscle and adipose tissue cells to increase glucose uptake by stimulating the translocation of the Glut4 glucose transporter protein to the plasma membrane [16, 17]. Combined, glycogenesis and cellular glucose uptake cause blood glucose levels to restore to normoglycemia. Conversely, alpha cells secrete increasing amounts of glucagon under the influence of nutrient stimulation, paracrine signaling and the autonomous nervous system [18]. Glucagon is released in an opposite manner from insulin, with increasing amounts as blood glucose levels are decreasing [19]. It mainly causes glycogenolysis in hepatocytes, releasing glucose from stored glycogen. This restores low blood glucose levels to normoglycemic levels. Glucagon also stimulates gluconeogenesis. In adipose tissue, it causes triglycerides to be broken down into glycerol and free fatty acids, which can be released into the bloodstream as cellular energy sources. In the absence of insulin, this secondary mechanism can cause ketoacidosis, as the pH of the blood drops after the release of ketone bodies (byproducts from the breakdown of free fatty acids) [20]. In turn, both glycogenolysis and gluconeogenesis are inhibited by the release of insulin [15, 21].

Diabetes mellitus is a chronic disease that is characterized by hyperglycemia. The disease is categorized into two main subtypes, type 1 diabetes mellitus (T1DM) is caused by an autoimmune destruction of beta cells, and type 2 diabetes mellitus (T2DM) is generally associated with insulin resistance in combination with islet dysfunction. Both types of the disease have the same pathological characteristics: the body cannot correctly clear glucose from the blood stream, which causes hyperglycemia. Short-term effects of diabetes mellitus include

osmotic diuresis, which causes fluid loss of the body due to polyuria, and ketoacidosis. Long-term effects include damage to blood vessel cells and nerve cells. This in turn can lead to retinopathy, cardiovascular disease, nephropathy and neuropathy. Blindness, the necessity to start renal replacement therapy and amputation of lower limbs are potential clinical consequences. Ultimately, people who suffer from diabetes mellitus have a shorter life expectancy than people without the disease [22, 23].

Current treatment of diabetes mellitus

The treatment of diabetes mellitus is currently symptomatic. Patients inject themselves with insulin or, in case of T2DM, use alternative drugs like metformin (inhibits gluconeogenesis and glycogenolysis), sulphonylureas (increase insulin release) and incretins (increase insulin release and decrease glucagon release) [24-27]. More recently, new technological advances have been made with the introduction of insulin pumps in combination with continuous blood glucose sensors, alleviating strain on patients to check and correct their blood glucose levels manually. This approach has been shown to improve average blood glucose levels and HbA1c (glycated hemoglobin, representing a three-month average blood glucose concentration) [28, 29]. Still, these forms of treatment are symptomatic by nature and will not cure diabetes mellitus.

T1DM patients suffer from an absence or severe lack of beta cells [30]. To cure these patients, lost beta cells must be replaced. For a small group with the most severe symptoms (i.e. severe difficulty to control glycemia, hypoglycemic unawareness), transplantation of a cadaveric pancreas available after organ donation is a potential cure for their disease [31]. Whole pancreas transplantation is regularly performed in patients with T1DM and end-stage kidney failure. Consequently, the procedure is often

combined with kidney transplantation. A successfully transplanted pancreas can completely reverse diabetes mellitus and restore blood glucose homeostasis, but the procedure is also associated with a relatively high morbidity and mortality [32]. An alternative therapy for patients with severe physical complications is the transplantation of islets of Langerhans [33, 34]. Isolation of pancreatic islets, as described in the Ricordi protocol [35], comprises physical and enzymatic digestion of the pancreas into small clumps of cells. Then, using a density gradient, islets of Langerhans are separated from exocrine pancreatic tissue. The obtained tissue can be transplanted as described in the Edmonton protocol [36] with islets being infused into the liver of patients through an intraportal injection. The islets can then engraft in the small portal vein branches of the liver and regulate blood glucose levels from this location [37].

Although the transplantation of islets of Langerhans is associated with a lower morbidity and mortality compared to whole pancreas transplantation, the technique suffers from a lower insulin restorative potential than whole pancreas transplantation. Even though insulin independence can be achieved in the first weeks to months following transplantation, this effect is often not permanent [37]. Loss of islet function after transplantation can be due to instant blood-mediated inflammatory response (IBMIR), poor engraftment and poor vascularization related to the disappearance of endothelial cells and destruction of islet basement membrane structures, and exposure to high levels of beta cell-toxic drugs in the portal system [38-40]. But, even without complete insulin independence, islets of Langerhans transplantation has great beneficial effects for recipients. Hypoglycemia unawareness is often cured, and patients often need to inject themselves less frequently with insulin and in lower doses, greatly improving quality of life [41].

Alternative transplantation strategies for islets of Langerhans

The liver is not considered the most optimal location for transplanted pancreatic islets [42-44]. Although nutrients and oxygen are readily available, due to the liver being highly vascularized, the negative effects the location has on transplanted islets, and inaccessibility of the tissue after transplantation make the location suboptimal at best. Because of this, alternative transplantation locations have been tested [45]. In order to safely and efficiently transplant islets in patients, islets need to be transplanted to a location that allows a rapid engraftment, which in turn allows an immediate exchange of nutrients, oxygen and hormones between the host and the transplanted cells. Rejection of transplanted tissue has to be prevented to achieve long-term islet survival [46]. Multiple alternative locations for transplantation are currently under investigation in a clinical setting [45]. These include the kidney capsule, skeletal muscle and the omentum (table 1).

To improve islet survival and function upon transplantation, much research effort is taken towards the development of transplantation vehicles called scaffolds. Scaffolds were traditionally designed using biocompatible and biodegradable synthetic polymers, like poly(lactic-co-glycolic acid) (PLGA) [47], polydimethylsiloxane (PDMS) [48], poly(ethylene-glycol) (PEG) [49], or natural polymers

like alginate [50]. These scaffolds can be used as solid drops, but can also be created as porous scaffolds that have a complex three dimensional structure, allowing a better interaction between transplanted cells and the environment because of an improved volume-surface-area ratio [51]. Porous scaffolds can be created in many ways, including printing, gas foaming and porogen leaching [52]. Where gas foaming and porogen leaching creates irregular and unpredictably shaped scaffolds, printing of scaffolds is a very controlled process, with a multitude of options considering the shapes that can be created, as designed by bio-CAD modelling [50, 53].

To improve survival and function of the transplanted cells, proteins and/or chemicals can be added that influence the transplanted cells or their environment. For example, binding interleukin-1 to PEG scaffolds can potentially protect transplanted islets from an immune response [54]. Also, binding of vascular factors like vascular endothelial growth factor A and platelet derived growth factor BB (in combination with recombinant fibronectin fragments) to scaffolds can enhance ingrowth of blood vessels into the scaffolds, which reduces revascularization time of transplanted islets and improves oxygenation [55]. Alternatively, oxygen can be incorporated, for example by including calcium peroxide in PDMS scaffolds [56]. These scaffolds release oxygen over more than three weeks, and thus help to prevent hypoxic dysfunction and death of islets of Langerhans shortly after transplantation.

	immunoprotection	Vascularization	# Islets for Normoglycemia	Ease of Transplantation	Islets in a Compact Pellet	Ease of Graft Recovery
Liver	-	++	+	+	-	--
Kidney Capsule	-	+	++	+	++	++
Skeletal Muscle	-	+	-	++	+	+
Omentum	+	?	-	-	-	+

Table 1: Characteristics of islet grafts transplanted into the liver, under the kidney capsule, into skeletal muscle or to the omentum. Grafts were judged based on immunoprotection, vascularization rate, the number of islets needed to restore normoglycemia, the ease of transplantation, the degree of compactness of islet grafts and the ease by which grafts can be retrieved. Ratings in "--" (very poor), "-" (poor), "+" (good) or "++" (excellent). Underdetermined data was noted as "?" [45, 46]

Polymer scaffolds are often biodegradable. To support and protect transplanted islets more permanently, a non-degradable scaffold has to be designed. Clinical trials are currently underway using two independent systems. The beta-air device allows subcutaneous transplantation of allogeneic islets whilst providing an oxygen supply and a protection from the immune system at the same time [57]. The device contains pancreatic islets in a layer of alginate, and creates a protective layer using teflon membranes that allow the exchange of macromolecules including glucose and insulin, but is impermeable for cells. Disadvantages are that patients need to inject oxygen into the device daily to maintain islet functionality, and the delay in insulin action due to the dead space in the device. The encaptra device is an alternative scaffold that has been used to transplant beta cell progenitors derived from embryonic stem (ES) cells [58]. It consists of a semi-permeable container that can be filled with immature, progenitor-like endocrine cells in a matrix. After transplantation, it takes several months for the cells to develop into mature endocrine cells. Within this time, the device becomes encapsulated and a dense vascular network is formed around it. Cells will become mature after this initial phase, start sensing glucose in the blood and regulate blood glucose by releasing insulin and glucagon.

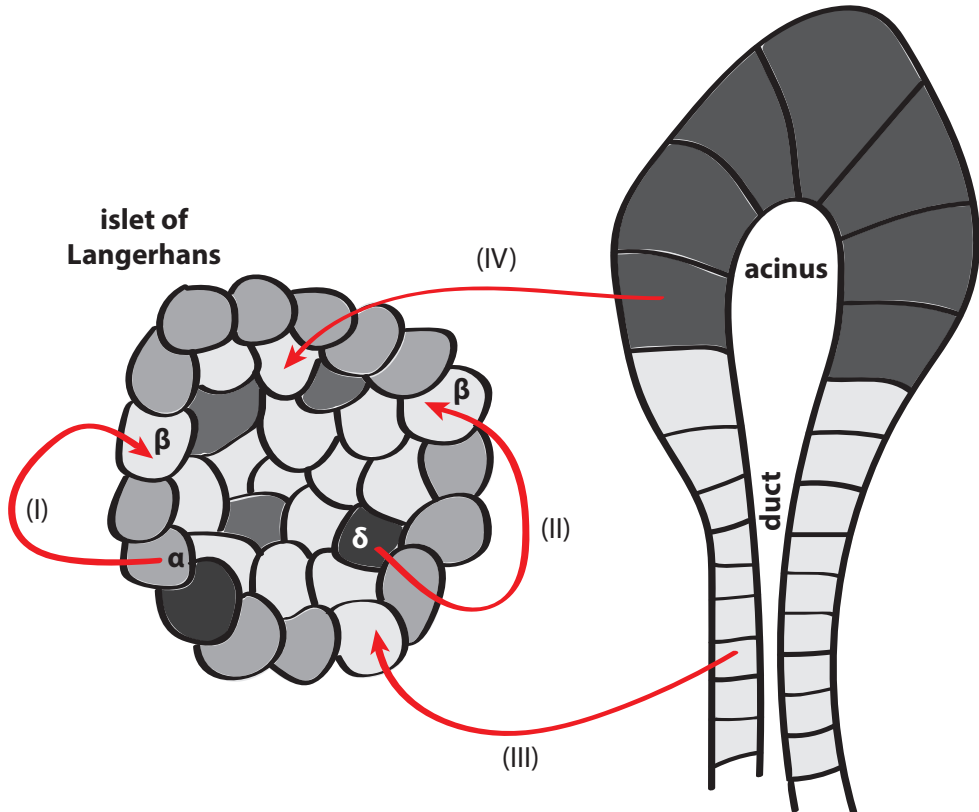
***In vitro* beta cell regeneration strategies**

Though whole pancreas and islets of Langerhans transplantation show great potential in curing diabetes mellitus, the number of patients being treated this way is very limited because of a shortage in available donor material [59]. Generating novel beta cells *in vitro* from alternative sources like ES cells, induced pluripotent stem (iPS) cells or adult progenitors is seen as a promising method to overcome this shortage [60, 61]. Considering ES and iPS cells, a complex protocol is normally required that utilizes

multiple culturing stages. This way, cells start differentiating towards increasingly more mature pancreatic endocrine cells, differentiating into islet cells. This process has multiple advantages. The supply of starting material is potentially unlimited due to the fact that ES cells, obtained from the inner cell mass of blastocysts, can theoretically be kept in culture indefinitely [62]. Moreover, iPS cells can be generated from patients' own mature cells, like skin cells, by overexpressing *Sox2*, *cMyc*, *Oct4* and *Klf4* [63], thereby limiting complications caused by allograft transplantation. On the downside, ES and iPS cells have been associated with teratoma formation, and the use of ES cells is considered an ethically sensitive subject [62, 64].

The first used protocols differentiated ES cells into embryoid bodies and then used beta cell specific selection markers to get rid of non-beta cell types [65]. This procedure already showed its potential, being able to cure hyperglycemia in over 70% of mice transplanted with these cells. After this initial breakthrough, differentiation took form in a more directed process, mimicking developmental processes in the pancreas. First, human ES cells were differentiated into definitive endoderm using specific culture conditions and selection of C-X-C chemokine receptor type 4-positive cells [66]. Then, definitive endoderm cells were differentiated into hormone-expressing endocrine cells using a five-stage differentiation protocol [67]. These cells express insulin and pancreatic and duodenal homeobox 1 (*Pdx1*) and respond to external stimuli like potassium chloride, though insulin content of these cells is lower than that of actual beta cells. To become fully mature beta cells, these cells were then transplanted into hyperglycemic mice. Over a three-month maturation period, these cells increasingly improved in glucose-stimulated insulin and c-peptide secretion [68]. More recently, alternative protocols using human iPS cells to generate definitive endoderm, were shown to be able to create glucose-responsive beta-like cells *in vitro* [69,

Figure 1: Regeneration of the pancreas using adult progenitors can be achieved through almost all cell types in the pancreas. In case of beta cell deficiency, alpha cells can transdifferentiate into beta cells at low rates (I). Delta cells can reprogram into beta cells in young mice (II). The exocrine pancreas has the potency to transdifferentiate into novel beta cells by contribution of both ductal (III) and acinar cells (IV) [79, 80, 83, 87]. For more details, read the paragraph “In vivo transdifferentiation strategies”



70]. These cells mimic beta cell behavior closely, and hierarchical clustering based on gene expression profiling also showed a close relation between mature beta cells and the differentiated iPS cells. Transplantation to hyperglycemic mice showed recovery to normoglycemia and normal response to glucose stimulation within two weeks after transplantation suggesting that *in vivo* differentiation was not needed for these cells to become functional. This procedure was recently also reported to work in a clinical setting for iPS cells from subjects with T1DM, opening a potential therapeutic application using autotransplantation of iPS cell-differentiated

beta cells [71].

***In vivo* transdifferentiation strategies**

An alternative to ES and iPS cell differentiation is the use of progenitor cells found in the adult pancreas [72]. Often, *in vivo* maturation steps are needed to fully mature these cells, making it more difficult to interpret how these cells develop into adult cells [73, 74]. After complete maturation, these cells have the capacity to reverse hyperglycemia [75, 76] with fewer disadvantages than ES and iPS cells. This

includes ethical considerations [77], teratoma formation [64], genomic instability [78] and allograft/xenograft rejection for grafts that were obtained from external sources.

Alternatively, transdifferentiation of mature cells towards beta cells may be considered a very interesting strategy for curing diabetes mellitus, with cells that are phenotypically close to beta cells being the most likely candidates to replace them [60]. Of the endocrine pancreas, both alpha and delta cells have shown some capacity to transdifferentiate [79, 80], though alpha cells only in very limited amounts and delta cells only in mice before they reach puberty. Also, the number of endocrine cells in the pancreas is very limited, often even more so in patients with diabetes mellitus. Lineage tracing experiments have indicated that ductal and acinar cells can potentially be used for beta cell regeneration [81]; ductal and islet cells share a common progenitor during development [82, 83]. *In vitro* expanded duct cells can generate novel beta cells in a low abundance after *in vivo* transplantation [84]. In a damage model like partial duct ligation, which atrophies the tail of the pancreas, beta cell mass could be expanded *in vivo* [85, 86]. Alternatively, treating hyperglycemic mice with epidermal growth factor (Egf) and ciliary neurotrophic factor (Cntf) resulted in a return to normoglycemia for most mice [87]. Taken together, the exocrine pancreas contains a very interesting subset of cells that can potentially be used for beta cell regeneration. Unfortunately, although some processes involved in transdifferentiation have been identified, the exact mechanisms remains unclear. An overview of *in vivo* transdifferentiation strategies is illustrated in Figure 1.

Embryonic pancreas development

The principles underlying many differentiation protocols, both from the ES and iPS as well as the adult progenitor studies, find their origin

in embryonic development of the pancreas [88]. In mice, development of the pancreas starts around embryonic day 8.5 (E8.5) when a cluster of cells in the foregut of the embryo becomes positive for Pdx1 [89]. These epithelial, Pdx1-positive cells start proliferating into the ventral and dorsal pancreatic bud, which will form the head, and the body and tail during a phase called the primary transition, respectively. During this phase, from approximately E8.5 to E12.5, the pancreatic buds increase in size through proliferation and the epithelial cells will start polarizing into apical and basal domains [90, 91]. As a result, the pancreatic buds form a basal lamina on the outside and tubular structures inside the epithelial buds. These tubular structures then start forming in a tree-like fashion, with a main duct leading from the foregut into the pancreatic epithelium, branching into increasingly smaller ducts [92, 93].

In the next developmental phase, called the secondary transition (E12.5 to E15.5), cells become more functionally and spatially organized. During this time the ducts of the developing pancreas segregate into tip and trunk domains. The tip regions contain a group of cells that are considered multipotent (multipotent cells; MPCs) [94], though not all tip cells are necessarily MPCs [81]. These MPCs are proliferating cells that elongate the ductal structures, and undergo branching morphogenesis [95] to exponentially expand the pancreas and increase its size. Furthermore, MPCs have the capacity to form all the lineages of the mature pancreas: acinar, ductal and endocrine cells. Multipotency in these cells is not maintained during the entire process of embryonic development, as MPCs gradually become unipotent and differentiate towards an acinar phenotype [81]. Specific markers for the tip region include carboxypeptidase A1 (Cpa1), pancreas specific transcription factor 1 alpha (Ptf1a) and myelocytomatosis oncogene (cMyc) [94]. Unfortunately, these genes mark the tip region during the secondary transition, but are not necessarily specific

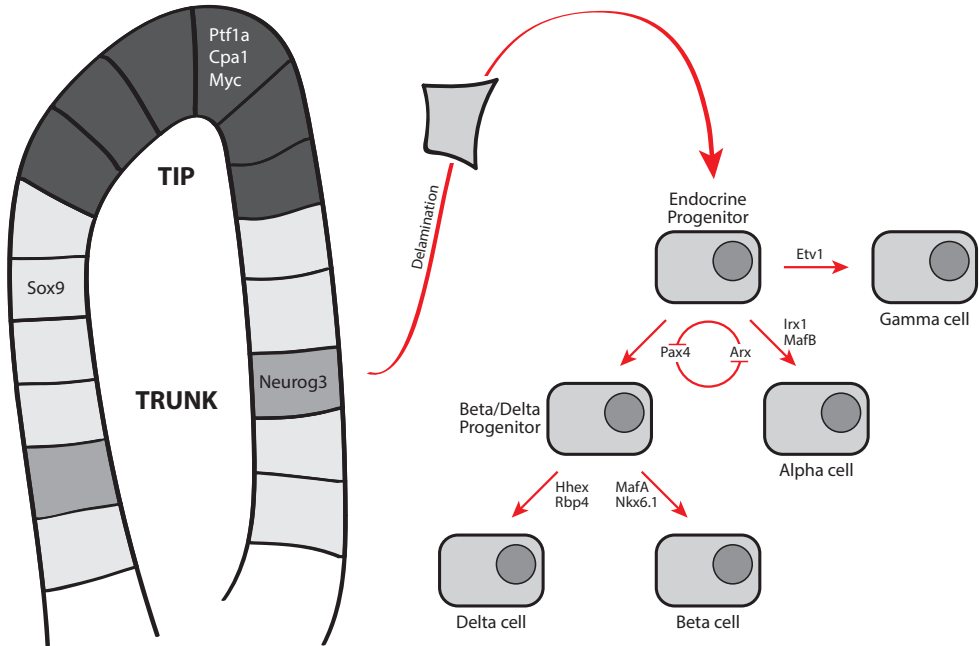
markers for MPCs. For example, *Cpa1* and *Ptf1a* not only mark tip cells, but also all mature acinar cells [96]. Because the tip structures differentiate into acinar cells, the mature acini are by definition located at the extremities of the ductal structures [92]. Cells in the trunk area are considered to be bipotent, either forming ductal or endocrine cells [97, 98]. During the secondary transition, a subset of these bipotent cells upregulate neurogenin 3 (*Neurog3*) [99] and delaminate from the ductal lining to form clusters of cells called the islets of Langerhans in the mesenchyme surrounding the pancreatic epithelium [100]. After delamination, endocrine progenitors undergo a brief mesenchymal interphase, where they upregulate genes like snail (*Snai1*), slug (*Snai2*) and vimentin (*Vim*) [100, 101].

Canonical Notch signaling is a key process that regulates cell fate determination during the secondary transition of the embryonic pancreas development [102], occurring through key players like delta-like 1 (*Dll1*) and hairy and enhancer of split 1 (*Hes1*), which are controlled by pancreas developmental factors like *Ptf1a* and *Neurog3* [103]. Lateral inhibition determines which cells will remain progenitor cells and proliferate, and which will differentiate to any given pancreatic lineage. In MPCs in the tip, *Dll1* stimulates proliferation, and is induced by *Hes1*-dependent expression of *Ptf1a* [102]. In the trunk, *Hes1* and *Neurog3* expression is mutually exclusive. Endocrine progenitor cells express *Neurog3*, a marker of endocrine cell fate commitment. *Neurog3* expression upregulates *Dll1*, which in turn stimulates surrounding cells to upregulate *Hes1*, blocking *Neurog3* expression and committing them to a ductal cell fate [104]. This process spatiotemporally limits the number of cells that delaminate and become mature endocrine cells. With lateral inhibition being the main discriminator between endocrine and ductal cell fates, bipotent cells are considered an interesting cell population in the hunt for neogenesis of beta cells *in vitro* [84].

Neurog3 is considered the master regulator for endocrine cell fate commitment [99]. It is expressed for a short period of time during delamination of endocrine progenitors from the ductal lining [97]. Lineage tracing of *Neurog3* positive cells during embryonic development results in specific labeling of endocrine cells in the islets of Langerhans and not the exocrine pancreas after birth [105], and downregulation of *Neurog3* expression during pancreas development leads to agenesis of the entire endocrine compartment of the pancreas and the development of severe diabetes [106]. Specific temporal upregulation of *Neurog3* in *Neurog3* knockout mice shows that *Neurog3* drives different endocrine cell fates at distinct developmental time points [107]. During the primary transition, the first *Neurog3* positive cells mainly differentiate towards alpha cells, where *Neurog3* positive cells during the first days of the secondary transition have a higher chance to become beta or gamma cells, and even later (after E14.5) *Neurog3* positive cells have a higher chance to end up forming delta cells.

Cell fate is not only determined by the temporal component of *Neurog3* expression; important transcription factors also define the direction in which cells are driven. After obtaining an endocrine cell fate, progenitor cells become positive for either one of the mutually inhibitory factors Aristaless related homeobox (*Arx*) or paired box 4 (*Pax4*) [108, 109]. Mice lacking the *Arx* gene produce islets that consist solely of beta and delta cells, and islets from mice without the *Pax4* gene contain only alpha and PP cells. Neurogenic differentiation 1 (*Neurod1*), another important developmental transcription factor, is only expressed in alpha and beta cells during development, not in PP or delta cells, thus helping further specialization [110]. Then, a cluster of genes is responsible for correct expression of beta cell-specific genes like *Pdx1* and insulin. These include the v-maf musculoaponeurotic fibrosarcoma oncogene family, protein A (*MafA*) [111], NK2 homeobox 2

Embryonic pancreas tissue during the secondary transition is segregated into tip and trunk domains. The tip contains multipotent cells that amplify pancreatic tissue, marked by expression of *Ptf1a*, *Cpa1* and *Myc*. The trunk contains bipotent cells that, under influence of Notch signaling, start expressing *Neurog3*. These cells delaminate and are progenitors to all endocrine pancreatic cell types. *Pax4* and *Arx* play pivotal roles in cell type specification, and each endocrine cell type expresses specific genes that define them [94, 99, 101, 106, 108, 114, 115]. For more details, read the paragraph “Embryonic pancreas development”



(*Nkx2.2*) [112] and NK6 homeobox 1 (*Nkx6.1*) [113]. An overview of embryonic development of islet cells is illustrated in Figure 2.

A comparison between murine and human pancreas development

Most studies concerning pancreatic development are performed in mice. In order to translate findings, a comparison between human and murine pancreas development is essential. Human and murine pancreas development shows many similarities with few, but very distinct, differences [116, 117]. For example, the timeline of development is much slower in human development (table 2). Besides timing, there are subtle differences in gene regulation between

human and murine pancreatic development, e.g. the expression of *Nkx2.2* in mouse MPCs, where *NKX2.2* is missing in human MPCs [89, 118]. Also, *SOX9* is expressed in human MPCs, leaving distinction between tip and trunk structures in the human pancreas based on *GATA4* expression [118]. Moreover, there is no early wave of endocrine differentiation in human pancreas development, where this is detected in mouse pancreatic development [119]. Islets containing alpha, beta, gamma and delta cells were first detected around 12-13 weeks post conception [120] and *NEUROG3* switches off before birth [121].

1

Scope of this thesis

In this thesis, we investigate how the endocrine embryonic pancreas develops from *Neurog3*-positive cells into the islets of Langerhans. For this, we use multiple novel techniques to investigate developmental processes that were difficult to study until now, like the migration of delaminated endocrine progenitors and the dynamic expression of genes in developing islet cells. Also, we investigate how transplanted islets of Langerhans engraft and survive after transplantation, both in an established setting by transplanting islets under the kidney capsule and using an alginate scaffolding system to transplant islets subcutaneously.

The kidney capsule has traditionally been the most and best described location for the transplantation of islets and embryonic pancreases in mice, but no tool was available to dynamically study engraftment and development in this location. In Chapter 2, a novel technique to dynamically study engraftment of tissue transplanted under the kidney capsule of immune-deficient mice using intravital microscopy is described. We make use of an imaging window that allows repeated intravital microscopy on tissue transplanted under the kidney capsule and validated this tool using fluorescently labeled islets of Langerhans, where

we can see gradual blood vessel ingrowth and a steady decline of relative beta cell mass. Then, transplanting embryonic pancreases under the kidney capsule, we show how grafts increase in size, and how beta cell mass exponentially increases and how individual islet cells form islets of Langerhans.

In Chapter 3, we implement the intravital microscopy technique described in chapter 2 to investigate the migratory capacity of islet cell progenitors during embryonic development. To do this, we make use of mouse-insulin-promoter green-fluorescent-protein (MIP-GFP) mice that express green fluorescent protein (GFP) under the transcriptional control of the mouse insulin promoter. GFP was found to be expressed not only in beta cells, but also in endocrine progenitors. After transplanting E12.5 embryonic pancreases under the kidney capsule, a subpopulation of GFP positive cells was found to display a migratory phenotype three days after transplantation, a time point that resembles pancreas development around E15.5. The number of migratory cells was diminished seven days after transplantation, a time point that resembles E18.5 embryonic pancreas.

In Chapter 4, we used a single cell transcriptomics approach to characterize tissue heterogeneity in the developing embryonic pancreas during the secondary transition. Using this tool,

	Human CS	Human DPC	Mouse stage
First PDX1 positive cells in the foregut	12	29-31	E9.0-9.5
Dorsal and ventral bud development	13	30-33	E9.5-10.0
Proliferation of MPCs	14-18	33-45	E10.0-14.0
Tip-trunk segregation	19	45-47	E10.5-11.5
First detection of NEUROG3	21	49-52	E12.0-12.5
Islet cell clusters have formed	NA	84-91	E17.5
Islets with GSIS	NA	140+	P8

Comparative analysis between first initiating events during human and murine pancreatic development. Timing is expressed as Carnegie Stages (CS) and Days Post Conception (DPC) for human, and as embryonic (E) or post-natal ages (P) for mouse development [116-118].

we found all known pancreatic cell types present in the developing pancreas, with cells becoming gradually more mature in later embryonic ages. By generating a lineage tree, we were able to create a pseudo timeline where clusters of cells were linked to represent endocrine differentiation for all islet cell types. We illustrated islet cell development by comparing successive endocrine clusters, and characterizing dynamic gene expression in pseudo time.

In Chapter 5, a novel alginate-based scaffolding system was introduced that allows transplantation of islets of Langerhans to subcutaneous sites. Scaffolds are created in a porous design using a 3D bioplotter that can produce regular-shaped scaffolds with a better surface to volume ratio than bulk scaffolds. 4% alginate mixed with 5% gelatin gave the best viability using beta cell line INS1E in bulk scaffolds, and plotting scaffolds in a porous manner increased this viability even further, although glucose diffusion and islet function were still impaired due to the density of the scaffold. Islet cells survived for at least 7 days after transplantation, but hormones could no longer be detected in these cells.

In Chapter 6, I conclude this thesis with a summarizing discussion.

References

- [1] Poudel A, Fowler JL, Zielinski MC, Kilimnik G, Hara M (2016) Stereological analyses of the whole human pancreas. *Sci Rep* 6: 34049
- [2] Brissova M, Fowler MJ, Nicholson WE, et al. (2005) Assessment of human pancreatic islet architecture and composition by laser scanning confocal microscopy. *J Histochem Cytochem* 53: 1087-1097
- [3] Thorens B (2008) Glucose sensing and the pathogenesis of obesity and type 2 diabetes. *Int J Obes (Lond)* 32 Suppl 6: S62-71
- [4] Hauge-Evans AC, King AJ, Carmignac D, et al. (2009) Somatostatin secreted by islet delta-cells fulfills multiple roles as a paracrine regulator of islet function. *Diabetes* 58: 403-411
- [5] Katsuura G, Asakawa A, Inui A (2002) Roles of pancreatic polypeptide in regulation of food intake. *Peptides* 23: 323-329
- [6] Wierup N, Svensson H, Mulder H, Sundler F (2002) The ghrelin cell: a novel developmentally regulated islet cell in the human pancreas. *Regul Pept* 107: 63-69
- [7] Muraro MJ, Dharmadhikari G, Grun D, et al. (2016) A Single-Cell Transcriptome Atlas of the Human Pancreas. *Cell Syst*
- [8] Li J, Klughammer J, Farlik M, et al. (2016) Single-cell transcriptomes reveal characteristic features of human pancreatic islet cell types. *EMBO Rep* 17: 178-187
- [9] Wang YJ, Schug J, Won KJ, et al. (2016) Single-Cell Transcriptomics of the Human Endocrine Pancreas. *Diabetes* 65: 3028-3038
- [10] Segerstolpe A, Palasantza A, Eliasson P, et al. (2016) Single-Cell Transcriptome Profiling of Human Pancreatic Islets in Health and Type 2 Diabetes. *Cell Metab* 24: 593-607
- [11] Baron M, Veres A, Wollock SL, et al. (2016) A Single-Cell Transcriptomic Map of the Human and Mouse Pancreas Reveals Inter- and Intra-cell Population Structure. *Cell Syst*
- [12] Xin Y, Kim J, Okamoto H, et al. (2016) RNA Sequencing of Single Human Islet Cells Reveals Type 2 Diabetes Genes. *Cell Metab* 24: 608-615
- [13] Lenzen S (2014) A fresh view of glycolysis and glucokinase regulation: history and current status. *J Biol Chem* 289: 12189-12194
- [14] Henquin JC (2000) Triggering and amplifying pathways of regulation of insulin secretion by glucose. *Diabetes* 49: 1751-1760
- [15] Dashty M (2013) A quick look at biochemistry: carbohydrate metabolism. *Clin Biochem* 46: 1339-1352
- [16] Belman JP, Habtemichael EN, Bogan JS (2014) A proteolytic pathway that controls glucose uptake in fat and muscle. *Rev Endocr Metab Disord* 15: 55-66
- [17] Gonzalez-Sanchez JL, Serrano-Rios M (2007) Molecular basis of insulin action. *Drug News Perspect* 20: 527-531
- [18] Gromada J, Franklin I, Wollheim CB (2007) Alpha-cells of the endocrine pancreas: 35 years of research but the enigma remains. *Endocr Rev* 28: 84-116
- [19] Rorsman P, Salehi SA, Abdulkader F, Braun M, MacDonald PE (2008) K(ATP)-channels and glucose-regulated glucagon secretion. *Trends*

Endocrinol Metab 19: 277-284

- [20] Wolfsdorf J, Glaser N, Sperling MA, American Diabetes A (2006) Diabetic ketoacidosis in infants, children, and adolescents: A consensus statement from the American Diabetes Association. *Diabetes Care* 29: 1150-1159
- [21] Rui L (2014) Energy metabolism in the liver. *Compr Physiol* 4: 177-197
- [22] Jorgensen ME, Almdal TP, Carstensen B (2013) Time trends in mortality rates in type 1 diabetes from 2002 to 2011. *Diabetologia* 56: 2401-2404
- [23] Miller RG, Secrest AM, Sharma RK, Songer TJ, Orchard TJ (2012) Improvements in the life expectancy of type 1 diabetes: the Pittsburgh Epidemiology of Diabetes Complications study cohort. *Diabetes* 61: 2987-2992
- [24] Marin-Penalver JJ, Martin-Timon I, Sevillano-Collantes C, Del Canizo-Gomez FJ (2016) Update on the treatment of type 2 diabetes mellitus. *World J Diabetes* 7: 354-395
- [25] Lim PC, Chong CP (2015) What's next after metformin? focus on sulphonylurea: add-on or combination therapy. *Pharm Pract (Granada)* 13: 606
- [26] Kawanami D, Matoba K, Sango K, Utsunomiya K (2016) Incretin-Based Therapies for Diabetic Complications: Basic Mechanisms and Clinical Evidence. *Int J Mol Sci* 17
- [27] Bahne E, Hansen M, Bronden A, Sonne DP, Vilsboll T, Knop FK (2016) Involvement of glucagon-like peptide-1 in the glucose-lowering effect of metformin. *Diabetes Obes Metab* 18: 955-961
- [28] Bergenstal RM, Tamborlane WV, Ahmann A, et al. (2010) Effectiveness of sensor-augmented insulin-pump therapy in type 1 diabetes. *N Engl J Med* 363: 311-320
- [29] Healy SJ, Dungan KM (2015) Monitoring glycemia in diabetes. *Med Clin North Am* 99: 35-45
- [30] Lohr M, Kloppel G (1987) Residual insulin positivity and pancreatic atrophy in relation to duration of chronic type 1 (insulin-dependent) diabetes mellitus and microangiopathy. *Diabetologia* 30: 757-762
- [31] Gruessner AC (2011) 2011 update on pancreas transplantation: comprehensive trend analysis of 25,000 cases followed up over the course of twenty-four years at the International Pancreas Transplant Registry (IPTR). *Rev Diabet Stud* 8: 6-16
- [32] Redfield RR, Rickels MR, Naji A, Odorico JS (2016) Pancreas Transplantation in the Modern Era. *Gastroenterol Clin North Am* 45: 145-166
- [33] Farney AC, Sutherland DE, Opara EC (2016) Evolution of Islet Transplantation for the Last 30 Years. *Pancreas* 45: 8-20
- [34] Robertson RP (2004) Islet transplantation as a treatment for diabetes - a work in progress. *N Engl J Med* 350: 694-705
- [35] Ricordi C, Lacy PE, Finke EH, Olack BJ, Scharp DW (1988) Automated method for isolation of human pancreatic islets. *Diabetes* 37: 413-420
- [36] Shapiro AM, Lakey JR, Ryan EA, et al. (2000) Islet transplantation in seven patients with type 1 diabetes mellitus using a glucocorticoid-free immunosuppressive regimen. *N Engl J Med* 343: 230-238
- [37] Ryan EA, Lakey JR, Rajotte RV, et al. (2001) Clinical outcomes and insulin secretion after islet transplantation with the Edmonton protocol. *Diabetes* 50: 710-719
- [38] Bennet W, Groth CG, Larsson R, Nilsson B, Korsgren O (2000) Isolated human islets trigger an instant blood mediated inflammatory reaction: implications for intraportal islet transplantation as a treatment for patients with type 1 diabetes. *Ups J Med Sci* 105: 125-133
- [39] Paraskevas S, Maysinger D, Wang R, Duguid TP, Rosenberg L (2000) Cell loss in isolated human islets occurs by apoptosis. *Pancreas* 20: 270-276
- [40] Shapiro AM, Gallant HL, Hao EG, et al. (2005) The portal immunosuppressive storm: relevance to islet transplantation? *Therapeutic drug monitoring* 27: 35-37
- [41] Holmes-Walker DJ, Kay TW (2016) Long-term effects of islet transplantation. *Curr Opin Organ Transplant* 21: 497-502
- [42] Toyofuku A, Yasunami Y, Nabeyama K, et al. (2006) Natural killer T-cells participate in rejection of islet allografts in the liver of mice. *Diabetes* 55: 34-39
- [43] Carlsson PO, Palm F, Andersson A, Liss P (2001) Markedly decreased oxygen tension in transplanted rat pancreatic islets irrespective of the implantation site. *Diabetes* 50: 489-495
- [44] Korsgren O, Lundgren T, Felldin M, et al. (2008) Optimising islet engraftment is critical for successful clinical islet transplantation. *Diabetologia* 51: 227-232
- [45] Kim HI, Yu JE, Park CG, Kim SJ (2010) Comparison of four pancreatic islet implantation sites. *J Korean Med Sci* 25: 203-210
- [46] Cantarelli E, Piemonti L (2011) Alternative transplantation sites for pancreatic islet grafts.

Curr Diab Rep 11: 364-374

- [47] Mao GH, Chen GA, Bai HY, Song TR, Wang YX (2009) The reversal of hyperglycaemia in diabetic mice using PLGA scaffolds seeded with islet-like cells derived from human embryonic stem cells. *Biomaterials* 30: 1706-1714
- [48] Brady AC, Martino MM, Pedraza E, et al. (2013) Proangiogenic hydrogels within macroporous scaffolds enhance islet engraftment in an extrahepatic site. *Tissue Eng Part A* 19: 2544-2552
- [49] Mason MN, Mahoney MJ (2010) A novel composite construct increases the vascularization potential of PEG hydrogels through the incorporation of large fibrin ribbons. *J Biomed Mater Res A* 95: 283-293
- [50] Marchioli G, van Gurp L, van Krieken PP, et al. (2015) Fabrication of three-dimensional bioplotting hydrogel scaffolds for islets of Langerhans transplantation. *Biofabrication* 7: 025009
- [51] Perez RA, Mestres G (2016) Role of pore size and morphology in musculo-skeletal tissue regeneration. *Mater Sci Eng C Mater Biol Appl* 61: 922-939
- [52] Janik H, Marzec M (2015) A review: fabrication of porous polyurethane scaffolds. *Mater Sci Eng C Mater Biol Appl* 48: 586-591
- [53] Marchioli G, Luca AD, de Koning E, et al. (2016) Hybrid Polycaprolactone/Alginate Scaffolds Functionalized with VEGF to Promote de Novo Vessel Formation for the Transplantation of Islets of Langerhans. *Adv Healthc Mater* 5: 1606-1616
- [54] Su J, Hu BH, Lowe WL, Jr., Kaufman DB, Messersmith PB (2010) Anti-inflammatory peptide-functionalized hydrogels for insulin-secreting cell encapsulation. *Biomaterials* 31: 308-314
- [55] Martino MM, Tortelli F, Mochizuki M, et al. (2011) Engineering the growth factor micro-environment with fibronectin domains to promote wound and bone tissue healing. *Sci Transl Med* 3: 100ra189
- [56] Pedraza E, Coronel MM, Fraker CA, Ricordi C, Stabler CL (2012) Preventing hypoxia-induced cell death in beta cells and islets via hydrolytically activated, oxygen-generating biomaterials. *Proc Natl Acad Sci U S A* 109: 4245-4250
- [57] Barkai U, Weir GC, Colton CK, et al. (2013) Enhanced oxygen supply improves islet viability in a new bioartificial pancreas. *Cell Transplant* 22: 1463-1476
- [58] Agulnick AD, Ambruzs DM, Moorman MA, et al. (2015) Insulin-Producing Endocrine Cells Differentiated *In Vitro* From Human Embryonic Stem Cells Function in Macroencapsulation Devices *In Vivo*. *Stem Cells Transl Med* 4: 1214-1222
- [59] Ekser B, Cooper DK, Tector AJ (2015) The need for xenotransplantation as a source of organs and cells for clinical transplantation. *Int J Surg* 23: 199-204
- [60] Chera S, Herrera PL (2016) Regeneration of pancreatic insulin-producing cells by in situ adaptive cell conversion. *Curr Opin Genet Dev* 40: 1-10
- [61] Shen J, Cheng Y, Han Q, Mu Y, Han W (2013) Generating insulin-producing cells for diabetic therapy: existing strategies and new development. *Ageing Res Rev* 12: 469-478
- [62] Simonson OE, Domogatskaya A, Volchkov P, Rodin S (2015) The safety of human pluripotent stem cells in clinical treatment. *Ann Med* 47: 370-380
- [63] Takahashi K, Tanabe K, Ohnuki M, et al. (2007) Induction of pluripotent stem cells from adult human fibroblasts by defined factors. *Cell* 131: 861-872
- [64] Abad M, Mosteiro L, Pantoja C, et al. (2013) Reprogramming *in vivo* produces teratomas and iPS cells with totipotency features. *Nature* 502: 340-345
- [65] Soria B, Roche E, Berna G, Leon-Quinto T, Reig JA, Martin F (2000) Insulin-secreting cells derived from embryonic stem cells normalize glycaemia in streptozotocin-induced diabetic mice. *Diabetes* 49: 157-162
- [66] D'Amour KA, Agulnick AD, Eliazar S, Kelly OG, Kroon E, Baetge EE (2005) Efficient differentiation of human embryonic stem cells to definitive endoderm. *Nat Biotechnol* 23: 1534-1541
- [67] D'Amour KA, Bang AG, Eliazar S, et al. (2006) Production of pancreatic hormone-expressing endocrine cells from human embryonic stem cells. *Nat Biotechnol* 24: 1392-1401
- [68] Kroon E, Martinson LA, Kadoya K, et al. (2008) Pancreatic endoderm derived from human embryonic stem cells generates glucose-responsive insulin-secreting cells *in vivo*. *Nat Biotechnol* 26: 443-452
- [69] Pagliuca FW, Millman JR, Gurtler M, et al. (2014) Generation of functional human pancreatic beta cells *in vitro*. *Cell* 159: 428-439
- [70] Rezanian A, Bruin JE, Arora P, et al. (2014) Reversal of diabetes with insulin-producing cells derived *in vitro* from human pluripotent stem cells. *Nat Biotechnol* 32: 1121-1133
- [71] Millman JR, Xie C, Van Dervort A, Gur-

- tlar M, Pagliuca FW, Melton DA (2016) Generation of stem cell-derived beta-cells from patients with type 1 diabetes. *Nat Commun* 7: 11463
- [72] Lysy PA, Weir GC, Bonner-Weir S (2013) Making beta cells from adult cells within the pancreas. *Curr Diab Rep* 13: 695-703
- [73] Huch M, Bonfanti P, Boj SF, et al. (2013) Unlimited *in vitro* expansion of adult bi-potent pancreas progenitors through the Lgr5/R-spondin axis. *EMBO J* 32: 2708-2721
- [74] Hohwieler M, Illing A, Hermann PC, et al. (2016) Human pluripotent stem cell-derived acinar/ductal organoids generate human pancreas upon orthotopic transplantation and allow disease modelling. *Gut*
- [75] El-Gohary Y, Wiersch J, Tulachan S, et al. (2016) Intraislet Pancreatic Ducts Can Give Rise to Insulin-Positive Cells. *Endocrinology* 157: 166-175
- [76] Inada A, Nienaber C, Katsuta H, et al. (2008) Carbonic anhydrase II-positive pancreatic cells are progenitors for both endocrine and exocrine pancreas after birth. *Proc Natl Acad Sci U S A* 105: 19915-19919
- [77] Power C, Rasko JE (2011) Will cell reprogramming resolve the embryonic stem cell controversy? A narrative review. *Ann Intern Med* 155: 114-121
- [78] Tavana O, Zhu C (2011) Too many breaks (brakes): pancreatic beta-cell senescence leads to diabetes. *Cell Cycle* 10: 2471-2484
- [79] Thorel F, Nepote V, Avril I, et al. (2010) Conversion of adult pancreatic alpha-cells to beta-cells after extreme beta-cell loss. *Nature* 464: 1149-1154
- [80] Chera S, Baronnier D, Ghila L, et al. (2014) Diabetes recovery by age-dependent conversion of pancreatic delta-cells into insulin producers. *Nature* 514: 503-507
- [81] Pan FC, Bankaitis ED, Boyer D, et al. (2013) Spatiotemporal patterns of multipotentiality in Ptf1a-expressing cells during pancreas organogenesis and injury-induced facultative restoration. *Development* 140: 751-764
- [82] Beucher A, Martin M, Spenle C, Poulet M, Collin C, Gradwohl G (2012) Competence of failed endocrine progenitors to give rise to acinar but not ductal cells is restricted to early pancreas development. *Dev Biol* 361: 277-285
- [83] Corritore E, Lee YS, Sokal EM, Lysy PA (2016) beta-cell replacement sources for type 1 diabetes: a focus on pancreatic ductal cells. *Ther Adv Endocrinol Metab* 7: 182-199
- [84] Bonner-Weir S, Toschi E, Inada A, et al. (2004) The pancreatic ductal epithelium serves as a potential pool of progenitor cells. *Pediatr Diabetes* 5 Suppl 2: 16-22
- [85] Wang RN, Kloppel G, Bouwens L (1995) Duct- to islet-cell differentiation and islet growth in the pancreas of duct-ligated adult rats. *Diabetologia* 38: 1405-1411
- [86] Xu X, D'Hoker J, Stange G, et al. (2008) Beta cells can be generated from endogenous progenitors in injured adult mouse pancreas. *Cell* 132: 197-207
- [87] Baeyens L, Lemper M, Leuckx G, et al. (2014) Transient cytokine treatment induces acinar cell reprogramming and regenerates functional beta cell mass in diabetic mice. *Nat Biotechnol* 32: 76-83
- [88] Avolio F, Pfeifer A, Courtney M, et al. (2013) From pancreas morphogenesis to beta-cell regeneration. *Curr Top Dev Biol* 106: 217-238
- [89] Jorgensen MC, Ahnfelt-Ronne J, Hald J, Madsen OD, Serup P, Hecksher-Sorensen J (2007) An illustrated review of early pancreas development in the mouse. *Endocr Rev* 28: 685-705
- [90] Villasenor A, Chong DC, Henkemeyer M, Cleaver O (2010) Epithelial dynamics of pancreatic branching morphogenesis. *Development* 137: 4295-4305
- [91] Hick AC, van Eyll JM, Cordi S, et al. (2009) Mechanism of primitive duct formation in the pancreas and submandibular glands: a role for SDF-1. *BMC Dev Biol* 9: 66
- [92] Benitez CM, Goodyer WR, Kim SK (2012) Deconstructing pancreas developmental biology. *Cold Spring Harb Perspect Biol* 4
- [93] Cano DA, Hebrok M, Zenker M (2007) Pancreatic development and disease. *Gastroenterology* 132: 745-762
- [94] Zhou Q, Law AC, Rajagopal J, Anderson WJ, Gray PA, Melton DA (2007) A multipotent progenitor domain guides pancreatic organogenesis. *Dev Cell* 13: 103-114
- [95] Puri S, Hebrok M (2007) Dynamics of embryonic pancreas development using real-time imaging. *Dev Biol* 306: 82-93
- [96] Hale MA, Swift GH, Hoang CQ, et al. (2014) The nuclear hormone receptor family member NR5A2 controls aspects of multipotent progenitor cell formation and acinar differentiation during pancreatic organogenesis. *Development* 141: 3123-3133
- [97] Bankaitis ED, Bechard ME, Wright CV (2015) Feedback control of growth, differentiation,

- and morphogenesis of pancreatic endocrine progenitors in an epithelial plexus niche. *Genes Dev* 29: 2203-2216
- [98] Solar M, Cardalda C, Houbracken I, et al. (2009) Pancreatic exocrine duct cells give rise to insulin-producing beta cells during embryogenesis but not after birth. *Dev Cell* 17: 849-860
- [99] Rukstalis JM, Habener JF (2009) Neurogenin3: a master regulator of pancreatic islet differentiation and regeneration. *Islets* 1: 177-184
- [100] Gouzi M, Kim YH, Katsumoto K, Johansson K, Grapin-Botton A (2011) Neurogenin3 initiates stepwise delamination of differentiating endocrine cells during pancreas development. *Dev Dyn* 240: 589-604
- [101] Cole L, Anderson M, Antin PB, Limesand SW (2009) One process for pancreatic beta-cell coalescence into islets involves an epithelial-mesenchymal transition. *J Endocrinol* 203: 19-31
- [102] Li XY, Zhai WJ, Teng CB (2016) Notch Signaling in Pancreatic Development. *Int J Mol Sci* 17
- [103] Ahnfelt-Ronne J, Jorgensen MC, Klinck R, et al. (2012) Ptf1a-mediated control of Dll1 reveals an alternative to the lateral inhibition mechanism. *Development* 139: 33-45
- [104] Lee JC, Smith SB, Watada H, et al. (2001) Regulation of the pancreatic pro-endocrine gene neurogenin3. *Diabetes* 50: 928-936
- [105] Gu G, Dubauskaite J, Melton DA (2002) Direct evidence for the pancreatic lineage: NGN3+ cells are islet progenitors and are distinct from duct progenitors. *Development* 129: 2447-2457
- [106] Gradwohl G, Dierich A, LeMeur M, Guillemot F (2000) neurogenin3 is required for the development of the four endocrine cell lineages of the pancreas. *Proc Natl Acad Sci U S A* 97: 1607-1611
- [107] Johansson KA, Dursun U, Jordan N, et al. (2007) Temporal control of neurogenin3 activity in pancreas progenitors reveals competence windows for the generation of different endocrine cell types. *Dev Cell* 12: 457-465
- [108] Collombat P, Hecksher-Sorensen J, Broccoli V, et al. (2005) The simultaneous loss of Arx and Pax4 genes promotes a somatostatin-producing cell fate specification at the expense of the alpha- and beta-cell lineages in the mouse endocrine pancreas. *Development* 132: 2969-2980
- [109] Collombat P, Mansouri A, Hecksher-Sorensen J, et al. (2003) Opposing actions of Arx and Pax4 in endocrine pancreas development. *Genes Dev* 17: 2591-2603
- [110] Itkin-Ansari P, Marcora E, Geron I, et al. (2005) NeuroD1 in the endocrine pancreas: localization and dual function as an activator and repressor. *Dev Dyn* 233: 946-953
- [111] Matsuoka TA, Artner I, Henderson E, Means A, Sander M, Stein R (2004) The MafA transcription factor appears to be responsible for tissue-specific expression of insulin. *Proc Natl Acad Sci U S A* 101: 2930-2933
- [112] Sussel L, Kalamaras J, Hartigan-O'Connor DJ, et al. (1998) Mice lacking the homeodomain transcription factor Nkx2.2 have diabetes due to arrested differentiation of pancreatic beta cells. *Development* 125: 2213-2221
- [113] Jensen J, Serup P, Karlens C, Nielsen TF, Madsen OD (1996) mRNA profiling of rat islet tumors reveals nkx 6.1 as a beta-cell-specific homeodomain transcription factor. *J Biol Chem* 271: 18749-18758
- [114] DiGruccio MR, Mawla AM, Donaldson CJ, et al. (2016) Comprehensive alpha, beta and delta cell transcriptomes reveal that ghrelin selectively activates delta cells and promotes somatostatin release from pancreatic islets. *Mol Metab* 5: 449-458
- [115] Benitez CM, Qu K, Sugiyama T, et al. (2014) An integrated cell purification and genomics strategy reveals multiple regulators of pancreas development. *PLoS Genet* 10: e1004645
- [116] Pan FC, Wright C (2011) Pancreas organogenesis: from bud to plexus to gland. *Dev Dyn* 240: 530-565
- [117] Jennings RE, Berry AA, Strutt JP, Gerrard DT, Hanley NA (2015) Human pancreas development. *Development* 142: 3126-3137
- [118] Jennings RE, Berry AA, Kirkwood-Wilson R, et al. (2013) Development of the human pancreas from foregut to endocrine commitment. *Diabetes* 62: 3514-3522
- [119] Villasenor A, Chong DC, Cleaver O (2008) Biphasic Ngn3 expression in the developing pancreas. *Dev Dyn* 237: 3270-3279
- [120] Piper K, Brickwood S, Turnpenny LW, et al. (2004) Beta cell differentiation during early human pancreas development. *J Endocrinol* 181: 11-23
- [121] Salisbury RJ, Blaylock J, Berry AA, et al. (2014) The window period of NEUROGENIN3 during human gestation. *Islets* 6: e954436

Sequential intravital imaging reveals *in vivo* dynamics of pancreatic tissue transplanted under the kidney capsule in mice

L. van Gorp¹, C.J.M. Loomans^{1,2}, P.P. van Krieken^{1,3}, G. Dharmadhikari¹,
E. Jansen^{1,4}, F.C.A.S. Ringnalda^{1,5}, E. Beerling⁶, J. van Rheenen⁶,
E.J.P. de Koning^{1,2}

2

1: Hubrecht Institute - KNAW and University Medical Center Utrecht, Uppsalalaan 8, 3584CT Utrecht, the Netherlands

2: Department of Internal Medicine, Leiden University Medical Center, Leiden, the Netherlands

3: The Rolf Luft Research Center for Diabetes and Endocrinology, Karolinska Institutet, Karolinska University Hospital, L1, Stockholm, Sweden

4: Department of Tumor Immunology, Radboudumc, Nijmegen, the Netherlands

5: Institute of Molecular Health Sciences, ETH Zürich, Zürich, Switzerland

6: Cancer Genomics Center, Hubrecht Institute—KNAW and University Medical Center Utrecht, Utrecht, the Netherlands

Abstract

Aims/hypothesis: Dynamic processes in pancreatic tissue are difficult to study. We aimed to develop an intravital imaging method to longitudinally examine engraftment, vascularisation, expansion and differentiation in mature islets or embryonic pancreases transplanted under the kidney capsule.

Methods: Isolated pancreatic islets from adult mice and murine embryonic day (E)12.5 pancreases containing fluorescent biomarkers were transplanted under the kidney capsule of immunodeficient recipient mice. Human islet cells were dispersed, transduced with a lentivirus expressing a fluorescent label and reaggregated before transplantation. Graft- containing kidneys were positioned subcutaneously and an imaging window was fitted into the skin on top of the kidney. Intravital imaging using multiphoton microscopy was performed for up to 2 weeks. Volumes of fluorescently labelled cells were determined as a measure of development and survival.

Results: Transplanted islets and embryonic pancreases showed good engraftment and remained viable. Engraftment and vascularisation could be longitudinally examined in murine and human islet cells. Murine islet beta cell volume was unchanged over time. Transplanted embryonic pancreases increased to up to 6.1 times of their original volume and beta cell volume increased 90 times during 2 weeks.

Conclusions/interpretation: This method allows for repeated intravital imaging of grafts containing various sources of pancreatic tissue transplanted under the kidney capsule. Using fluorescent markers, dynamic information concerning engraftment or differentiation can be visualised and measured.

Introduction

Islet cell development, dynamic processes involved in islet engraftment and changes in islet composition are difficult processes to study *in vivo*. To obtain longitudinal information in combination with functional data, new imaging methods are required that allow sequential measurements in individual animals.

Transplantation of pancreatic islets under the kidney capsule is considered the gold standard for the *in vivo* evaluation of graft insulin secretory capacity and survival in mice [1]. Isolated islets derived from humans and different animal species can be used for transplantation at this site [2]. After engraftment, there is good vascularisation of the transplanted islets, allowing the rapid release and action of insulin. Nephrectomy of the graft- containing kidney followed by determination of blood glucose values validates graft function [3]. By transplanting a cell pellet that remains compact after transplantation, grafts can easily be retrieved and histologically analysed.

In this study, we adapted our previously published method [4, 5] to perform intravital imaging on islets of Langerhans or embryonic pancreatic tissue transplanted under the kidney capsule using an abdominal imaging window. This method allows sequential measurements of survival, vascularisation, expansion and differentiation of these tissues for a period up to 2 weeks.

Methods

Mouse pancreatic islets and embryonic pancreas isolation

All experiments on animals were carried out in accordance with the guidelines of the Animal Welfare Committee of the Royal Netherlands Academy of Arts and Sciences. Mature pancreatic islets and intact E12.5 embryonic

Chapter 2: Sequential intravital imaging reveals *in vivo* dynamics of pancreatic tissue transplanted under the kidney capsule in mice

pancreases were isolated from mouse insulin promoter–enhanced green fluorescent protein (MIP-EGFP) (Jackson Laboratory, Bar Harbor, ME, USA, stock no. 006864) and cytomegalovirus–actin–globin promoter red fluorescent protein (CAG-DsRed) (Jackson Laboratory, stock no. 005441) mice. See ESM for further details.

Human pancreatic islets and lentiviral transduction

Human pancreatic islets were isolated at the Leiden University Medical Centre using standard procedures [6]. Isolated human islets could only be used with research consent and when the number and/or quality of the islets were insufficient for clinical islet transplantation, according to national laws. Islets were transduced with a human insulin promoter–GFP (HIP-GFP) virus before transplantation. See ESM for further details.

Islet transplantation and positioning of an intra-abdominal imaging window

NOD severe combined immunodeficiency gamma (NSG) mice (Jackson Laboratory, stock no. 005557) were anaesthetised and pancreatic islets or embryonic pancreases were transplanted under the kidney capsule. The kidney was fixed subcutaneously and an imaging window was placed in the skin (ESM Fig. 1a–f), as published previously [4]. See ESM for further details.

Intravital imaging

Intravital imaging was performed as described previously [5]. If visualisation of the vasculature was required, mice received an intravenous tail vein injection of 2.5 mg 70 kDa dextran–Texas Red conjugate (Thermo Fisher, Waltham, MA, USA, D-1830) in 100 μ l PBS directly before imaging. Images were acquired at resolutions between $0.6 \times 0.6 \times 1.0$ and $4.8 \times 4.8 \times 5.0$ μ m (xyz). Multiphoton excitation was performed at 960 nm, and the emission was

collected at 505–555 nm (EGFP), and 555–695 nm (DsRed, Texas Red).

Histological analysis

Graft-containing kidneys were either fixed for paraffin sectioning or for cryosectioning. Paraffin-embedded sections (4 μ m) were cut at and stained with haematoxylin and eosin for the determination of graft size and capsule thickness. Cryosections (10 μ m) were used for immunohistochemical staining for insulin and glucagon. See ESM for further details.

Microscopy data processing

See ESM for further details.

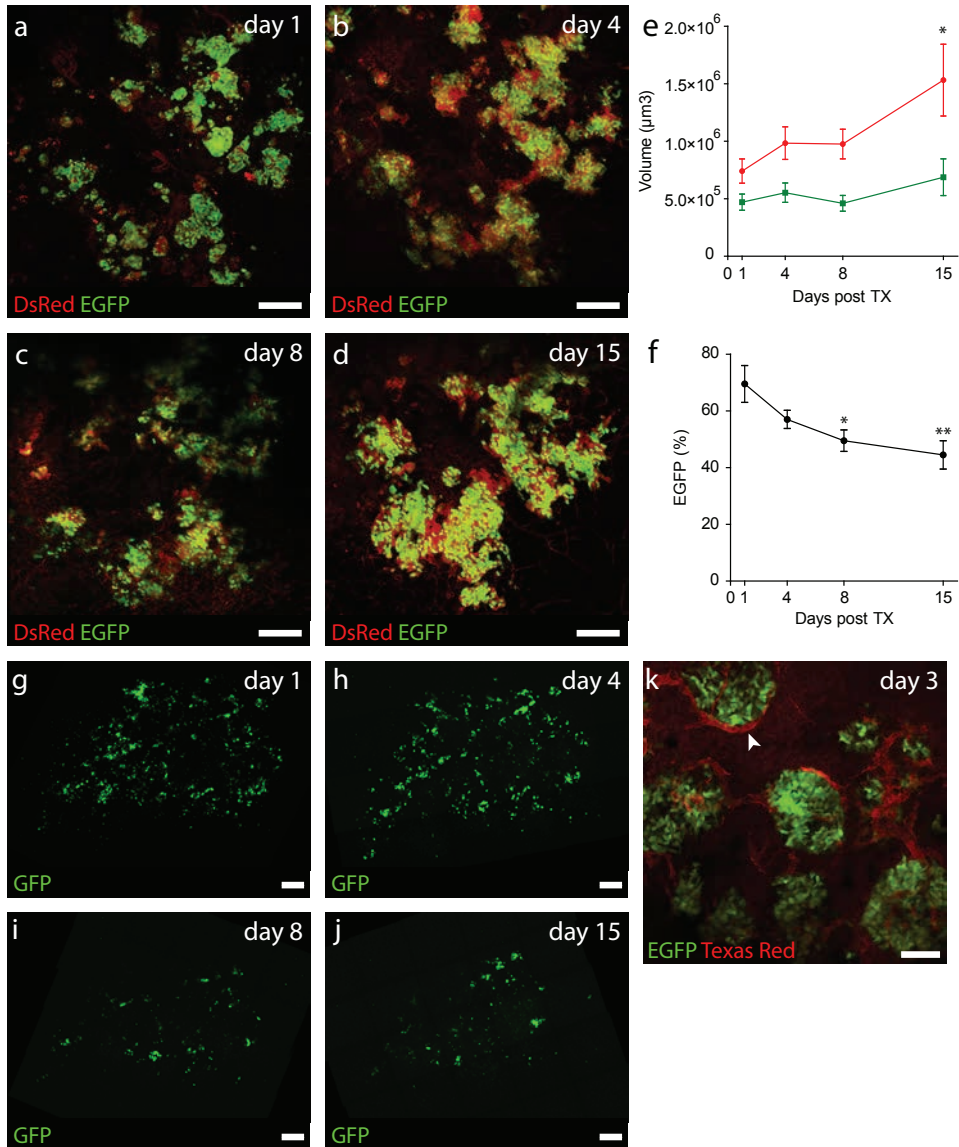
Statistical analysis

Data are presented as mean \pm SEM. R (www.R-project.org) was used to perform statistical analyses. IPGTT data were analysed using two-way ANOVA. All other statistical analyses were performed using independent two-way Student's t-tests. Data were considered significant if the p value was <0.05 .

Results

Transplanted islets function normally in mice fitted with an abdominal imaging window

Mice recovered quickly after surgery and were fully active after 1 h. There was no impairment of movement and mice did not show behaviour indicating pain or discomfort. Body weight increased normally after surgery (ESM Fig. 2a). To test if islet graft functionality was affected by the procedure, an IPGTT was performed and human C-peptide concentrations were measured in streptozotocin-induced hyperglycaemic NSG mice 4 weeks after transplantation of 2000 human islet equivalents. Both mice with an abdominal imaging window (AIW, n = 5) and controls (CTRL, n = 5) showed a normal response to an IPGTT (ESM Fig. 2b). Human



C-peptide concentrations were similar between the two groups 4 weeks after surgery (358 ± 157 pmol/l [AIW] and 384 ± 47 pmol/l [CTRL], $p = 0.88$; ESM Fig. 2c). Graft thickness (801 ± 86 μm [AIW] and 827 ± 51 μm [CTRL]) was unaffected ($p = 0.81$). Capsule thickness was not significantly increased (477 ± 64 μm [AIW] and 324 ± 34 μm [CTRL], $p = 0.09$; ESM Fig. 2d). The imaging window did not affect the

proportion of beta cells (relative to the total alpha and beta cells) in the transplanted islets (ESM Fig. 2e–g).

Transplanted islets can be repeatedly monitored during *in vivo* engraftment

To demonstrate that longitudinal intravital imaging of tissue grafts under the kidney

Chapter 2: Sequential intravital imaging reveals *in vivo* dynamics of pancreatic tissue transplanted under the kidney capsule in mice

*Figure 1: Vascularisation and survival of pancreatic islets transplanted under the kidney capsule of immune deficient NSG mice. (a–d) Maximum projection image (projecting all xy focal planes into a single 2D image) of murine MIP-EGFP/CAG-DsRed islets transplanted under the kidney capsule. The grafts were imaged on day 1, 4, 8 and 15. MIP-EGFP (green), CAG-DsRed (red). Scale bar, 250 μm . (e) Tissue volume of all pancreatic cells (CAG-DsRed, in red) and beta cells (MIP-EGFP, in green) in transplanted MIP-EGFP/CAG-DsRed islets over time. DsRed volume was significantly increased on day 15 compared with day 1. (f) Percentage of the volume of beta cells (EGFP %) over whole tissue volume (DsRed) in transplanted MIP-EGFP/CAG-DsRed islets over time. The percentage of beta cells was significantly decreased on day 8 and 15 compared to day 1. (g–j) Human pancreatic islets were dispersed into single cells, transduced with a lentivirus containing a HIP-GFP virus, and reaggregated overnight on ultra-low attachment plates. After 1 week in culture, islet cell aggregates were visually assessed and transplanted if at least 50% of the cells were fluorescent. Maximum projection images of transplanted islets were captured on day 1, 4, 8 and 15. HIP-GFP (green). Scale bar, 250 μm . (k) Image of a single xy focal plane of transplanted MIP-EGFP islets 3 days after transplantation. Blood vessels (red) were visualised after a tail vein injection of Texas Red-conjugated dextran solution. The arrowhead marks a transplanted islet of which several xy focal planes are merged into a mosaic in ESM Fig. 4. Scale bar, 100 μm . Data are mean \pm SEM. * $p < 0.05$, ** $p < 0.01$ vs day 1. TX, transplant*

capsule can be performed, normoglycaemic NSG mice ($n = 4$) were transplanted with 10–25 mouse MIP-EGFP/CAG-DsRed islets and fitted with an AIW. Imaging was performed on day 1, day 4, day 8 and day 15 after surgery (Fig. 1a–d). In total, 29 separate islet-containing regions of interest were identified. In these areas, beta cell and total cell volume were measured by volumetric calculation of the DsRed and EGFP signal. DsRed volume at 15 days was 2.1 times that at day 1 ($7.4 \times 10^5 \pm 1.1 \times 10^5 \mu\text{m}^3$ at day 1 vs $15.3 \times 10^5 \pm 3.1 \times 10^5 \mu\text{m}^3$ at day 15, $p = 0.029$), while EGFP volume did not significantly increase over this time ($4.7 \times 10^5 \pm 0.7 \times 10^5 \mu\text{m}^3$ at day 1 vs $6.9 \times 10^5 \pm 1.6 \times 10^5 \mu\text{m}^3$ at day 15, $p = 0.22$) (Fig. 1e). The relative EGFP content decreased from $69.5 \pm 6.5\%$ on day 1 to $44.5 \pm 5.0\%$ on day 15 ($p = 0.004$) (Fig. 1f). To show that human islet cells can also be sequentially imaged, HIP-GFP-transduced human islet cell aggregates were transplanted under the kidney capsule. Approximately 50% of all transplanted cells expressed GFP after transduction prior to transplantation (ESM Fig. 3). Beta cells expressing GFP could be clearly visualised on days 1, 4, 8 and 15 after transplantation under the kidney capsule (Fig. 1g–j).

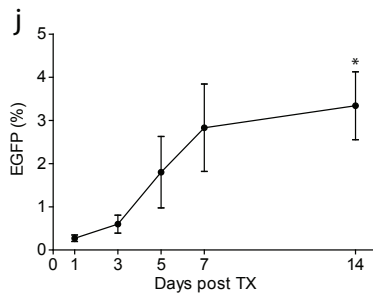
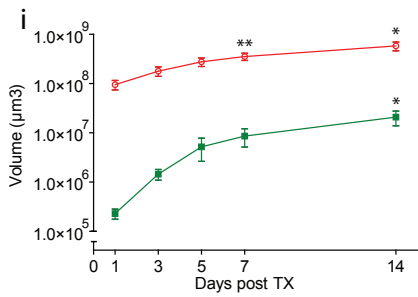
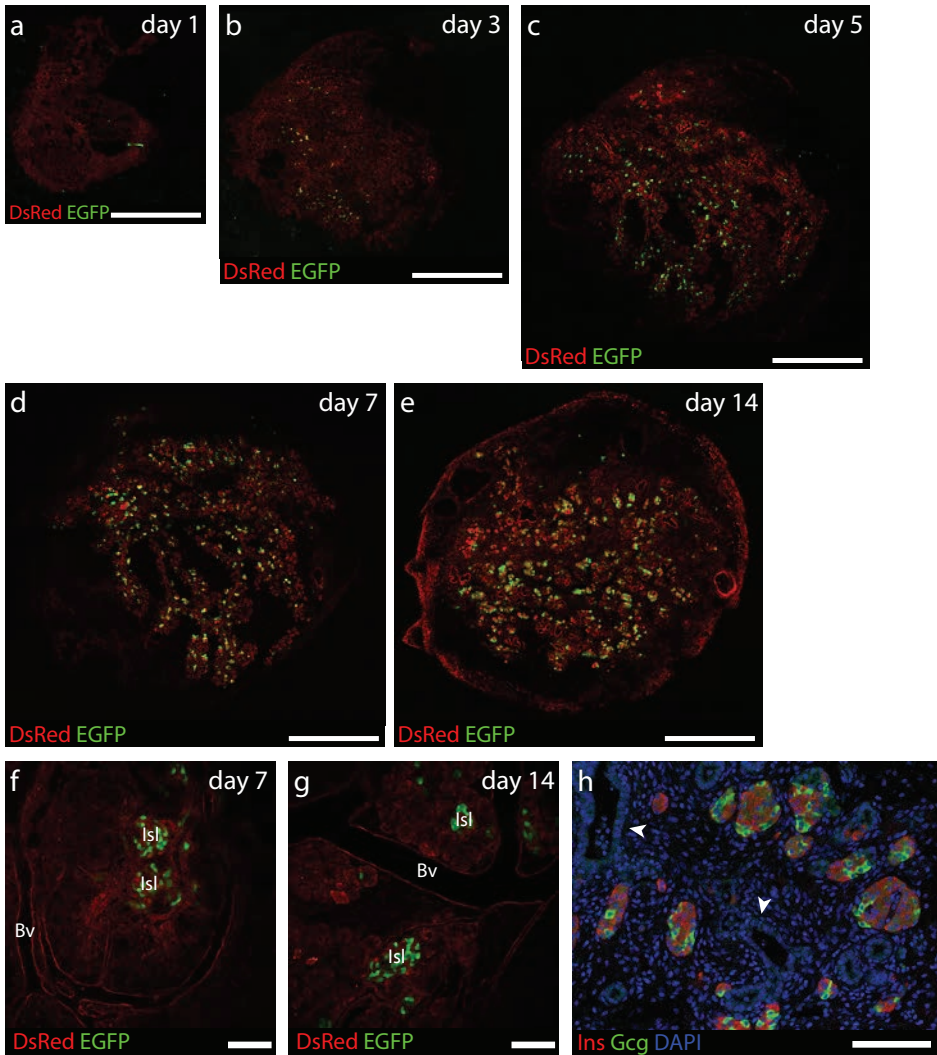
Visualisation of islet graft vasculature and blood flow

Blood vessels were visualised in MIP-EGFP islet grafts after injection of Texas Red-labelled dextrans into the tail vein. The first signs of vascularisation were recorded 3 days after transplantation, when blood vessels could be identified within and surrounding the islets (Fig. 1k, ESM Fig. 4).

Transplanted embryonic pancreas increases in size and forms islets within 2 weeks

To demonstrate that large tissue grafts can be visualised and to monitor pancreatic development in a quantitative fashion, we transplanted two to four E12.5 embryonic pancreases from pregnant MIP-EGFP/CAG-DsRed mice under the kidney capsule of NSG mice before an AIW was fitted ($n = 7$). One day after transplantation, 27.3 ± 3.6 EGFP-positive cells were present per embryonic pancreas ($n = 18$). These cells were usually single and dispersed throughout the embryonic pancreas (Fig. 2a). When multiple pancreases were transplanted, the grafts joined together over time (Fig. 2a–e). After 7 days, the first islet-like clusters were visible in the grafts (Fig. 2f, ESM movie). Mature islets were present 2 weeks after transplantation, as illustrated by rounded and separated EGFP-positive cell clusters during intravital imaging (Fig. 2g) and immunohistochemical staining for

2



Chapter 2: Sequential intravital imaging reveals *in vivo* dynamics of pancreatic tissue transplanted under the kidney capsule in mice

*Figure 2: Expansion and differentiation of MIP-EGFP/CAG-DsRed embryonic pancreas (E12.5) under the kidney capsule of immunodeficient NSG mice. (a–e) Images of individual xy focal planes of embryonic pancreases from MIP-EGFP/CAG-DsRed mice transplanted under the kidney capsule and imaged on day 1, 3, 5, 7 and 14. MIP-EGFP (green), CAG-DsRed (red). Scale bar, 1000 μm . (f–g) Higher magnification of individual xy focal planes showing islets in the transplanted embryonic pancreas (red) on day 7 and 14 after transplantation. Blood vessels (Bv) and islets (Is) can be clearly distinguished. MIP-EGFP (green), CAG-DsRed (red). Scale bar, 250 μm . (h) Immunohistochemical staining for insulin (red), glucagon (green) and DAPI (blue) 14 days after transplantation of embryonic pancreatic tissue. Arrowheads mark ductal structures. Scale bar, 250 μm . (i) Volume of the total embryonic pancreatic tissue (CAG-DsRed, in red) and the insulin-expressing cells (MIP-EGFP, in green) after transplantation. DsRed volume was significantly increased on day 7 and 14 compared with day 1, and EGFP volume was significantly increased on day 14 compared with day 1. (j) Percentage of the volume of the insulin-expressing cells (EGFP %) out of the total embryonic pancreatic tissue volume (DsRed) after transplantation. EGFP volume was significantly increased on day 14 compared with day 1. Data are mean \pm SEM. * $p < 0.05$ and ** $p < 0.01$ vs day 1. TX, transplant*

insulin and glucagon (Fig. 2h). DsRed volume at 14 days was 6.1 times that at day 1 ($9.5 \pm 2.1 \times 10^7 \mu\text{m}^3$ at day 1 vs $5.8 \pm 1.2 \times 10^8 \mu\text{m}^3$ at day 14, $p = 0.014$), and EGFP volume was 90 times that at day 1 ($2.3 \pm 0.5 \times 10^5 \mu\text{m}^3$ at day 1 vs $2.1 \pm 0.7 \times 10^7 \mu\text{m}^3$ day 14, $p = 0.04$) (Fig. 2i). After 2 weeks, the EGFP-positive cells represented $3.34 \pm 0.78\%$ of the DsRed-positive cells (Fig. 2j).

Discussion

Here we describe a novel intravital imaging model to study mature islet cells and developing pancreatic tissue using an abdominal imaging window. Tissues transplanted under the kidney capsule, which is considered the gold standard site for studying islet grafts, can be sequentially imaged for at least 2 weeks. Using fluorescent markers, we longitudinally measured engraftment, expansion, differentiation and vascularisation in transplanted developing pancreatic tissue and mature islets.

Alternative intravital imaging methods have been used to study islet function, survival and vascularisation over time. While the anterior chamber of the eye model allows prolonged (up to 6 months) sequential intravital imaging of transplanted pancreatic islets [7], it is limited by the tissue volume that can be transplanted. This reduces options to transplant large amounts of

tissue, or tissues with expansion capacity over time.

Our model allows the dynamic characterisation of the embryonic pancreas, which undergoes further development and expansion after transplantation under the kidney capsule [8]. Fetal pancreases are by nature highly proliferative [9]. The time course of growth and differentiation of embryonic pancreases transplanted under the kidney capsule is very similar to that observed in eutopic pancreatic development [10]. Sequential intravital imaging shows the process of islet neogenesis, as indicated by the appearance of rounded clusters of fluorescent cells. In the majority of embryonic pancreatic tissue transplants no acinar tissue was observed, as reported previously [8]. This is probably the reason why the percentage of beta cells in our grafts is relatively high compared with normal pancreatic development.

We were also able to dynamically assess transplanted islet grafts. Islets were connected to the host vasculature within 3 days, which is in line with previous findings [7]. Generally, placement of an imaging window did not affect survival or function of islets transplanted under the kidney capsule.

Important processes such as engraftment, vascularisation, expansion and differentiation can be studied using this imaging method. The

technique can therefore be a valuable tool in beta cell replacement therapy using progenitor cells, islet inflammation and rejection. In conclusion, we have developed a novel method to dynamically image both mature islet cells and developing pancreatic tissue.

Abbreviations

AIW: Abdominal imaging window

CAG-DsRed: Cytomegalovirus–actin–globin promoter red fluorescent protein

GFP: Green fluorescent protein

HIP-GFP: Human insulin promoter-green fluorescent protein

MIP-EGFP: Mouse insulin promoter-enhanced green fluorescent protein

NSG mice: NOD severe combined immunodeficiency gamma mice

References

- [1] Sakata N, Tan A, Chan N et al (2009) Efficacy comparison between intraportal and subcapsular islet transplants in a murine diabetic model. *Transplant Proc* 41:346–349
- [2] Loganathan G, Graham ML, Radosevich DM et al (2013) Factors affecting transplant outcomes in diabetic nude mice receiving human, porcine, and nonhuman primate islets: analysis of 335 transplants. *Transplantation* 95:1439–1447
- [3] Gao J, Tian L, Weng G, O'Brien TD, Luo J, Guo Z (2011) Stimulating beta-cell replication and improving islet graft function by AR231453, A gpr119 agonist. *Transplant Proc* 43:3217–3220
- [4] Ritsma L, Steller EJ, Beerling E et al (2012) Intravital microscopy through an abdominal imaging window reveals a pre-micrometastasis stage during liver metastasis. *Sci Transl Med* 4:158ra145
- [5] Ritsma L, Steller EJ, Ellenbroek SI, Kranenburg O, Borel Rinkes IH, van Rheenen J (2013) Surgical implantation of an abdominal imaging window for intravital microscopy. *Nat Protoc* 8:583–594
- [6] Ricordi C, Lacy PE, Finke EH, Olack BJ, Scharp DW (1988) Automated method for isolation of human pancreatic islets. *Diabetes* 37:413–420
- [7] Speier S, Nyqvist D, Cabrera O et al (2008) Noninvasive *in vivo* imaging of pancreatic islet cell biology. *Nat Med* 14:574–578
- [8] Brown J, Molnar IG, Clark W, Mullen Y (1974) Control of experimental diabetes mellitus in rats by transplantation of fetal pancreases. *Science* 184:1377–1379
- [9] Castaing M, Peault B, Basmaciogullari A, Casal I, Czernichow P, Scharfmann R (2001) Blood glucose normalization upon transplantation of human embryonic pancreas into beta-cell-deficient SCID mice. *Diabetologia* 44:2066–2076
- [10] Mullen YS, Clark WR, Molnar IG, Brown J (1977) Complete reversal of experimental diabetes mellitus in rats by a single fetal pancreas. *Science* 195:68–70

Legends ESM figures

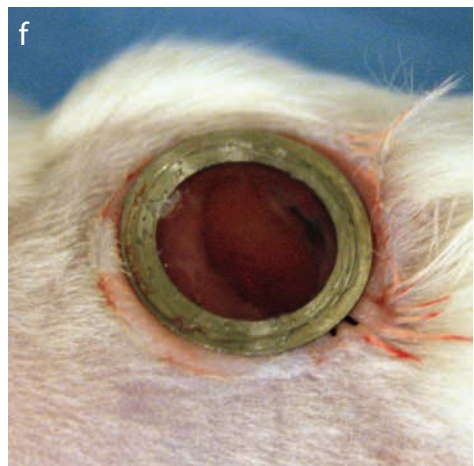
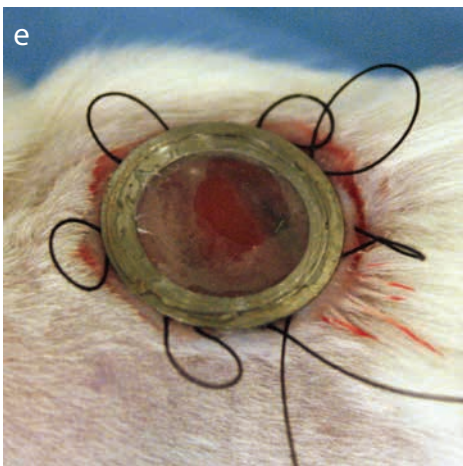
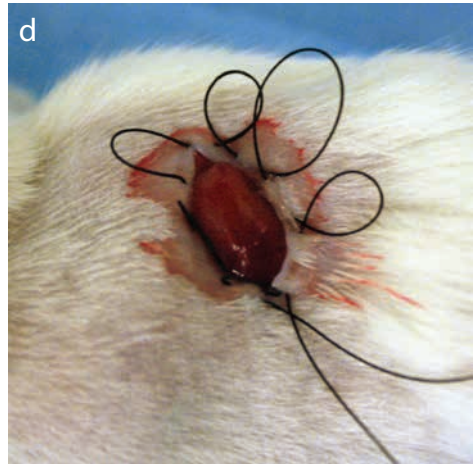
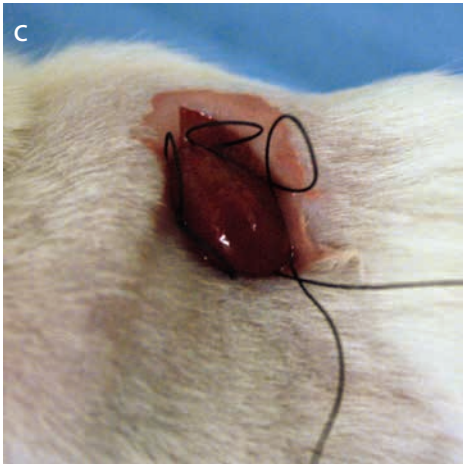
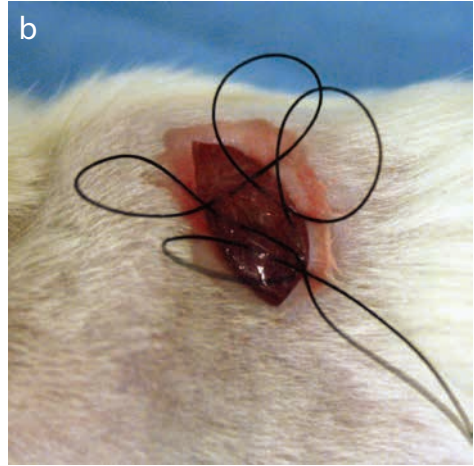
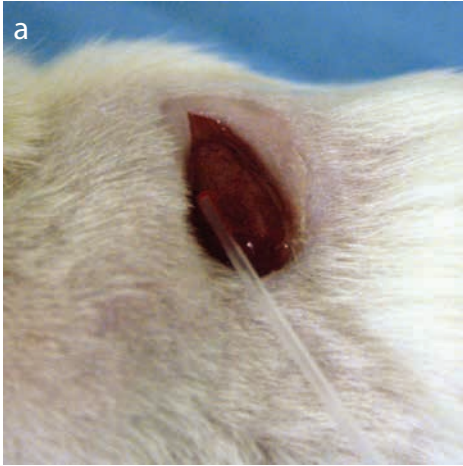
ESM figure 1 Procedures for abdominal window insertion [4] and intravital microscopy of grafts transplanted under the kidney capsule. (a) The skin and abdominal muscle of the left flank are opened, the kidney is surfaced and pancreatic islets or embryonic pancreases are transplanted using standard procedures. (b) The kidney is replaced into the retroperitoneal space and a purse-string suture is made in the abdominal wall. (c) The kidney is repositioned outside the abdominal wall and the purse-string suture is tightened so that the kidney is now positioned in the subcutaneous space. (d) A similar purse-string suture is made into the skin surrounding the incision. (e) An abdominal imaging window is placed into the incision in the skin. (f) Tightening the purse-string suture in the skin fixes the window in place, creating an airtight barrier.

ESM figure 2 Effects of an abdominal imaging window insertion. NSG mice were treated with a single intraperitoneal injection of 130 mg/kg streptozotocin (Sigma Aldrich, S0130) to induce hyperglycemia. Insulin glargine (Lantus, Sanofi-Aventis) was administered subcutaneously if blood glucose concentrations were >20mmol/l. (a) Change in body weight of mice with (AIW) or without (CTRL) an abdominal imaging window after transplantation of 2000 IEQ human islets (n=5 per group). (b) An IP-GTT was performed on AIW and CTRL mice that were fasted for 16 hours, 28 days after surgery. Baseline blood glucose was measured, after which mice received a 3 mg/kg intraperitoneal injection of glucose. Blood glucose concentrations were determined at 15, 30, 60 and 120 minutes post injection. (c) Human C-peptide concentrations on day 28 after surgery in AIW and CTRL NSG mice transplanted with human islets. (d) Islet graft size and fibrous capsule thickness. (e-f) Immunohistochemical staining for insulin and glucagon in sections from human islet grafts 28 days after transplantation.

(g) Percentage of insulin positive cells with respect to all insulin and glucagon positive cells. CTRL = lines & open circles, or white bars. AIW = dotted lines & closed squares, or black bars. Data are mean \pm SEM. Scale bar 250 μ m.

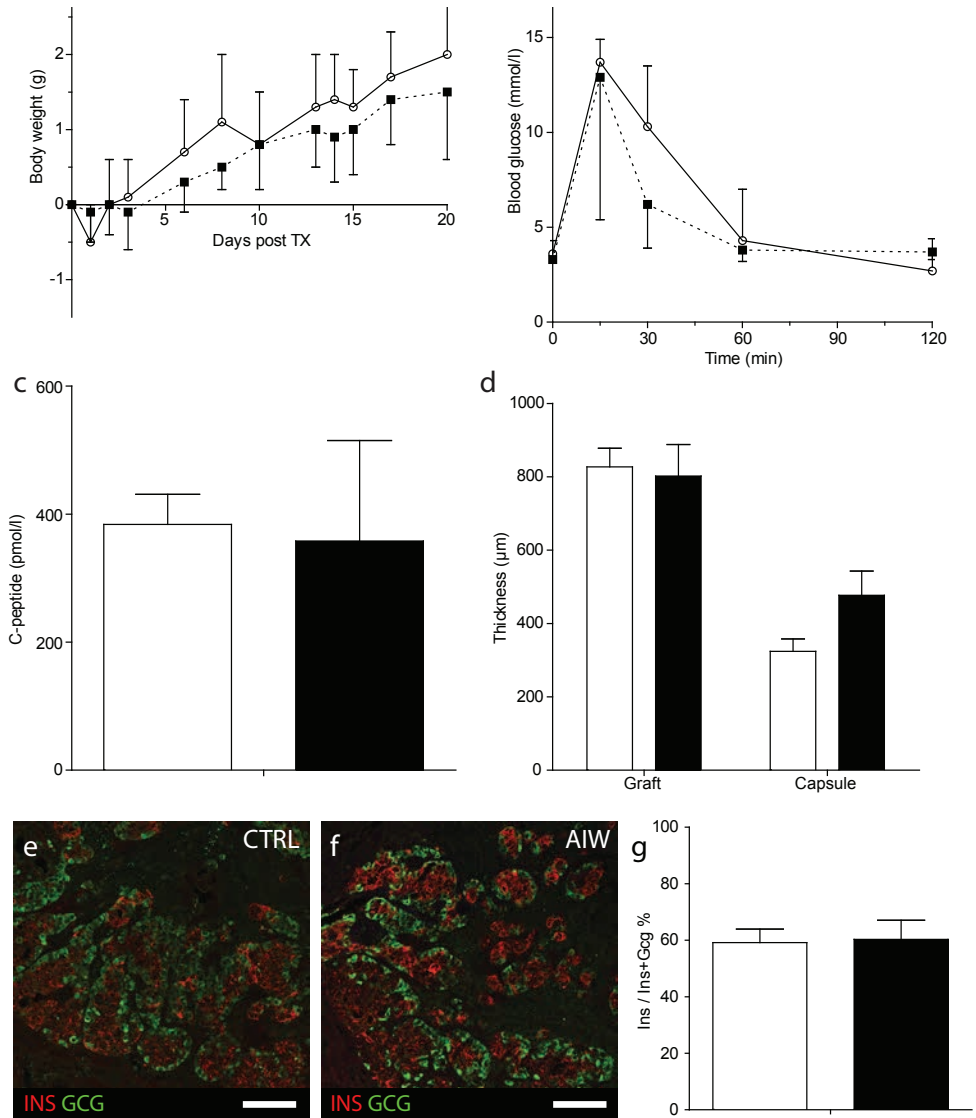
ESM figure 3 Transduction efficiency of human islet aggregates after a single-cell transduction with a HIP-GFP virus, reaggregation and culture for 7 days. HIP-GFP: Green fluorescent protein (GFP) under the transcriptional regulation of the human insulin promoter (HIP). Scale bar 250 μ m.

ESM figure 4 w Mosaic of individual XY focal plane images of MIP-EGFP islets three days after transplantation, and Texas Red labelled blood vessels inside these islets. The distance between individual images is 2 μ m. Arrowheads indicate a blood vessel surrounding the islet, arrows indicate a blood vessel inside the islet. Scale bar 100 μ m.



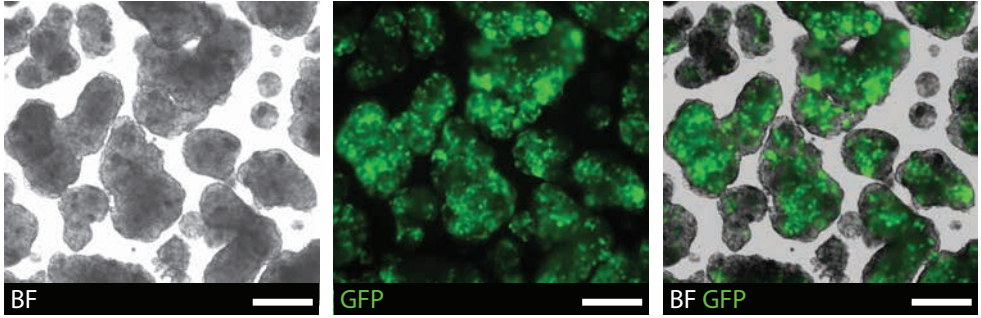
ESM figure 1

Chapter 2: Sequential intravital imaging reveals *in vivo* dynamics of pancreatic tissue transplanted under the kidney capsule in mice



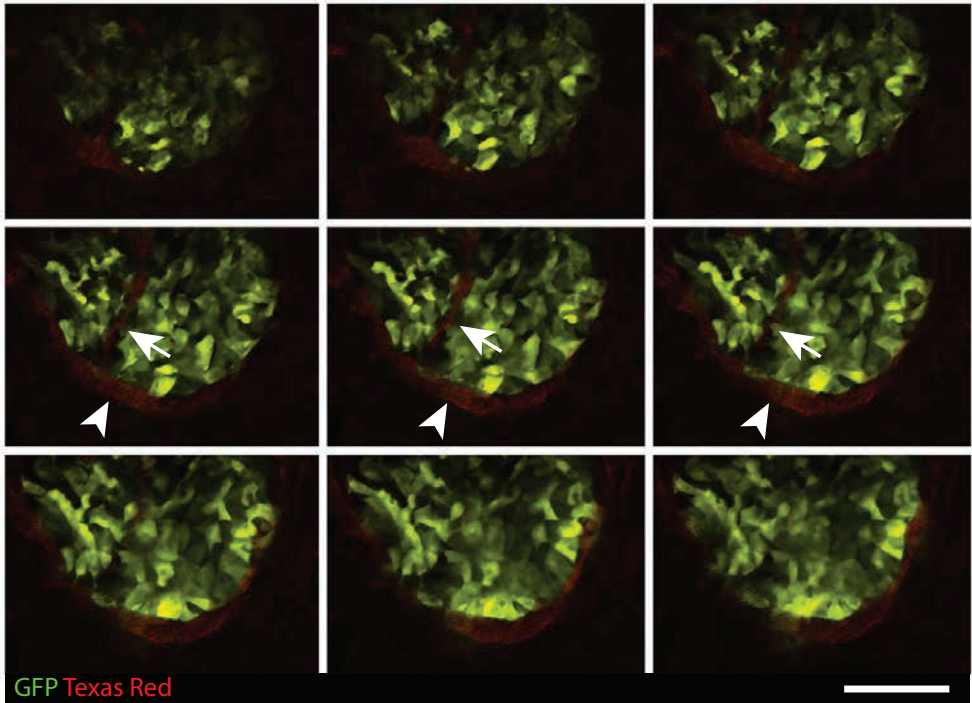
ESM figure 2

2



ESM figure 3

ESM figure 4



ESM Methods

Mouse pancreatic islet isolation

Animals between 7 and 12 weeks of age were killed after which pancreases were dissected from the animals. Pancreatic tissue was then dissected into small pieces (approximately 1 mm³). These pieces were incubated in 3ml RPMI medium (Thermo Fisher, 72400-021) containing 3mg/ml collagenase (Sigma Aldrich, St. Louis, MO, USA, C9263) in a shaking incubator at 37°C until a homogenous digest was obtained. Islets were immediately washed in RPMI medium containing 10% FBS, handpicked based on EGFP expression and transplanted within 4 hours after isolation.

Mouse embryonic pancreas isolation

Embryonic pancreases were dissected from E12.5 mouse embryos as described before [1] and kept in BME medium (Thermo Fisher, 4101-026) containing 100U/ml penicillin-streptomycin (Thermo Fisher, 15140-122), 50µg/ml gentamicin (Thermo Fisher, 15710-049), 1% glutamax (Thermo Fisher, 35050-061) and 10% FBS on ice until transplantation.

Human pancreatic islets and lentiviral transduction

For lentiviral transduction, the human islets were first dispersed into single cells using TrypLE (Thermo Fisher, 12605-010) containing 10µg/ml pulmozyme (Roche, Basel, Switzerland). A lentivirus containing a green fluorescent protein (GFP) under transcriptional regulation of the human insulin promoter (HIP) [2] was used. The HIP-GFP lentivirus was added to the dispersed cells at 20µg/ml, centrifuged at 300g for 1 hour, followed by incubation at 37°C for 3 hours. Cells were washed in PBS and cultured in RPMI medium containing 10% FBS on ultra-low attachment plates (Corning, Corning, NY, USA, 3471) during which spon-

taneous reaggregation occurred.

Islet or embryonic pancreas transplantation and positioning of an intra-abdominal imaging window

NSG mice were anesthetized using isoflurane. The lateral abdominal area on the left flank was shaved and an incision was made in both skin and abdominal muscle over the left kidney. The kidney was exposed and either 10-25 mouse islets, 2000 human islet equivalents (IEQ) or 2-4 embryonic pancreases were transplanted under the kidney capsule. A purse-string suture was made in the abdominal muscle and the kidney was fixed in place by tightening the suture which prevented the kidney from recoiling into the abdominal cavity, while blood vessels and ureter remained intact. A second purse-string suture was made in the skin and an abdominal imaging window (AIW) [3] was fitted into the incision. Tightening the suture fixed the window in the skin, leaving the graft directly underneath it (sFig 1). Mice received a single dose of 3µg buprenorphin (Temgesic, RB Pharmaceuticals Ltd, Richmond, VA, USA) as post-surgical pain relief. In control animals, no AIW was fitted, and the kidney was returned to the retroperitoneal space before muscle and skin closure using standard procedures.

Histological analysis

After killing the mice, the graft-containing kidney was removed and either fixed overnight in a 4% paraformaldehyde solution and embedded in paraffin, or fixed overnight in 1% paraformaldehyde solution in PBS containing 2.12mg/ml sodium periodate and 75mM l-lysine, cryoprotected in 30% sucrose for 6 hours and frozen in tissue freezing medium (Leica, Wetzlar, Germany, #14020108926). Paraffin sections were cut at 4µm and stained with haematoxylin and eosin for the determination of graft size and capsule thickness. Six to nine haematoxylin and eosin stained tissue

sections per graft were analysed with sections being 100-150µm apart. The measurement in every section comprised the largest diameter of the graft and capsule using Leica LAS AF 2.6 software. A mean diameter for graft and capsule per mouse was calculated. Cryosections were used for immunohistochemical staining. Primary antibodies against insulin (1:100, Ab7842, Abcam, Cambridge, UK) and glucagon (1:100, VP-G806, Vector labs, Burlingame, CA, USA) were used. Biotin-conjugated donkey anti rabbit (1:200, 711-065-152, Jackson ImmunoResearch Ltd, West Grove, PA, USA), TRITC anti guinea-pig (1:400, 706-025-148, Jackson ImmunoResearch Ltd) and Alexa 488 streptavidin (1:200, S-11223, Life Technologies) were used as secondary antibodies. Bright field images were acquired using a DM4000 microscope (Leica) with LAS AF software version 3.1. Fluorescent images were acquired using an inverted TCS SP5 microscope (Leica) with a 4W multiphoton chameleon Ti:Sapphire-pumped optical parametric oscillator (Coherent Inc, Santa Clara, CA, USA). For DAPI, multiphoton excitation was performed at 780nm. Other fluorophores were excited using single photon laser lines. Alexa488 and EGFP were excited at 488nm, and Alexa568, TRITC and DsRed at 561nm. Emission was collected at 400-460nm for DAPI, 510-550nm for Alexa488 and EGFP, and 570-610nm for Alexa568, TRITC and DsRed.

Image stacks from grafts that covered multiple fields of view were stitched together and exported using LAS AF software 2.6 (Leica). Maximum projection images were generated using ImageJ 1.49k. Reconstructions in 3D and volumetric calculations were made using Volocity software version 6.0 (PerkinElmer, Waltham, MA, USA).

Supplemental references

[1] Petzold KM, Spagnoli FM (2012) A system for ex vivo culturing of embryonic pancreas. *Journal of visualized experiments : JoVE*: e3979

[2] Zaldumbide A, Alkemade G, Carlotti F, et al. (2013) Genetically engineered human islets protected from CD8-mediated autoimmune destruction *in vivo*. *Molecular therapy : the journal of the American Society of Gene Therapy* 21: 1592-1601

[3] Ritsma L, Steller EJ, Ellenbroek SI, Kranenburg O, Borel Rinkes IH, van Rheenen J (2013) Surgical implantation of an abdominal imaging window for intravital microscopy. *Nature protocols* 8: 583-594

In vivo assessment of the migratory capacity of endocrine pancreatic progenitors during development

L. van Gulp¹, L. Seneby¹, T. Dielen¹, K. Koekkoek¹, J. van Rheenen²,
E.J.P. de Koning^{1,3}

3

1: Hubrecht Institute, Royal Netherlands Academy of Arts and Sciences and University Medical Centre Utrecht, Utrecht, The Netherlands

2: Cancer Genomics Center, Hubrecht Institute, Royal Netherlands Academy of Arts and Sciences and University Medical Centre Utrecht

3: Department of Nephrology, Leiden University Medical Center, Leiden, The Netherlands

Manuscript in preparation for publication

Abstract

Introduction and aim: The existence of endocrine progenitors in the pancreas with a mesenchymal phenotype has been previously described, but these cells have been poorly characterized due to the lack of a good model. We aimed to use a novel intravital microscopy technique to dynamically characterize migratory behavior of endocrine progenitors in the developing pancreas.

Methods and Results: Adult and embryonic pancreases from mouse insulin promoter-green fluorescent protein (MIP-GFP) mice were stained for GFP, insulin and glucagon to confirm that GFP-positive cells from MIP-GFP mice contain a subpopulation of endocrine progenitors during development. Embryonic age (E)12.5 pancreases were transplanted under the kidney capsule and the grafts were analyzed three and seven days after transplantation. Histological comparison of day three and day seven grafts to E15.5 and E18.5 embryonic pancreas, respectively, revealed that endocrine pancreas development appeared to be similar in transplanted embryonic pancreas grafts compared to eutopic embryonic pancreas development. Time lapse intravital imaging on day three and day seven grafts showed that 9.1% of all GFP positive cells expressed a migratory phenotype three days after transplantation. A lower number of migratory cells (4.0%) was observed seven days after transplantation.

Conclusions: Using intravital microscopy on transplanted embryonic pancreases, migration of endocrine progenitors can be further characterized.

Introduction

Beta cells arise from *Sox9* expressing trunk cells in the pancreatic epithelium during development. Under influence of Notch signaling [1], these cells start expressing neurogenin 3, delaminate from the ductal lining [2] and undergo epithelial-to-mesenchymal transition (EMT) [3]. Delaminated cells originating from neurogenin 3-positive cells mature towards endocrine cells [4, 5]. Under the influence of several important transcription factors, these cells will make a fate choice to end up in islets of Langerhans as either alpha, beta, gamma, delta or epsilon cells [6]. Although gene regulatory networks have been widely characterized [7], few studies have investigated cellular behavior during *in vivo* development. Islet cell progenitors, after delamination, express vimentin and members of the snail family indicating a mesenchymal phase [8]. Although it is known that after birth stretches of endocrine cells break into smaller pieces that start proliferating to form islets of Langerhans [9], little data is available on the prenatal behavior of delaminated endocrine precursors and the initial formation of islet cell aggregates.

Intravital microscopy using body imaging windows is a powerful technique that allows dynamic characterization of tissues and cells *in vivo* [10, 11]. We developed a method to intravitaly image tissue transplanted under the kidney capsule [12] whereby islets showed good engraftment and function after transplantation. Additionally, under the kidney capsule transplanted embryonic pancreases were shown to be able to reverse hyperglycemia [13, 14]. Histological analysis of these transplanted embryonic pancreases also revealed normal development of ductal structures and islets of Langerhans, but a complete agenesis of acinar tissue [13]. We found that islet-like structures could already be identified one week after transplantation of embryonic pancreases, and mature islets of Langerhans were found as early as two weeks

after transplantation [12].

Mice expressing green fluorescent protein under the mouse insulin promoter (MIP-GFP transgenic mice) show green fluorescence in beta cells [15]. Although all GFP-positive cells express insulin, almost half of these cells co-express other pancreatic endocrine hormones such as glucagon, somatostatin and pancreatic polypeptide in adult mice. In embryonic age (E)15.5 embryonic pancreases, this co-expression occurred in 60% of cells. Notably, more than 10% of all GFP-positive cells at E15.5 co-expressed neurogenin 3 [16]. These findings clearly indicate that during embryonic development besides GFP-positive mature beta cells, also a subpopulation of immature, progenitor-like cells is present. However, these findings are solely based on RNA expression profiling [16].

In this study, we show that the developmental time line is comparable between eutopic embryonic pancreases and transplanted embryonic pancreases. We confirm that GFP positive cells in the developing pancreas contain a subpopulation of endocrine progenitor cells based on protein stainings, and we performed time lapse intravital imaging on MIP-GFP grafts transplanted under the kidney capsule to study the migratory capacity of GFP positive cells in the developing pancreas.

Methods

Mouse models

Adult and embryonic pancreas tissue was isolated from mice expressing a combination of green fluorescent protein under transcriptional control of the mouse insulin promoter (MIP-GFP; the Jackson Laboratory #006864), red fluorescent protein under transcriptional control of the cytomegalovirus-actin-globulin promoter (CAG-DsRed; The Jackson Laboratory #005441) and/or monomeric cyan fluorescent

protein under transcriptional control of the cadherin 1 promoter (Ecad-CFP; The Jackson laboratory #016933). Transplantation was performed in NOD severe combined immunodeficiency gamma mice (NSG; The Jackson Laboratory #005557).

Tissue isolation

Embryonic tissue was isolated as described previously [17]. In short, uteri from pregnant female mice were collected at E12.5, E15.5 or E18.5. Embryonic pancreases were then isolated from the embryos by dissection. Adult pancreases were isolated from mice between seven and twelve weeks.

Embryonic pancreas transplantation

After isolation, embryonic pancreases were stored in BME medium (Thermo Fisher #4101026) containing 100 U/ml penicillin-streptomycin (Thermo Fisher #15140122), 50 µg/ml gentamicin (Thermo Fisher #15710-049), 1% glutamax (Thermo Fisher #35050061) and 10% FBS. The embryonic pancreases were transplanted as described previously [12]. In short, an incision was made on the left flank of the mouse. The kidney was exposed and 3-4 E12.5 embryonic pancreases were transplanted under the kidney capsule. Using a purse-string suture to reduce the size of the incision in the abdominal wall, the kidney was prevented from recoiling into the abdominal cavity. A second purse-string suture in the skin allowed the fixing of an abdominal imaging window (AIW) on top of the graft containing kidney so that microscopy of the transplanted tissue could be performed. Mice were sacrificed three or seven days after transplantation, and graft-containing kidneys were retrieved for histological analysis. In mice that were used only for histology, no AIW was placed, and the kidney was returned to the abdominal cavity after transplantation of the embryonic pancreases and both the abdominal wall and the skin were closed using standard procedures.

Intravital microscopy and image analysis

Intravital imaging was performed as described previously [11, 12]. In short, mice were anesthetized using isoflurane and positioned in a specially designed imaging box in such a way that the AIW would be located directly on top of the objective of an inverted TCS SP5 microscope (Leica) fitted with a 4W multiphoton laser (chameleon Ti:Sapphire-pumped optical parametric oscillator, Coherent Inc). The imaging box with the mouse was inserted into the climate chamber (ambient temperature 35.5°C). Images were acquired at resolutions between 0.6x0.6x2.0 μm and 2.4x2.4x5.0 μm (xyz) with 15 minute intervals for seven hours. For CFP, multiphoton excitation was performed at 840 nm, and the emission was collected at 455-505 nm. For GFP and DsRed, multiphoton excitation was performed at 960 nm, and the emission was collected at 505-555 nm (GFP), and/or 555-695 nm (DsRed). Images obtained from intravital imaging were corrected for xy and z drift using in-house developed software [18-20]. After correction, individual xy-focal planes from multiple regions of interest (ROI) in which GFP-positive cells, CFP-positive cells and/or clearly recognizable DsRed-positive structures could be identified, were selected. Movement of these cells or structures was measured using Fiji (ImageJ) with the manual cell tracking plugin. Speed was calculated by dividing distance and time after every time point, in $\mu\text{m}/\text{min}$. Displacement was calculated by measuring the vector between the first and last time point, in μm . GFP-positive cells were considered migratory if they displayed a higher speed and/or displacement than the average CFP-positive cells and DsRed-positive structures plus two standard deviations. Per time point, the percentage of GFP-positive migratory cells out of all GFP-positive cells was determined.

Histology

Graft containing kidneys were dissected so that only the graft and the directly surrounding

kidney tissue remained. All grafts and E12.5, E15.5 and E18.5 embryonic pancreases were fixed in freshly prepared 4% paraformaldehyde solution for two hours. For paraffin sectioning, tissue was dehydrated and embedded in paraffin blocks. For cryosectioning, tissue was cryoprotected in 30% sucrose solution for six hours or overnight and frozen in tissue freezing medium (Leica #14020108926). Sections were cut at 4 μm for paraffin, or 10 μm for cryo.

For immunohistochemical stainings, the following antibodies were used: guinea pig anti insulin (Abcam #Ab7842, 1:100), rabbit anti glucagon (Vector Labs #VP-G806, 1:200), mouse anti GFP (Roche #11814460001, 1:200), rabbit anti Mafk (Atlas Antibodies #HPA005653, 1:250), rabbit anti chromogranin A (Abcam #Ab45179, 1:200), mouse anti cadherin 1 (BD Biosciences #610182, 1:500), rabbit anti neurogenin 3 (Millipore #Ab10535, 1:500), rabbit anti Ki67 (Abcam #Ab16667, 1:500), biotin conjugated donkey anti rabbit (Jackson ImmunoResearch Ltd #711-065-152, 1:200), Alexa488 conjugated goat anti rabbit (Thermo Fisher #A11008, 1:200), Alexa488 conjugated goat anti mouse (Thermo Fisher #A11029, 1:200), Alexa568 conjugated goat anti rat (Thermo Fisher #A11077, 1:200), Tritc conjugated donkey anti guinea pig (Jackson ImmunoResearch #706-025-148, 1:200), Alexa633 conjugated goat anti mouse (Thermo Fisher #A21050, 1:200), Alexa647 conjugated goat anti rabbit (Thermo Fisher #A21244, 1:200), Streptavidin Alexa488 (Thermo Fisher #S11223, 1:200). Cell death was visualized using a TUNEL assay conjugated with Alexa647 (Thermo Fisher #C10619). Nuclei were stained using DAPI (Sigma Aldrich #D9542, 20 $\mu\text{g}/\text{ml}$).

Three adult pancreases from MIP-GFP mice and three E15.5 embryonic pancreases from MIP-GFP mice were stained for insulin, glucagon and GFP. All insulin-positive, GFP-positive, and/or glucagon-positive cells were counted. In adult pancreas, 10⁶ 167 cells were counted. In E15.5 embryonic pancreas,

Chapter 3: *In vivo* assessment of the migratory capacity of endocrine pancreatic progenitors during development

1'039 cells were counted. The percentage of insulin-positive cells out of all GFP-positive cells, the percentage GFP-positive cells out of all insulin-positive cells and the percentage of glucagon-positive cells out of all GFP-positive cells was determined.

Sections from E15.5 and E18.5, and from grafts three or seven days after transplantation, were immunohistochemically stained for cadherin 1, chromogranin A, neurogenin 3,

Ki67, and for apoptosis using TUNEL assay. DAPI-positive nuclei were counted automatically. The DAPI channel was transformed into a greyscale 8-bit image, thresholding was performed manually so that all nuclei were visible with the highest possible contrast, the image was watershedded to separate nuclei that were close together and the nuclei were counted using particle analysis (size 50-20000, circularity 0.00-1.00). Cadherin 1, chromogranin A, and neurogenin 3-positive cells were calculated man-

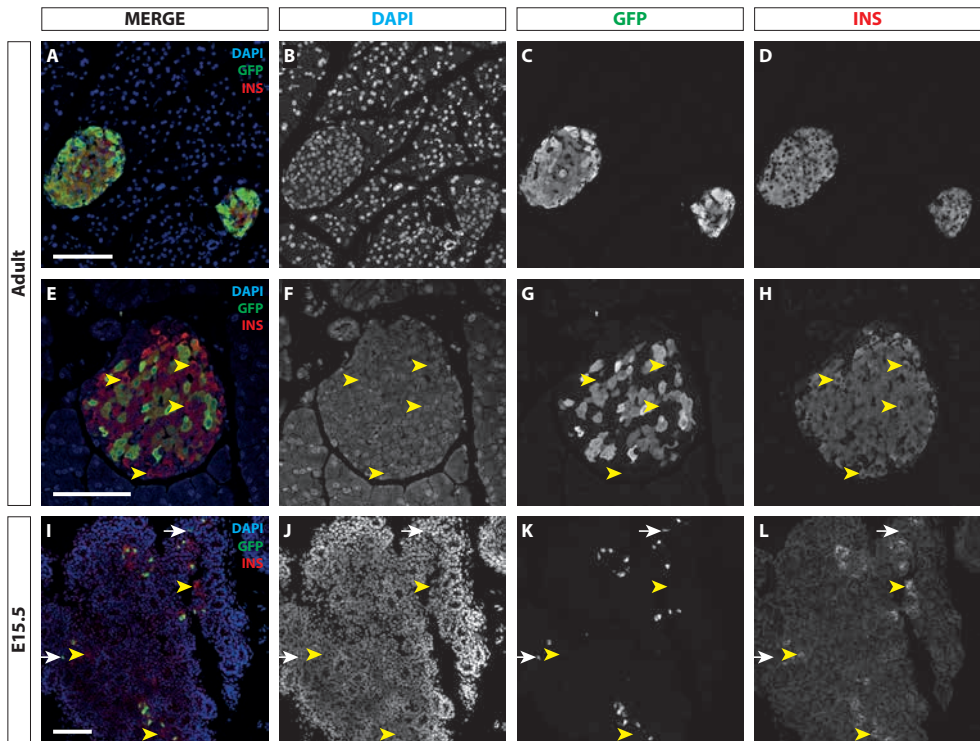


Figure 1: Not all insulin positive cells are GFP positive in the adult pancreas, and not all GFP positive cells are insulin positive in embryonic pancreas. A) Representative image of islets in the adult pancreas where almost all the insulin positive cells are also GFP positive. DAPI in blue, GFP in green, insulin in red. Scale bar 100 μ m. B-D) Greyscale images of DAPI, GFP and insulin channels from panel A. E) Representative image of islets in the adult pancreas where many insulin positive cells are negative for GFP. Yellow arrowheads indicate examples of cells that are negative for GFP and positive for insulin. DAPI in blue, GFP in green, insulin in red. Scale bar 100 μ m. F-H) Greyscale images of DAPI, GFP and insulin channels from panel E. I) Representative image of islet cells in the embryonic pancreas at E15.5. Yellow arrowheads indicate examples of cells that are negative for GFP and positive for insulin. White arrows indicate cells that are positive for GFP and negative for insulin. DAPI in blue, GFP in green, insulin in red. Scale bar 100 μ m. J-L) Greyscale images of DAPI, GFP and insulin channels from panel I.

Figure 2: Transplanted embryonic pancreas develops similarly compared to normal embryonic pancreas development. A-D) Staining for Chga and Cdh1 in embryonic pancreatic tissue 3 days after transplantation, E15.5 pancreas, embryonic pancreatic tissue 7 days after transplantation and E18.5 pancreas. DAPI in blue, Chga in green and Cdh1 in red. Scale bar 100 μ m. E-H) Staining for Neurog3 and Cdh1 in embryonic pancreatic tissue 3 days after transplantation, E15.5 pancreas, embryonic pancreatic tissue 7 days after transplantation and E18.5 pancreas. DAPI in blue, Neurog3 in green and Cdh1 in red. White dotted line in panel E indicates borders of the graft. Scale bar 100 μ m. I-L) Staining for Ki67 and Cdh1 in embryonic pancreatic tissue 3 days after transplantation, E15.5 pancreas, embryonic pancreatic tissue 7 days after transplantation and E18.5 pancreas. DAPI in blue, Ki67 in green and Cdh1 in red. Scale bar 100 μ m. M-P) Staining for TUNEL and Cdh1 in embryonic pancreatic tissue 3 days after transplantation, E15.5 pancreas, embryonic pancreatic tissue 7 days after transplantation and E18.5 pancreas. DAPI in blue, TUNEL in green and Cdh1 in red. Yellow arrowheads indicate examples of Cdh1 positive cells that are positive for TUNEL. Scale bar 100 μ m. Q-U) Percentages of Cdh1 (Q), Chga (R) and Neurog3 (S) positive cells compared to the total DAPI positive nuclei, and the percentages of Ki67 (T) and TUNEL (U) positive cells compared to the total Cdh1 positive cells. Charts are ordered from 3 day old grafts (lightest grey) to E15.5 pancreas, 7 day old grafts and E18.5 pancreas (darkest grey).

ually using Fiji (ImageJ) with the cell counter plugin, and were expressed as percentages out of the total number of DAPI nuclei per image, while Ki67 and TUNEL-positive cells were manually counted and expressed as percentages of cadherin 1-positive cells.

Statistical analysis

Differences between groups were calculated using two-way Student's t-tests. Data were considered significant when $p < 0.05$. All statistical analyses were performed using R (www.R-project.org).

Results

GFP from MIP-GFP mice is beta cell specific in adult pancreas but not in E15.5 embryonic pancreas

Pancreas sections from three adult MIP-GFP mice were immunohistochemically stained for GFP, insulin and glucagon. In total, 39.3 ± 8.5 islets per mouse were counted. In some islets almost all GFP-positive cells were positive for insulin (Figure 1a-d), while in some islets more than 50% of the insulin-positive cells were not positive for GFP (Figure 1e-h). On average, $78.4 \pm 11.34\%$ of insulin-positive

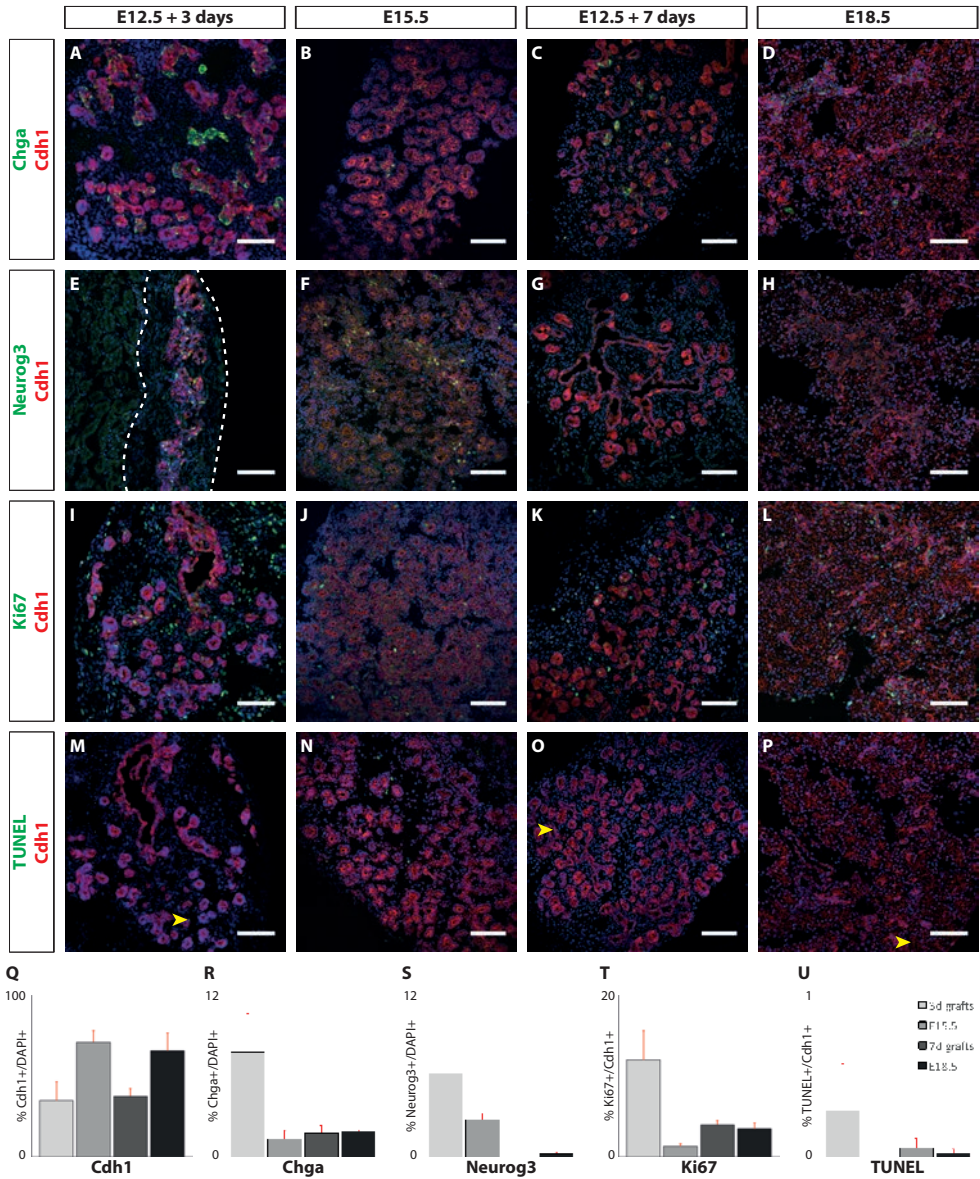
cells were also positive for GFP. Out of 6218 counted cells, only one cell was positive for GFP but negative for insulin. We identified five cells that were positive for both GFP and glucagon out of 3949 counted cells.

Sections from three E15.5 embryonic pancreases from MIP-GFP mice were also stained for GFP, insulin and glucagon. Islets did not yet form in these tissues, so individual cells were counted. In total, 441 cells that were positive for GFP and/or insulin were counted to investigate the relation between GFP and insulin. Of these cells, $53.6 \pm 9.0\%$ were double positive for GFP and insulin, while $38.0 \pm 11.8\%$ were only positive for insulin. We identified $8.4 \pm 3.6\%$ of all cells to be negative for GFP but positive for insulin (Figure 1i-l). All GFP and/or insulin-positive cells were positive for Mafb (supplemental Figure 1). Only two cells out of 596 GFP and/or glucagon-positive cells were found that co-expressed GFP and glucagon.

Similar development of endocrine cells in transplanted and eutopic embryonic pancreas

Three days after transplantation of E12.5 embryonic pancreases, there was a non-significant lower percentage of cadherin 1-positive cells compared to E15.5 embryonic pancreases

Chapter 3: *In vivo* assessment of the migratory capacity of endocrine pancreatic progenitors during development



(34.9±11.6% vs. 71.0±7.1%, respectively; $p=0.07$) (figure 2a-b, q). Seven days after transplantation, there was a non-significant lower percentage of cadherin 1-positive cells compared to E18.5 embryonic pancreases (37.5±4.7% vs. 65.7±11.1%, respectively; $p=0.11$) (Figure 2c-d, q). Neurogenin 3-positive cells were present in three days old grafts and

in E15.5 embryonic pancreases (6.2±3.6% and 2.8±0.5%, respectively; $p=0.44$) (Figure 2e-f, s), while neurogenin 3-positive cells could not be detected in seven days old grafts and only in a very limited number in E18.5 pancreases (0.26±0.12%) (Figure 2g-h, s). Chromogranin A-positive cells were detected in all tissues with no significant differences between any of the

tissues, although there was a trend for more chromogranin A-positive cells in three days old grafts compared to E15.5 pancreas ($7.8 \pm 2.9\%$ vs. $1.3 \pm 0.6\%$, respectively; $p=0.15$) (Figure 2a-d, r). Ki67-positive cells were detected in all tissues, with a trend towards more Ki67-positive, cadherin 1-positive cells, as an indicator for proliferation epithelial cells, in three days old grafts compared to E15.5 pancreas ($12.01 \pm 3.63\%$ vs. $1.31 \pm 0.30\%$, respectively; $p=0.10$) (Figure 2i-l, t). TUNEL-positive, cadherin 1-positive cells, as an indicator for apoptotic epithelial cells, were uncommon ($<1\%$ in all tissues) (Figure 2m-p, u).

Embryonic pancreas grafts contain a GFP population with a migratory phenotype

Time lapse imaging was performed on E12.5 pancreases from MIP-GFP/CAG-DsRed or MIP-GFP/Ecad-CFP mice three and seven days after transplantation under the kidney capsule of NSG mice in order to determine migration capacity of GFP-positive cells. For both three days and seven days after transplantation, NSG mice were transplanted with three or four embryonic pancreases per mouse. Due to expansion and fusion of the embryonic tissue, separate embryonic pancreases could not be distinguished in a graft. Intravital time lapse imaging could be performed in three mice with three day old grafts, and in three mice with seven day old grafts.

Migratory GFP-positive cells could be clearly identified on day three after transplantation (Figure 3a-d). Many of these cells had a mesenchymal-like shape. A total of 515 GFP-positive cells and 266-CFP positive cells or DsRed-positive structures as control were measured for speed and displacement (Figure 3i). Of the GFP-positive cells, 34 cells showed higher speed and 15 cells showed higher displacement compared to background. Of these cells, 2 cells had both a higher speed and displacement compared to background. In total 9.1% of all GFP-positive cells showed a migratory phenotype (figure

3j).

On day seven after transplantation, islet like structures could be detected in the grafts (Figure 3e-h). These grafts also contained GFP-positive cells with a mesenchymal phenotype but the frequency of these cells was reduced compared to day three grafts. A total of 348 GFP-positive cells and 113 CFP-positive cells or DsRed-positive structures were measured for speed and displacement (Figure 3k). Four cells were identified with a higher speed, and 10 cells with a higher displacement compared to background. Of these, 3 cells showed both a higher speed and displacement than the background cells and structures. In total, 4.0% of the GFP-positive cells on day seven showed a migratory phenotype (Figure 3l).

For both day three and day seven grafts, no positive relationship between speed and displacement was found (figure 3j,l).

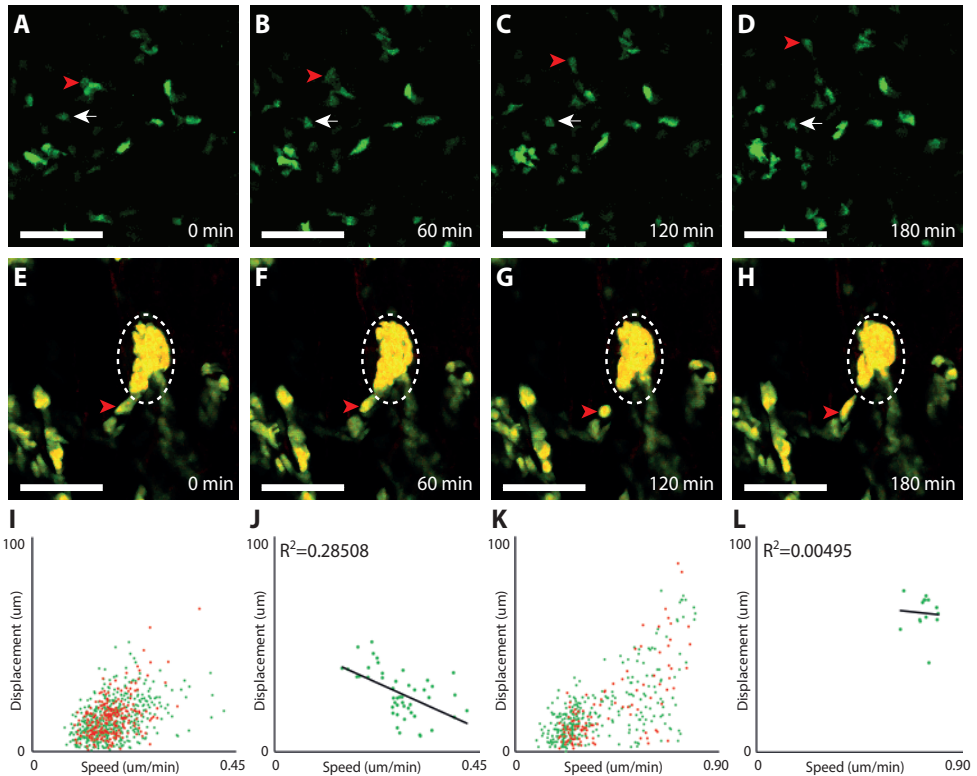
Discussion

Here we describe the migration characteristics of a subpopulation of cells expressing the insulin gene in embryonic pancreatic tissue from MIP-GFP mice transplanted under the kidney capsule. Migration of islet cell progenitors has previously been investigated using immunohistochemical stainings [3], *in vitro* culturing [21] and lineage tracing [22]. These methods confirm a migratory interphase of endocrine progenitors in which delaminated cells temporarily exist, but characterizing these cells has proven difficult because of limitations of the chosen method. Immunohistochemical staining does not capture the dynamic behavior of cells, embryonic pancreases cultured *in vitro* develop distinctly different from the *in vivo* situation, and lineage tracing gives information about the end-point of cells, not of the in-between phase.

The grafts that were imaged showed no significant difference in beta cell composition compared to embryonic pancreases from

Chapter 3: *In vivo* assessment of the migratory capacity of endocrine pancreatic progenitors during development

Figure 3: A subpopulation of GFP positive cells shows a migratory phenotype three days and seven days after transplantation of E12.5 embryonic pancreas under the kidney capsule. A-D) Time lapse images of E12.5 MIP-GFP pancreas three days after transplantation, with 60 minute intervals. Migratory cells can be identified in the red dotted circle. GFP positive cells in green. Red arrowhead indicates an example of a cell that shows a migratory phenotype. White arrow indicates an example of a cell that does not show a migratory phenotype. Scale bar 100 μm . E-H) Time lapse images of E12.5 MIP-GFP/CAG-DsRed pancreas seven days after transplantation, with 60 minute intervals. Migratory cells can be identified in the red dotted circle. GFP positive cells in green, DsRed positive cells in red. Red arrowhead indicates an example of a cell that shows a migratory phenotype. White dotted circle indicates an islet-like structure. Scale bar 100 μm . I) Scatterplot of all GFP positive cells (green) and all background cells (red) in grafts three days after transplantation. J) Scatterplot of all migratory GFP positive cells (green) in grafts three days after transplantation. The trendline with R-square value indicates the relation between speed and displacement. K) Scatterplot of all GFP positive cells (green) and all background cells (red) in grafts seven days after transplantation. L) Scatterplot of all migratory GFP positive cells (green) in grafts seven days after transplantation. The trendline with R-square value indicates the relation between speed and displacement.



comparable time points during development. However, there is an absence of acinar cells in transplanted embryonic tissue which is in line with previous findings [13, 14]. These findings might also explain the trend towards fewer cadherin 1-positive cells in the grafts. In

general, islet cell development in transplanted embryonic pancreases under the kidney capsule appears to be very similar to eutopic embryonic pancreatic development, although trends for increased chromogranin A and Ki67 in three days old grafts indicate a more active neogenesis

process. By using intravital microscopy of the developing pancreas under the kidney capsule, our method is the first to dynamically capture behavior of migratory endocrine cells in the developing pancreas.

By making a distinction between speed and displacement, an estimation can be made regarding directionality of the migrating cells [23]. Cells with both a high speed and displacement are migrating directionally, while cells with high speed but a low displacement are moving non-directionally, potentially ending up in the same spot as where they started. In our data, there does not seem to be a relation between speed and displacement, indicating that cells do not migrate directionally.

A limitation of our study is that we are not able to more clearly characterize the GFP-positive cells with a migratory phenotype. The MIP-GFP construct is not specifically expressed in beta cells during development, but also in other endocrine cell types and endocrine progenitors. This has previously been illustrated by multiplex qPCR on single cells showing that many multi-hormonal cells are present during development, where GFP-positive cells were detected that expressed neurogenin 3 [16]. The current study further confirms this by showing that during development, GFP-positive cells can be negative for insulin protein as well. These cells, although negative for insulin, were positive for the endocrine marker *Mafb*. During time lapse imaging, we observed that the migrating cells have a mesenchymal phenotype. Further characterization of migratory cells must be performed in order to investigate how islets of Langerhans are formed.

Another limitation of our study is the software we used for image analyses. The in-house software can correct for xy and z drift in tissue over time but not for rotation, zoom or deformation, which causes background movement. We solved this issue by correcting our findings of GFP positive cells with data on movement

of background structures, such as CFP positive epithelial cells or DsRed positive structures in the grafts. There was a considerable difference between the degree of background movement we encountered in mice, mostly caused by breathing.

In conclusion, we developed a method to track migratory endocrine progenitor cells during islet development *in vivo*. This method will allow the identification of factors that can modulate this migration.

References

- [1] Ahnfelt-Ronne J, Jorgensen MC, Klinck R, et al. (2012) Ptf1a-mediated control of Dll1 reveals an alternative to the lateral inhibition mechanism. *Development* 139: 33-45
- [2] Bankaitis ED, Bechard ME, Wright CV (2015) Feedback control of growth, differentiation, and morphogenesis of pancreatic endocrine progenitors in an epithelial plexus niche. *Genes Dev* 29: 2203-2216
- [3] Rukstalis JM, Habener JF (2007) *Snail2*, a mediator of epithelial-mesenchymal transitions, expressed in progenitor cells of the developing endocrine pancreas. *Gene Expr Patterns* 7: 471-479
- [4] Gu G, Dubauskaite J, Melton DA (2002) Direct evidence for the pancreatic lineage: NGN3+ cells are islet progenitors and are distinct from duct progenitors. *Development* 129: 2447-2457
- [5] Mellitzer G, Martin M, Sidhoum-Jenny M, et al. (2004) Pancreatic islet progenitor cells in neurogenin 3-yellow fluorescent protein knock-add-on mice. *Mol Endocrinol* 18: 2765-2776
- [6] Dassaye R, Naidoo S, Cerf ME (2016) Transcription factor regulation of pancreatic organogenesis, differentiation and maturation. *Islets* 8: 13-34
- [7] Arda HE, Benitez CM, Kim SK (2013) Gene regulatory networks governing pancreas development. *Dev Cell* 25: 5-13
- [8] Cole L, Anderson M, Antin PB, Limesand SW (2009) One process for pancreatic beta-cell coalescence into islets involves an epithelial-mesenchymal transition. *J Endocrinol* 203: 19-31
- [9] Miller K, Kim A, Kilimnik G, et al. (2009) Islet formation during the neonatal development in mice. *PLoS One* 4: e7739
- [10] Ellenbroek SI, van Rheenen J (2014)

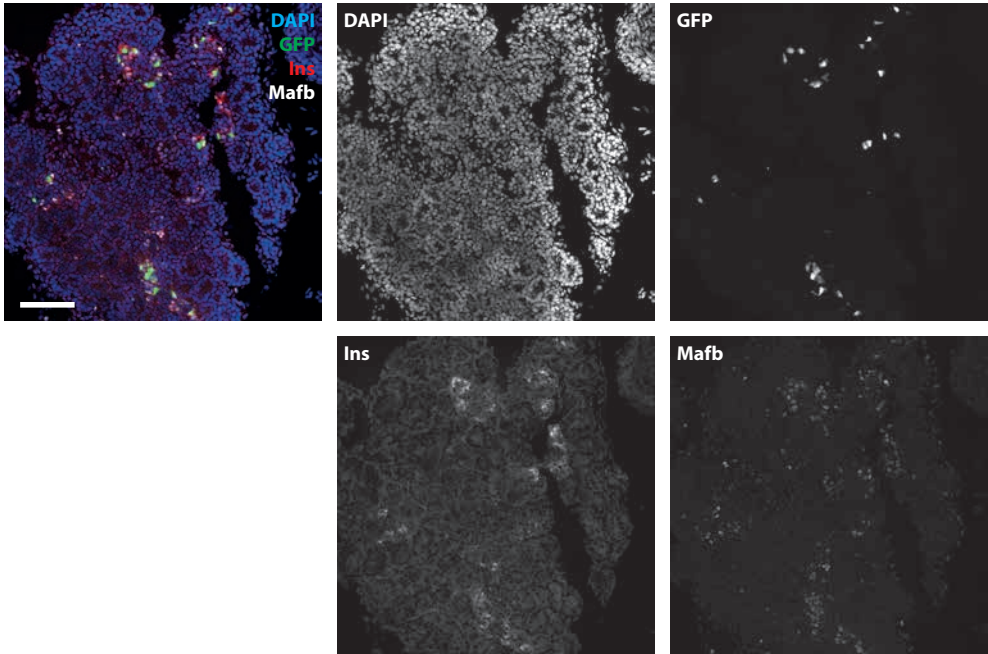
Chapter 3: *In vivo* assessment of the migratory capacity of endocrine pancreatic progenitors during development

Imaging hallmarks of cancer in living mice. *Nat Rev Cancer* 14: 406-418

cell migration. *Nat Protoc* 9: 1931-1943

- [11] Ritsma L, Steller EJ, Beerling E, et al. (2012) Intravital microscopy through an abdominal imaging window reveals a pre-micrometastasis stage during liver metastasis. *Sci Transl Med* 4: 158ra145
- [12] van Gurp L, Loomans CJ, van Krieken PP, et al. (2016) Sequential intravital imaging reveals *in vivo* dynamics of pancreatic tissue transplanted under the kidney capsule in mice. *Diabetologia*
- [13] Brown J, Molnar IG, Clark W, Mullen Y (1974) Control of experimental diabetes mellitus in rats by transplantation of fetal pancreases. *Science* 184: 1377-1379
- [14] Mullen YS, Clark WR, Molnar IG, Brown J (1977) Complete reversal of experimental diabetes mellitus in rats by a single fetal pancreas. *Science* 195: 68-70
- [15] Hara M, Wang X, Kawamura T, et al. (2003) Transgenic mice with green fluorescent protein-labeled pancreatic beta -cells. *Am J Physiol Endocrinol Metab* 284: E177-183
- [16] Katsuta H, Akashi T, Katsuta R, et al. (2010) Single pancreatic beta cells co-express multiple islet hormone genes in mice. *Diabetologia* 53: 128-138
- [17] Petzold KM, Spagnoli FM (2012) A system for ex vivo culturing of embryonic pancreas. *J Vis Exp*: e3979
- [18] Beerling E, Seinstra D, de Wit E, et al. (2016) Plasticity between Epithelial and Mesenchymal States Unlinks EMT from Metastasis-Enhancing Stem Cell Capacity. *Cell Rep* 14: 2281-2288
- [19] Zomer A, Maynard C, Verweij FJ, et al. (2015) *In Vivo* imaging reveals extracellular vesicle-mediated phenocopying of metastatic behavior. *Cell* 161: 1046-1057
- [20] Ritsma L, Ellenbroek SI, Zomer A, et al. (2014) Intestinal crypt homeostasis revealed at single-stem-cell level by *in vivo* live imaging. *Nature* 507: 362-365
- [21] Puri S, Hebrok M (2007) Dynamics of embryonic pancreas development using real-time imaging. *Dev Biol* 306: 82-93
- [22] Kim YH, Larsen HL, Rue P, Lemaire LA, Ferrer J, Grapin-Botton A (2015) Cell cycle-dependent differentiation dynamics balances growth and endocrine differentiation in the pancreas. *PLoS Biol* 13: e1002111
- [23] Gorelik R, Gautreau A (2014) Quantitative and unbiased analysis of directional persistence in

3



Supplemental figure 1: All GFP and insulin positive cells are also positive for endocrine marker MafB. Insulin in red, GFP in green, MafB in white, DAPI in blue. Greyscale images show positivity for individual proteins. Scale bar 100 μ m.

Dynamics of pancreas development using single cell transcriptome sequencing

L. van Gurp^{1,2}, M.J. Muraro^{1,2}, L. Seneby¹, T. Dielen¹, G. Dharmadhikari¹,
A. van Oudenaarden¹, E.J.P. de Koning^{1,3}

4

1: Hubrecht Institute, Royal Netherlands Academy of Arts and Sciences and University Medical Centre
Utrecht, Utrecht, The Netherlands

2: These authors contributed equally to this work

3: Department of Nephrology, Leiden University Medical Center, Leiden, The Netherlands

Manuscript in preparation for publication

Abstract

Single cell transcriptome sequencing characterizes all different cell types in heterogeneous tissues. We used this technique to investigate how cells from different populations in the developing pancreas interact, and how genes are dynamically regulated during embryonic differentiation. Cells were isolated from embryonic pancreases during the secondary transition of development. These cells were processed, mapped and clustered using SORT-seq. In total, 17 clusters with different cell types were identified, including epithelial tip and trunk structures, cells with an endocrine cell fate and various stages of endocrine progenitor cells. Tissue maturation was confirmed by comparing cells from different embryonic ages, and by generating a lineage tree. Gene expression could be visualized in pseudotime and revealed three distinct endocrine progenitor clusters: a cluster specifically expressing *Neurog3*, a cluster expressing high levels of *Vim* and *Chgb* and a cluster from which all endocrine cell types appear to originate, expressing many well described genes involved in endocrine differentiation, such as *Arx*, *Isl1*, *Rbp4*, *Pyy*, *Glud1*, *Pax6* and *Neurod1*. The generated transcriptome map of pancreas development reveals tissue complexity and dynamic behaviour of gene expression during pancreas organogenesis.

Introduction

Mouse pancreatic development is characterized by two main differentiation phases: the primary and secondary transition. The secondary transitional phase, characterized by segregation of the pancreatic epithelium into ductal tip and trunk domains and generally takes place between embryonic age 12.5 and 15.5 (E12.5 and E15.5) [1, 2]. In the trunk region, lateral inhibition determines which cells will differentiate into mature ductal cells, and which cells

will differentiate towards an endocrine cell fate [3-5].

Neurogenin 3 (*Neurog3*) is a key transcription factor involved in endocrine differentiation [6]. Upon expression of *Neurog3*, endocrine progenitors delaminate from the ductal lining to form the islets of Langerhans in the mesenchyme surrounding the pancreatic epithelium [7, 8]. These endocrine progenitors, which stop proliferation after committing to the endocrine lineage [9], make fate choices based on expression of key transcription factors as such to determine which endocrine cell type they will assume upon maturation. A first choice is imposed by the expression of mutually inhibitory genes *Pax4* or *Arx*, which push cells towards an alpha, beta or delta cell phenotype [10-12]. Later fate choices towards a beta cell phenotype involve *Pax6*, *Neurod1*, *Nkx2.2*, *Nkx6.1*, *Mafa* and *Mafb* [13-16]. Expression of these markers is well described, but dynamic patterns of these transcription factors remain poorly understood.

Single cell transcriptomics is a relatively new approach that provides information on gene expression from individual cells [17-20]. The two main advantages over traditional bulk sequencing are the possibility to investigate cell heterogeneity within tissues, and the identification of uncommon cell types that are masked by the most common cell types [21]. We and others have recently provided resources of gene expression in mature human and murine pancreatic tissue at a single cell level [22-27]. These resources show how single cells from the endocrine and exocrine pancreas can be clustered based on expression profiles into alpha, beta, gamma, delta, epsilon, ductal and acinar clusters. Heterogeneity within these clusters could be detected, which was used to subdivide clusters and identify rare subpopulations of cells [22, 23, 25]. A new challenge lies in the unbiased identification of progenitor cells, which can for example be achieved using cellular entropy [28] in combination with connectivity of cell clusters [29].

Here, we describe how individual cells from multiple time points during the secondary transition of the pancreas can be pooled into a single dataset, and divided into separate clusters representing all cell types of the embryonic pancreas using SORT-seq [22]. This dataset can then be used to identify tissue maturation through time, to characterize progenitor clusters, identify the distinct endocrine cell types of the pancreas that arise from these progenitors and to reveal dynamic regulation of genes involved in these fate choices.

Methods

Tissue preparation

Mouse embryos that express green fluorescent protein under transcriptional control of the mouse insulin promoter (MIP-GFP mice, Jackson Laboratories #006864) were isolated at embryonic age (E)12.5, E13.5, E14.5, E15.5 and E18.5 as described previously [30]. Tissues were digested into single cells using TrypLE (Thermo Fisher #12605010) containing 10 µg/ml pulmozyme (Roche, Basel, Switzerland), and washed with phosphate buffered saline (PBS) containing 10% fetal bovine serum (FBS, Thermo Fisher #10500064). Cells were stored on ice until they were sorted using FACS. DAPI (Sigma Aldrich #D9542, 20 µg/ml) or TO-PRO3 (Thermo Fisher #T3605, 1 µM) was added to cell suspensions immediately before sorting to distinguish between live and dead cells.

FACS sorting

Cells were then sorted as single cells into hard-shell 384 wells PCR plates (BioRad) containing 100 or 200 nl of reverse transcription (RT) primers, dNTPs and ERCC spike-ins, and 5 µl vapor-lock (Qiagen) using a FACSJazz or FACSaria II (BD biosciences) as described previously [22]. For every embryonic age, one 384 wells plate was sorted with ungated live cells, and one plate was sorted with MIP-GFP-pos-

itive cells to enrich for endocrine cell types. Sorted cells in plates were snap frozen on dry ice and stored at -80°C.

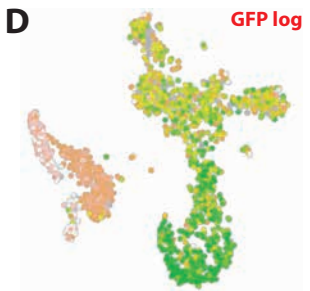
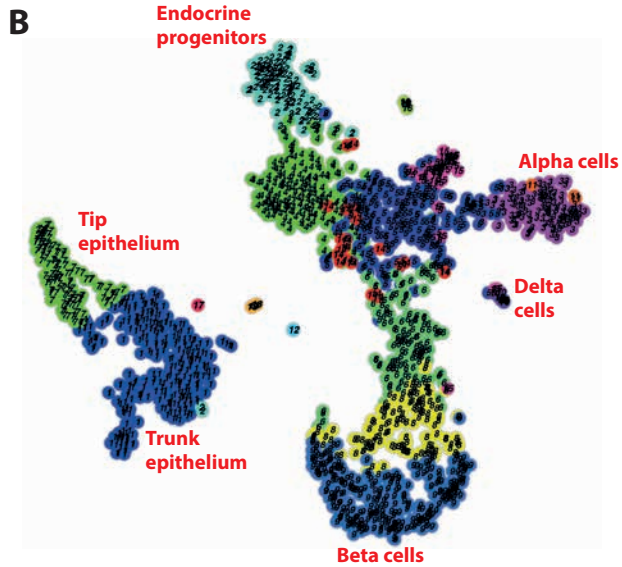
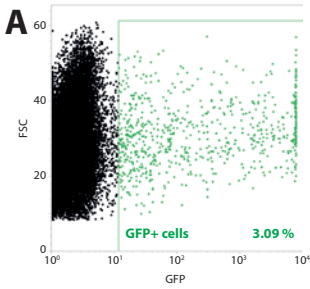
Processing of sorted cells

Cells were processed using SORT-seq as described previously [22]. In short, cells were thawed on ice and lysed at 65°C, after which RT and second strand reactions were done. RT reactions were performed using primers containing a polyT tail, a four or six base pair unique molecular identifier (UMI) sequence, a cell-specific barcode sequence (eight base pairs), an illumina 5' adapter and a T7 promoter sequence. After RT, each mRNA molecule was thus uniquely labeled. Contents from all wells in a plate were pooled into a single library after second strand reactions. The mRNA in these libraries underwent linear amplification using *in vitro* transcription, followed by fragmentation to lengths between 200 and 1000 base pairs, another RT reaction using random hexamer primers containing the illumina 3' adapter and exponential amplification using PCR. Sequencing was performed on Illumina NextSeq (paired-end, 75 bp).

Data processing

Sequenced reads were mapped to the transcriptome based on the mouse genome release mm10 as described previously [18, 22]. In short, reads with the same UMI – barcode – transcript combination were likely caused by PCR over-amplification and were thus counted as a single read, and the number of reads per transcript per cell were used to calculate transcript abundance using poissonian counting statistics [18].

Data from all plates were pooled into a single dataset. Data was downsampled to 6000 transcripts per cell, and cells with fewer transcripts were excluded. Genes needed to be expressed with a minimum of 5 transcripts in at least two cells or they were excluded from fur-



4

C

Clust.nr	# Cells	Top 10 upregulated genes in the cluster						Identify
1	315	Spp1 Sparc	Adams1 Hes1	Cyr61 Wfdc2	Cxcl12 Vim	Ccnd1 Zfp361		Trunk epithelium
2	121	Neurog3 Miat	Epb4.2 Gadd45a	Nhlh1 Btdb17	Neurod2 Cck	Amotl2 Pax4		Neurog3 progenitors
3	135	Gcg Tmem27	Cartpt Peg10	Irx1 Slc38a5	Irx2 Ttr	Asb4 Etv1		Alpha cells
4	204	Fev Cacna2d1	Chgb Glud1	Runx1t1 Pax4	Ids Neurod1	Hmgn3 St18		Mesenchymal endocrine progenitors
5	222	Peg10 Rbp4	Arx Gast	Zcchc18 Asb4	Slc38a5 Irx2	Isl1 Meis2		Late endocrine progenitors
6	134	Npy Atp2a2	Mapt Sytl4	Nnat Mafb	Gng12 Tshz1	Adra2a Ppp1r1a		Early beta cell progenitors
7	134	Ctrb1 Clps	Pnliprp1 Cela3b	Cela2a Spink3	Amy2b Cel	Try10 Try5		Tip epithelium
8	132	Nnat Arhgap36	Npy Iapp	Sytl4 Ero1lb	Ppp1r1a Gng12	Scg2 Atp2a2		Late beta cell progenitors
9	271	Prlr Scg2	Prss53 Ero1lb	G6pc2 Sytl4	Slc30a8 Chga	Hyou1 Gpx3		Beta cells
10	12	Sst Pyy	Hhex Cd200	Arg1 Cd24a	Fam159b Ppy	Rbp4 Isl1		Delta cells
11	3	Wnt4 Celf4	Rab37 Ctsz	Gpx3 Etv1	Resp18 Tmem27	Edn3 Ccnd2		Alpha cell subpopulation
12	2	S100a9 Camp	Ngp Gm5483	S100a8 Stfa3	Stfa1 Lyz1	BC100530 Stfa2		Intestinal cells
13	6	Stmn2 Phox2a	Gap43 Tubb2b	Rtn1 Elavl3	Prph Tagln3	Phox2b L1cam		Neuronal cells
14	23	Dbpht2 Chgb	1700086L19Rik Atp2a2	Meis2 Mid1ip1	Fam159b Pak3	Mapt Isnm1		Endocrine progenitor subpopulation
15	34	Ppy Lrrprc	Ppy Arx	Gast Tmem27	Gm4216 Etv1	Peg10 Isl1		Gamma cells
16	8	Ghr1 Maged2	Irs4 Anpep	Acs1 Alcam	Mboat4 Cdkn1a	Nefm Lrrprc		Epsilon cells
17	2	Cpa3 Rac2	Srgn Arhgdib	Hdc Ifitm1	Gpr65 Fcer1g	Laptm5 Lcp2		Immune cells

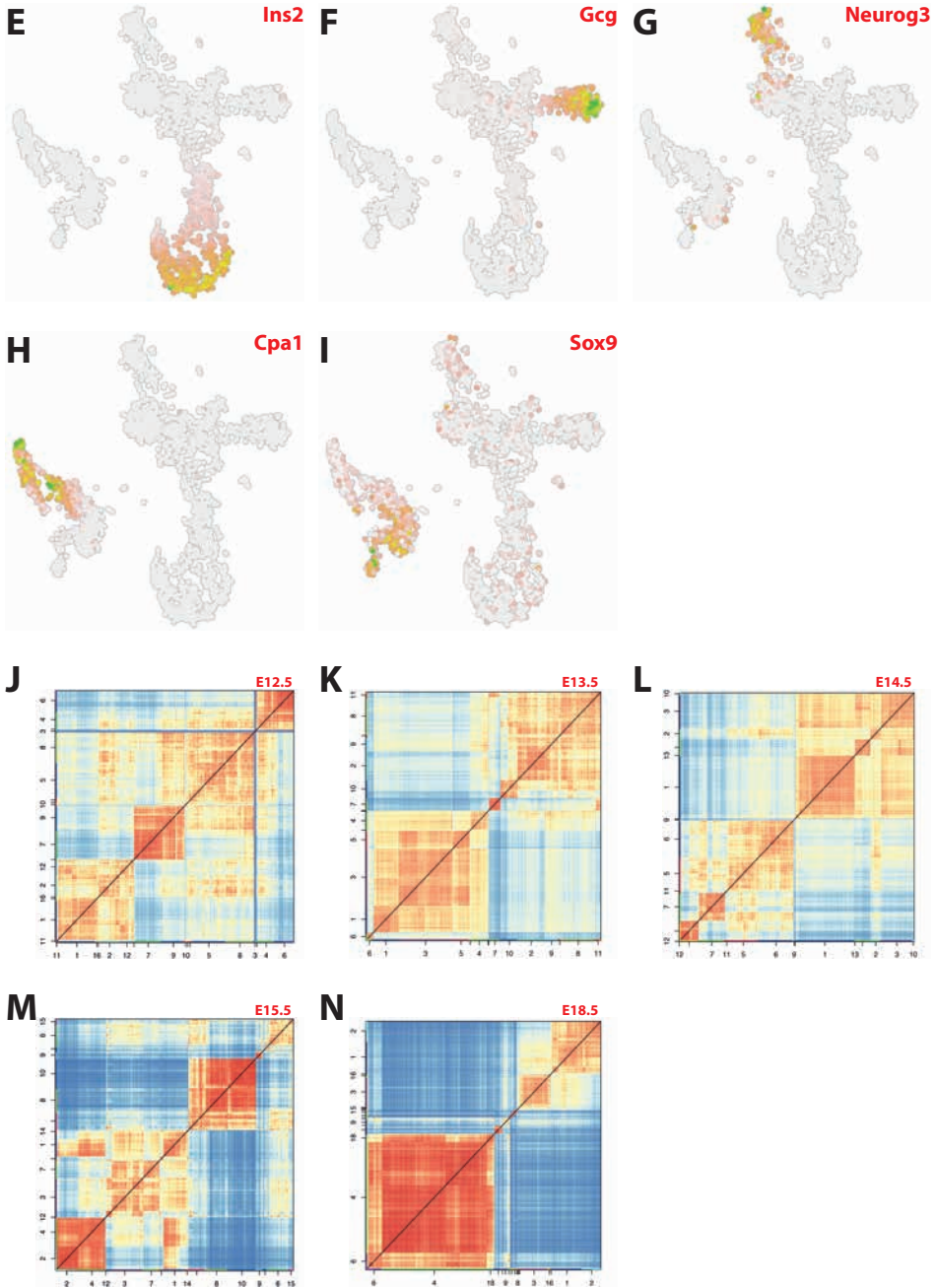


*Figure 1: Single cells from embryonic pancreases from multiple time points during embryonic development can be clustered to represent all pancreatic cell types present during development. a) FACS sorting of MIP-GFP embryonic pancreases revealed approximately 3% of all cells positive for GFP. b) Overlaying GFP intensity during FACS sorting upon TSNE maps reveals all endocrine cell types and all endocrine progenitors as positive for GFP. c) TSNE clustering of E12.5, E13.5, E14.5, E15.5 and E18.5 embryonic pancreases. d) Identification of individual clusters based on upregulated genes of every cluster compared to all other clusters. e-i) TSNE maps showing expression of *Ins2*, *Gcg*, *Neurog3*, *Cpa1* and *Sox9* to illustrate the location of beta cells, alpha cells, endocrine progenitor cells, tip cells and trunk cells. j-n) Heatmaps of correlations between individual cells. At later time points, correlations of cells within clusters become higher, while correlations outside the clusters become lower.*

ther analysis. Cells expressing more than 3 transcripts *Apoe*, 3 transcripts *Cd93*, 5 transcripts *Col1a1*, or 5 transcripts *Hbb-y* were excluded, as they represented cell populations unrelated to the pancreas (immune cells, blood vessel cells, mesenchymal cells or erythrocytes, respectively). The genes *Malat1*, *Lars2* and *Rn45s*, which are strongly upregulated in some libraries and are linked to cellular stress [31-33], were excluded from the dataset.

K-medoids clustering and outlier detection was performed using the RaceID algorithm [18, 22], and differential expression between clusters was calculated as described previously [34]. Connectivity and stemness of clusters was calculated using the StemID algorithm [29]. In short, a lineage tree is calculated between clusters whereby every cluster in the dataset receives a stemID score, which is based on connectivity of that cluster in the lineage tree in combination with the median entropy (transcriptome specificity) of that cluster. Stem cell clusters receive higher scores, based on lower transcriptome specificity and higher connectivity to other clusters, compared to more mature cell clusters.

Gene ontology (GO) biological processes analysis was performed using the enrichment analysis from the gene ontology consortium (www.geneontology.org). All data were processed using R (www.r-project.org).

For a graphical overview of the entire procedure, see supplemental figure 1.

Results

Embryonic pancreatic tissue can be subdivided in all pancreatic cell types using a single cell transcriptomics approach

To obtain transcriptome information from different embryonic ages during the secondary transition of mouse pancreas development, embryonic pancreata were collected from embryos at E12.5, E13.5, E14.5, E15.5 and E18.5. Sorting of cells was performed on single cell suspensions containing embryonic pancreata from multiple embryos. Increasingly fewer embryos were needed to obtain enough cells as organs were increasing in size: 34 embryos were isolated to sort for E12.5, 14 embryos for E13.5, 10 embryos for E14.5, 8 embryos for E15.5 and 2 embryos for E18.5.

Data from ungated live cells and MIP-GFP-positive live cells from every embryonic age were pooled into a single dataset. Approximately 3% of all cells was positive for MIP-GFP during FACS sorting (Figure 1a). After downsampling, k-medoids clustering of 1758 cells based on expression of 3230 genes revealed 17 clusters, as represented in TSNE mapping (Figure 1b). Differential expression between cells of individual clusters and all other cells revealed which genes were upregulated in cells of these clusters, after which identification of the main cell types in these clusters could be performed (Figure 1c) (supplemental data 1c). MIP-GFP positive cells enriched the dataset for all endocrine cell types, and all endocrine pro-

genitor cells (figure 1d). Gene expression levels of *Ins2*, *Gcg*, *Neurog3*, *Cpa1* and *Sox9* reveals which clusters can be designated as beta cell, alpha cell, endocrine progenitor, epithelial cell from the tip region and from the trunk region of the ductal tree, respectively. (Figure 1e-i).

K-medoid clustering of pancreatic cells from a specific embryonic age resulted in smaller datasets. Hierarchical clustering of correlations between cells revealed increasingly smaller correlations between cells of different clusters at later time points, indicating that cells become more specialized over time (Figure 1j-n). Pan-

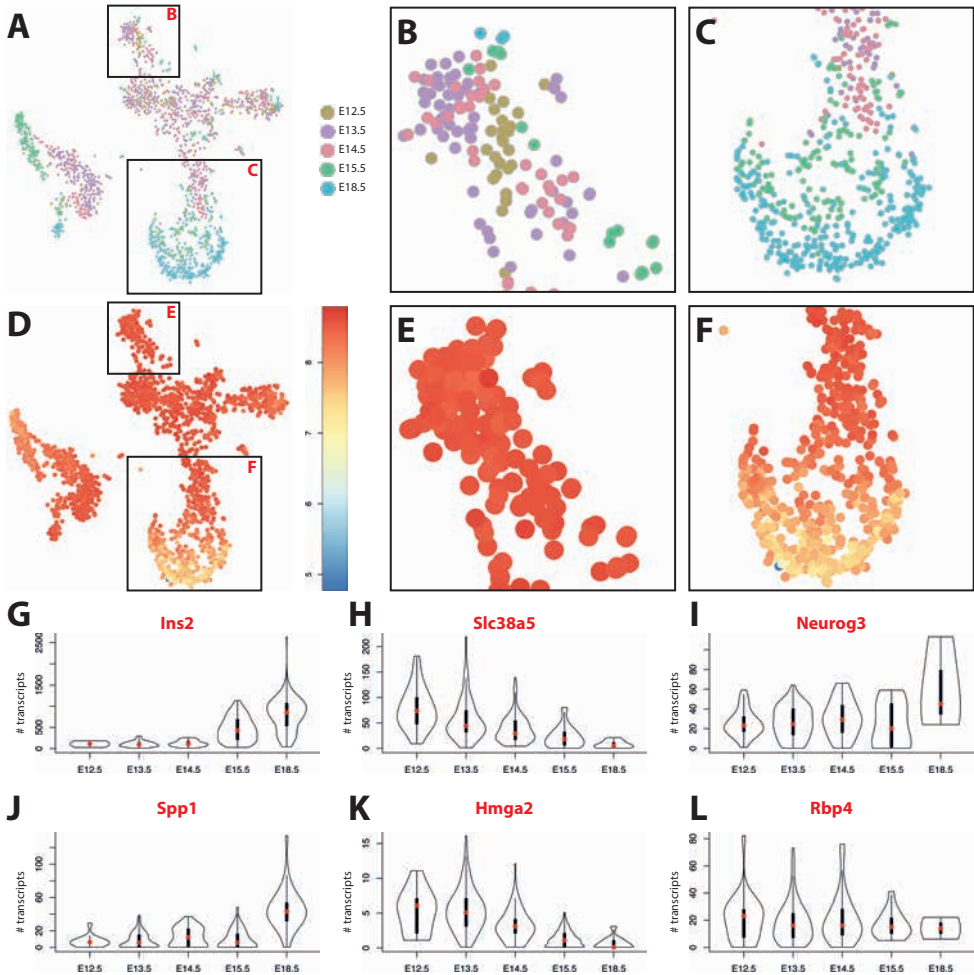
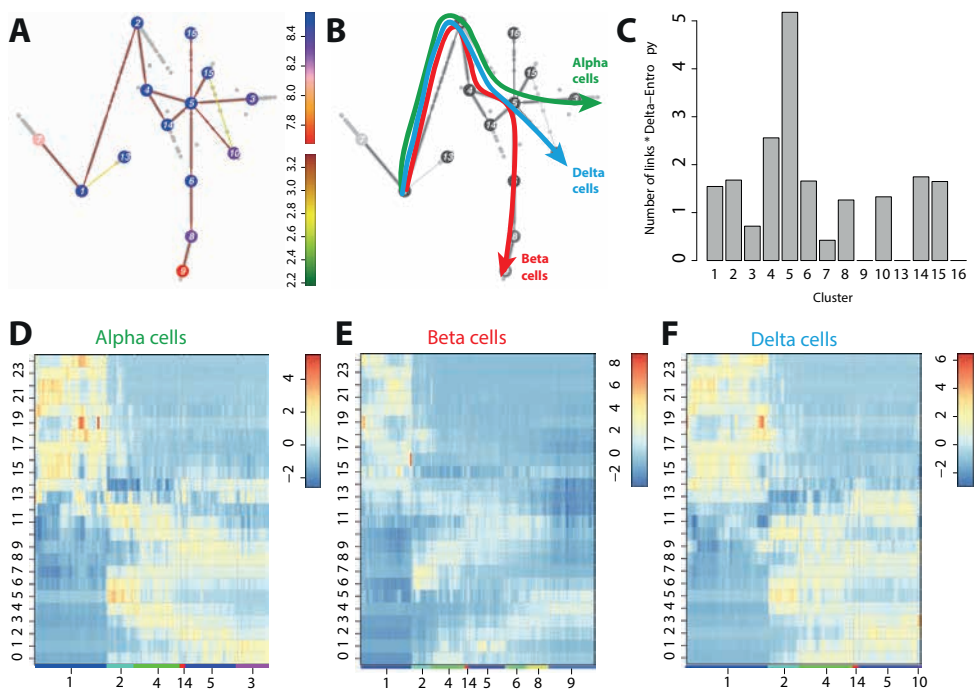


Figure 2: Contribution and temporal characteristics of cells from different embryonic ages to the dataset. a) Distribution of cells from different embryonic ages in the dataset. b) Zoom of panel A for endocrine progenitor cluster 2. c) Zoom of panel A for beta cell clusters 6, 8 and 9. d) Entropy of cells in the dataset. e) Zoom for entropy of panel D for endocrine cluster 2. f) Zoom for entropy of panel D for beta cell clusters 6, 8 and 9. g-l) Violin plots of expression for *Ins2* in clusters 6, 8 and 9 (g), *Slc38a5* in clusters 5 and 3 (h), *Neurog3* in cluster 2 (i), *Spp1* in cluster 1 and 7 (j), *Hmga2* in clusters 1 and 7 (k) and *Rbp4* in clusters 5 and 3 (l) for E12.5, E13.5, E14.5, E15.5 and E18.5 cells.

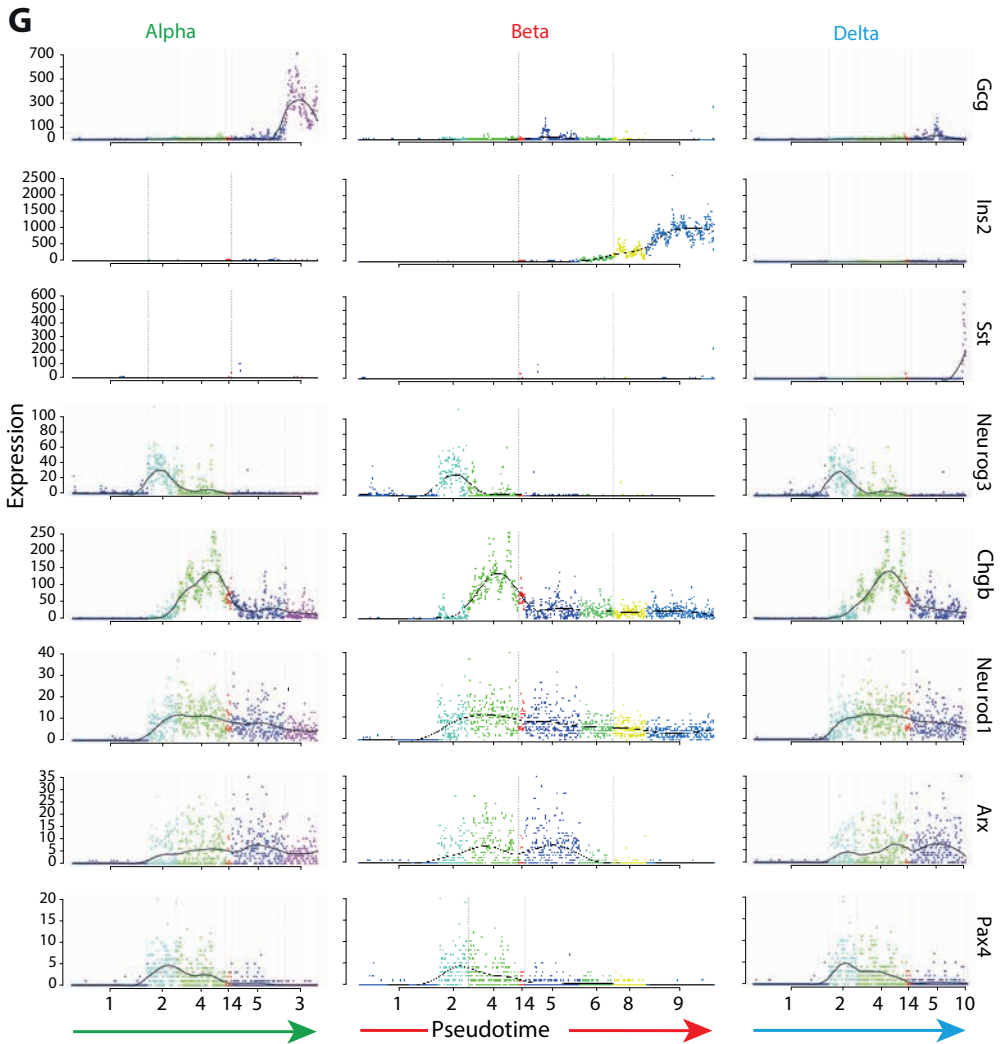
Figure 3: Determination of a lineage tree leads to establishment of alpha, beta and delta cell branches of development and allows for identification of dynamic expression patterns for genes involved in endocrine cells using self-organizing maps. a) Lineage tree determination for the dataset using the StemID algorithm. b) Identification of pseudotemporal branches for alpha, beta and delta cell development. c) StemID identification of most stem-like cluster. Cluster 5 is the last endocrine progenitor cluster before the specific endocrine cell types start forming. d-f) Self-organizing maps for alpha, beta and delta cell differentiation. Data is compressed into two dimensions, with pseudo time on the x-axis and clusters of genes with similar temporal expression patterns on the y-axis. g) Gene expression in pseudo time for alpha, beta and delta cell branches for Gcg, Ins2, Sst, Neurog3, Chgb, Neurod1, Arx and Pax4. Pseudo-time is plotted on the x-axis, gene expression levels are plotted on the y-axis.



creas data from each embryonic age contains clusters of cells representing beta cells, alpha cells, endocrine progenitors, and cells from the tip and trunk epithelium, except for the E18.5 dataset. This dataset does not contain any *Cpa1* expressing cells indicative of epithelial cells in the tip region of the ductal tree in earlier datasets (supplemental Figure 2). Small non-pancreatic clusters were also identified, containing intestinal, neuronal and immune cells.

Cells from different time points can show distinct temporal expression patterns

In order to identify temporal fingerprints within our dataset, we investigated how pancreatic cells from different embryonic ages were represented within the clusters of cells. It was found that most clusters contained a heterogeneously mixed population of cells from all embryonic ages, such as the Neurog3 expressing endocrine progenitor cluster (Figure 2a-b).



Some clusters could be subdivided based on the embryonic ages of the collected cells, such as the beta cell cluster (Figure 2a,c). This temporal expression pattern correlates with the entropy of these cells, defined as the transcriptome uniformity [28]. A higher entropy value represents a more uniform transcriptome, which is associated with multipotency or stemness of cells [35]. Entropy was found to be uniformly expressed in clusters with a heterogenous mix of cells from different embryonic ages (Figure 2d-e), but showed a decreasing gradient in clusters

in which mature cell types are being formed, such as the beta cell cluster (Figure 2d,f), the epithelial tip cluster (cluster 7) and the alpha cell cluster (cluster 3).

Gene expression levels can be temporally affected. Some genes, like *Ins2* and *Spp1*, become increasingly more highly expressed at later embryonic ages (figure 2g,j). Other genes, like *Slc38a5* and *Hmga2*, show decreasing expression at later embryonic ages (figure 2h,k). Many genes do not show clear temporal expression

patterns, as illustrated by the temporal expression profiles of *Neurog3* and *Rbp4* (figure 2i,l).

Generation of a pseudo timeline for alpha, beta and delta cell development

A lineage tree was calculated using the entire dataset (Figure 3a) as described previously [29]. We identified a pathway from the epithelial trunk (cluster 1) through *Neurog3* cells (cluster 2) to three clusters of endocrine progenitor cells (clusters 4, 14 and 5). From cluster 5, many branches appear that lead to the different endocrine cell types. A beta cell branch leads from cluster 5 through clusters 6 and 8 towards cluster 9. Other branches from cluster 5 lead towards more mature alpha cells (cluster 5 to 3), delta cell (cluster 5 to 10), gamma cells (cluster 5 to 15) and epsilon cells (cluster 5 to 16) (Figure 3b). Cluster 5 was further recognized by the StemID algorithm as the most stem-like cluster in the dataset (Figure 3c).

We then created three pseudo timelines, one for alpha cell differentiation (linking clusters 1, 2, 4, 14, 5 and 3), one for beta cell differentiation (linking clusters 1, 2, 4, 14, 5, 6, 8 and 9) and one for delta cell differentiation (linking clusters 1, 2, 4, 14, 5 and 10). Cells were ranked in pseudotime for every branch. Subsequently, all differentially expressed genes in the dataset were clustered into 25 groups, based on their expression profile in pseudotime. In the alpha cell branch, groups 0, 1 and 8 contained genes with high expression at the end of the pseudotime axis. Group 0 contained familiar genes like *Arx* and *Etv1*, group 1 contained more mature genes like *Gcg*, *Irx1*, *Irx2* and *Ttr*. Interestingly, in group 8 no generally known genes involved in alpha cell maturation or functioning were found to be highly expressed (Figure 3d) (supplemental data 3d). In the beta cell branch, group 4 and 5 contained genes with high expression at the end of the pseudo timeline for beta cell development. Group 4 contained many mature beta cell genes like *Iapp*, *Ins1*, *Ins2* and *Nkx6.1*, and also the delta cell specific *Sst* (Fig-

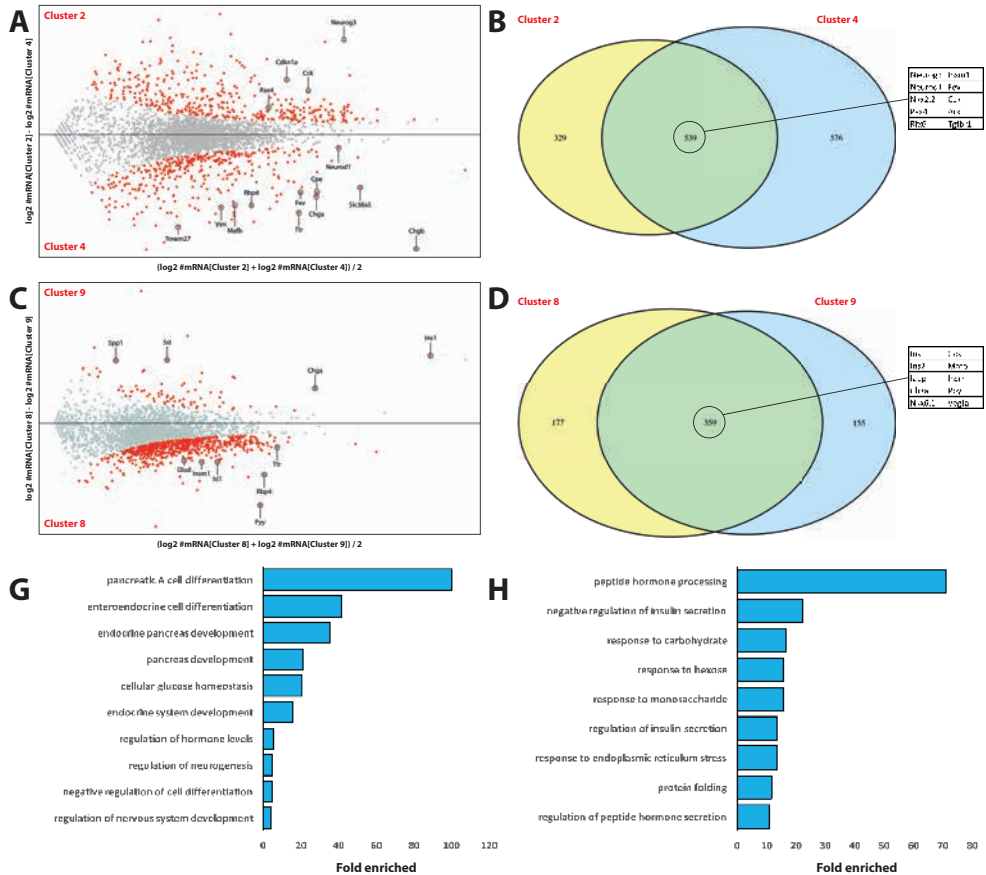
ure 3e) (supplemental data 3e). Group 5 did not contain any generally known genes involved in beta cell maturation or functioning. In the delta cell branch, group 3 was the only group with strong expression at the end of the delta branch pseudo timeline, which contained *Sst* and *Foxo1* (Figure 3f) (supplemental data 3f).

Different expression profiles were also observed for key endocrine genes using these pseudo timelines. To illustrate this, we plotted *Gcg*, *Ins2*, *Sst* and *Neurog3* in the alpha, beta and delta branches (Figure 3g). *Gcg*, *Ins2* and *Sst* were all found to be strongly upregulated at the end of the pseudo timeline for their representative branches (*Gcg* in the alpha cell branch, *Ins2* in the beta cell branch and *Sst* in the delta cell branch, respectively), while *Neurog3* was upregulated in cluster 2 of every branch. By plotting *Chgb*, *Neurod1*, *Arx* and *Pax4* we could illustrate how genes are organized in pseudotime for the alpha cell, beta cell and delta cell branches.

Differential expression between linked clusters identifies stages of endocrine pancreas development

To compare different stages of endocrine progenitor cells we determined differential expression between clusters 2 and 4. We identified 480 genes that were significantly upregulated in cluster 2, including genes such as *Neurog3*, *Cdkn1a* and *Cck*. In cluster 4, we identified 484 differentially expressed genes, including genes like *Chgb*, *Mafb*, *Cldn4* and *Vim* (figure 4a) (supplemental data 4a). For both clusters, differentially upregulated genes were identified compared to all other cells in the dataset, and overlap in these lists of differentially upregulated genes was calculated. Cells in cluster 2 differentially upregulated 868 genes compared to all other cells, while cells in cluster 4 differentially upregulated in 1115 genes compared to all other cells. Of these genes, 539 genes were differentially upregulated in both cluster 2 and 4 (Figure 4b) (supplemental data 4b). Amongst

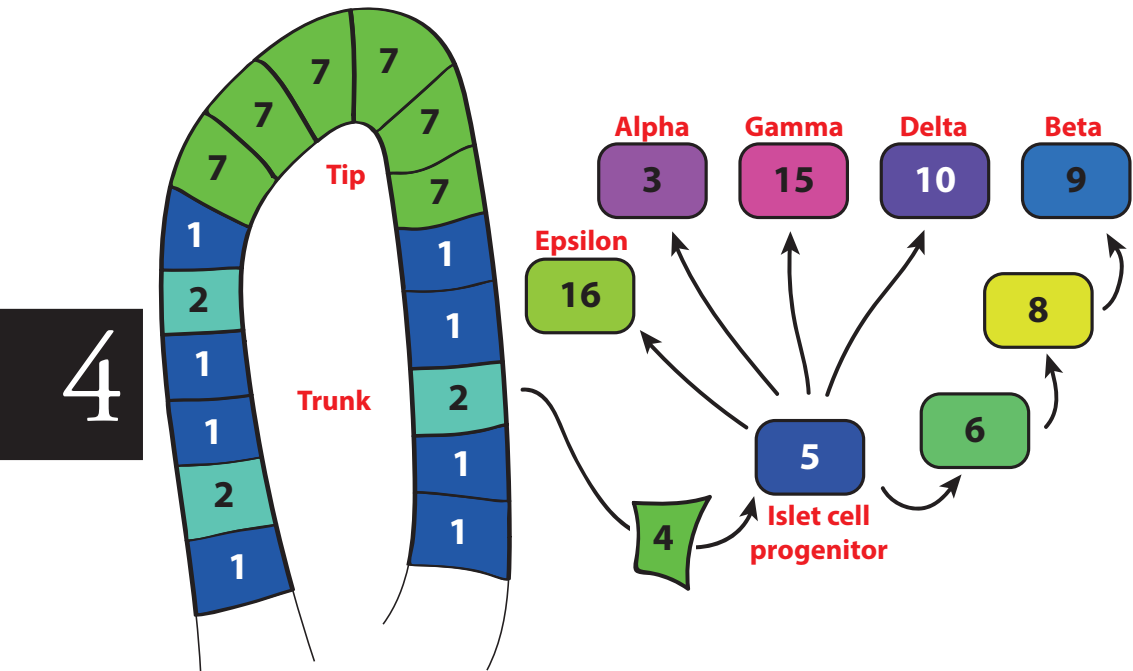
Figure 4: Comparison between clusters that are linked in the lineage tree allows for the identification of similarly and differentially expressed genes. a) MA plot for differential expression between clusters 2 and 4. b) Venn diagram showing overlap in differentially upregulated genes in clusters 2 and 4. A short list with familiar genes that overlap between clusters 2 and 4 is provided. c) MA-plot for differential expression between clusters 8 and cluster 9. d) Venn diagram showing overlap in differentially upregulated genes in clusters 8 and cluster 9. A short list with familiar genes that overlap between these clusters is provided. e) Most highly enriched GO terms related to the top 100 overlapping genes between clusters 2 and 4. f) Most highly enriched GO terms related to the top 100 overlapping genes between cluster 8 and cluster 9.



these genes were many genes that are known to be upregulated in endocrine progenitor cells, like *Neurod1*, *Nkx2.2*, *Pax4*, *Arx* and *Rfx6*. When using the top 100 overlapping genes between clusters 2 and 4 in a GO term analysis, we predominantly identified ontology terms related to pancreas and endocrine pancreas development, like *Pax4*, *Arx*, *Nkx2.2*, *Neurog3* and *Neurod1* (Figure 4e).

In a similar fashion, we identified differential gene expression of cells in beta cell cluster 8, and cluster 9 (Figure 4c) (supplemental data 4c). In cluster 8 we identified 692 differentially expressed genes, including *Glud1*, *Insm1*, *Isl1* and *Rbp4*. In cluster 9, a total of 77 genes were differentially expressed, including the more mature beta cell genes *Ins1* and *Chga*. After calculating differential expression between cluster 8

Figure 5: Graphical summary of single cell clustering analysis in the developing pancreas. All clusters present in the developing pancreas have been identified in our dataset, and different stages of endocrine differentiation are linked through a lineage tree. Using this tree to create a pseudo temporal differentiation map, dynamic behavior of genes involved in endocrine differentiation could be investigated.



and all other cells in the dataset, we found 536 gene differentially expressed. In cluster 9, 514 genes were differentially upregulated compared to all other cells in the dataset. When comparing the differentially expressed genes from clusters 8 and 9, 359 genes were upregulated in both clusters (figure 4d) (supplemental data 4d). The list of overlapping genes contained many genes known to be linked to beta cells and beta cell maturation, like *Ins1*, *Ins2*, *Chga*, *Iapp*, *Nkx6.1* and *Mafb*. GO term analysis of the top 100 genes from this list revealed hormone processing and insulin secretion terms to be strongly enriched (Figure 4f).

Discussion

The main results of our study show tissue heterogeneity and cellular maturation at a single cell level during the secondary transition of embryonic pancreatic development using a single cell transcriptomics approach. Using this protocol, we were able to identify the common embryonic pancreatic cell types, such as epithelial cells from the tip and trunk structures, endocrine progenitor populations and cells that have already committed to a specific endocrine cell fate. Cells from later time points in development showed a more defined transcriptome based on cellular entropy, which correlates with cells becoming gradually more mature during development. We were able to plot a lineage tree that defines the pseudo-temporal signature of endocrine pancreatic development for each of

the five endocrine cell types. From the epithelial trunk to *Neurog3* positive endocrine progenitors, to *Vim* and *Chgb* positive endocrine progenitors and finally a late common endocrine progenitor, before cells start differentiating towards alpha, beta, gamma, delta or epsilon cell types.

Enrichment for endocrine cell types was accomplished by specifically selecting GFP-positive cells during FACS sorting. While the GFP signal is reported to be very specifically expressed in adult beta cells [36], there are also many GFP-positive cells that express multiple hormones, and *Neurog3* can be detected in a subpopulation of GFP-positive cells during embryonic development [37]. We detected GFP expression in all endocrine cell types and in all the endocrine progenitors including *Neurog3* expressing cells. As such, the MIP-GFP mouse is a valuable asset to study endocrine development.

By looking at tissue heterogeneity on a single cell level, the dataset gave a unique view on endocrine differentiation. Three clusters of endocrine progenitor with specific characteristics could be identified. Cluster 2 contained the cells with strong *Neurog3* expression, the gene involved in the delamination of endocrine progenitors from the ductal lining [7, 8]. Cells in cluster 4 not only showed increased expression of typical endocrine genes such as *Pax4*, *Arx*, *Neurod1* and *Nkx2.2*, but also displayed differential expression of *Vim* and *Cldn4*. *Vim* is a well-known marker gene for mesenchymal cells [38] and *Cldn4* has been previously linked to Epithelial-to-Mesenchymal Transition (EMT) [39-41]. These cells most likely represent the mesenchymal interphase of endocrine progenitors after delamination before they form islets of Langerhans. Cells in cluster 5 expressed a large number of genes that have previously been linked to endocrine development and maturation of endocrine cells, like *Arx* [11, 42], *Isl1* [43, 44], *Irx2* [45], *Ttr* [46, 47], *Etv1* [48], *Pax6* [16, 49], *Neurod1* [14, 50] and *Mafb* [13,

51]. We identified cluster 5 using the StemID algorithm [29] as the most stem-like cluster regarding endocrine differentiation. This suggests that cluster 5 is the common point of departure for differentiation towards more mature endocrine cells, although additional steps to full maturation are likely to be necessary. Beta cells are known to go through a proliferation phase after birth, only fully maturing 3 weeks after birth when mice switch from high-fat to high-carb nutrients [52]. The dataset allows us to investigate signatures of progenitor cell differentiation towards a specific islet cell type.

In conclusion, we generated a comprehensive single cell transcriptome map of the developing pancreas. Our analysis reveals dynamics of tissue maturation over time, and how this affects tissue complexity, transcriptomic uniformity and gene expression.

Supplemental data can be downloaded through the following link: <https://dl.dropboxusercontent.com/u/1630051/Supplemental%20data%20chapter%204.zip>

References

- [1] Zhou Q, Law AC, Rajagopal J, Anderson WJ, Gray PA, Melton DA (2007) A multipotent progenitor domain guides pancreatic organogenesis. *Dev Cell* 13: 103-114
- [2] Pan FC, Bankaitis ED, Boyer D, et al. (2013) Spatiotemporal patterns of multipotentiality in *Ptf1a*-expressing cells during pancreas organogenesis and injury-induced facultative restoration. *Development* 140: 751-764
- [3] Magenheimer J, Klein AM, Stanger BZ, et al. (2011) *Ngn3*(+) endocrine progenitor cells control the fate and morphogenesis of pancreatic ductal epithelium. *Dev Biol* 359: 26-36
- [4] Shih HP, Kopp JL, Sandhu M, et al. (2012) A Notch-dependent molecular circuitry initiates pancreatic endocrine and ductal cell differentiation. *Development* 139: 2488-2499
- [5] Kim YH, Larsen HL, Rue P, Lemaire LA, Ferrer J, Grapin-Botton A (2015) Cell cycle-dependent differentiation dynamics balances growth and endocrine differentiation in the pancreas. *PLoS Biol* 13: e1002111

- [6] Gu G, Dubauskaite J, Melton DA (2002) Direct evidence for the pancreatic lineage: NGN3+ cells are islet progenitors and are distinct from duct progenitors. *Development* 129: 2447-2457
- [7] Seymour PA, Freude KK, Tran MN, et al. (2007) SOX9 is required for maintenance of the pancreatic progenitor cell pool. *Proc Natl Acad Sci U S A* 104: 1865-1870
- [8] Grapin-Botton A, Seymour PA, Gradwohl G (2015) Pairing-up SOX to kick-start beta cell genesis. *Diabetologia* 58: 859-861
- [9] Miyatsuka T, Kosaka Y, Kim H, German MS (2011) Neurogenin3 inhibits proliferation in endocrine progenitors by inducing Cdkn1a. *Proc Natl Acad Sci U S A* 108: 185-190
- [10] Collombat P, Hecksher-Sorensen J, Broccoli V, et al. (2005) The simultaneous loss of Arx and Pax4 genes promotes a somatostatin-producing cell fate specification at the expense of the alpha- and beta-cell lineages in the mouse endocrine pancreas. *Development* 132: 2969-2980
- [11] Collombat P, Mansouri A, Hecksher-Sorensen J, et al. (2003) Opposing actions of Arx and Pax4 in endocrine pancreas development. *Genes Dev* 17: 2591-2603
- [12] Sosa-Pineda B, Chowdhury K, Torres M, Oliver G, Gruss P (1997) The Pax4 gene is essential for differentiation of insulin-producing beta cells in the mammalian pancreas. *Nature* 386: 399-402
- [13] Artner I, Hang Y, Mazur M, et al. (2010) MafA and MafB regulate genes critical to beta-cells in a unique temporal manner. *Diabetes* 59: 2530-2539
- [14] Mastracci TL, Anderson KR, Papizan JB, Sussel L (2013) Regulation of Neurod1 contributes to the lineage potential of Neurogenin3+ endocrine precursor cells in the pancreas. *PLoS Genet* 9: e1003278
- [15] Schaffer AE, Taylor BL, Benthuyzen JR, et al. (2013) Nkx6.1 controls a gene regulatory network required for establishing and maintaining pancreatic Beta cell identity. *PLoS Genet* 9: e1003274
- [16] St-Onge L, Sosa-Pineda B, Chowdhury K, Mansouri A, Gruss P (1997) Pax6 is required for differentiation of glucagon-producing alpha-cells in mouse pancreas. *Nature* 387: 406-409
- [17] Kolodziejczyk AA, Kim JK, Svensson V, Marioni JC, Teichmann SA (2015) The technology and biology of single-cell RNA sequencing. *Mol Cell* 58: 610-620
- [18] Grun D, Lyubimova A, Kester L, et al. (2015) Single-cell messenger RNA sequencing reveals rare intestinal cell types. *Nature* 525: 251-255
- [19] Grun D, van Oudenaarden A (2015) Design and Analysis of Single-Cell Sequencing Experiments. *Cell* 163: 799-810
- [20] Hashimshony T, Senderovich N, Avital G, et al. (2016) CEL-Seq2: sensitive highly-multiplexed single-cell RNA-Seq. *Genome Biol* 17: 77
- [21] Kanter I, Kalisky T (2015) Single cell transcriptomics: methods and applications. *Front Oncol* 5: 53
- [22] Muraro MJ, Dharmadhikari G, Grun D, et al. (2016) A Single-Cell Transcriptome Atlas of the Human Pancreas. *Cell Syst*
- [23] Segerstolpe A, Palasantza A, Eliasson P, et al. (2016) Single-Cell Transcriptome Profiling of Human Pancreatic Islets in Health and Type 2 Diabetes. *Cell Metab* 24: 593-607
- [24] Baron M, Veres A, Wolock SL, et al. (2016) A Single-Cell Transcriptomic Map of the Human and Mouse Pancreas Reveals Inter- and Intra-cell Population Structure. *Cell Syst*
- [25] Wang YJ, Schug J, Won KJ, et al. (2016) Single-Cell Transcriptomics of the Human Endocrine Pancreas. *Diabetes* 65: 3028-3038
- [26] Li J, Klughammer J, Farlik M, et al. (2016) Single-cell transcriptomes reveal characteristic features of human pancreatic islet cell types. *EMBO Rep* 17: 178-187
- [27] Xin Y, Kim J, Okamoto H, et al. (2016) RNA Sequencing of Single Human Islet Cells Reveals Type 2 Diabetes Genes. *Cell Metab* 24: 608-615
- [28] Banerji CR, Miranda-Saavedra D, Severini S, et al. (2013) Cellular network entropy as the energy potential in Waddington's differentiation landscape. *Sci Rep* 3: 3039
- [29] Grun D, Muraro MJ, Boisset JC, et al. (2016) De Novo Prediction of Stem Cell Identity using Single-Cell Transcriptome Data. *Cell Stem Cell* 19: 266-277
- [30] Petzold KM, Spagnoli FM (2012) A system for ex vivo culturing of embryonic pancreas. *J Vis Exp*: e3979
- [31] Yao J, Wang XQ, Li YJ, et al. (2016) Long non-coding RNA MALAT1 regulates retinal neurodegeneration through CREB signaling. *EMBO Mol Med* 8: 346-362
- [32] Schild C, Hahn D, Schaller A, et al. (2014) Mitochondrial leucine tRNA level and PTCD1 are regulated in response to leucine starvation. *Amino Acids* 46: 1775-1783
- [33] Yoshikawa M, Fujii YR (2016) Human Ribosomal RNA-Derived Resident MicroRNAs as

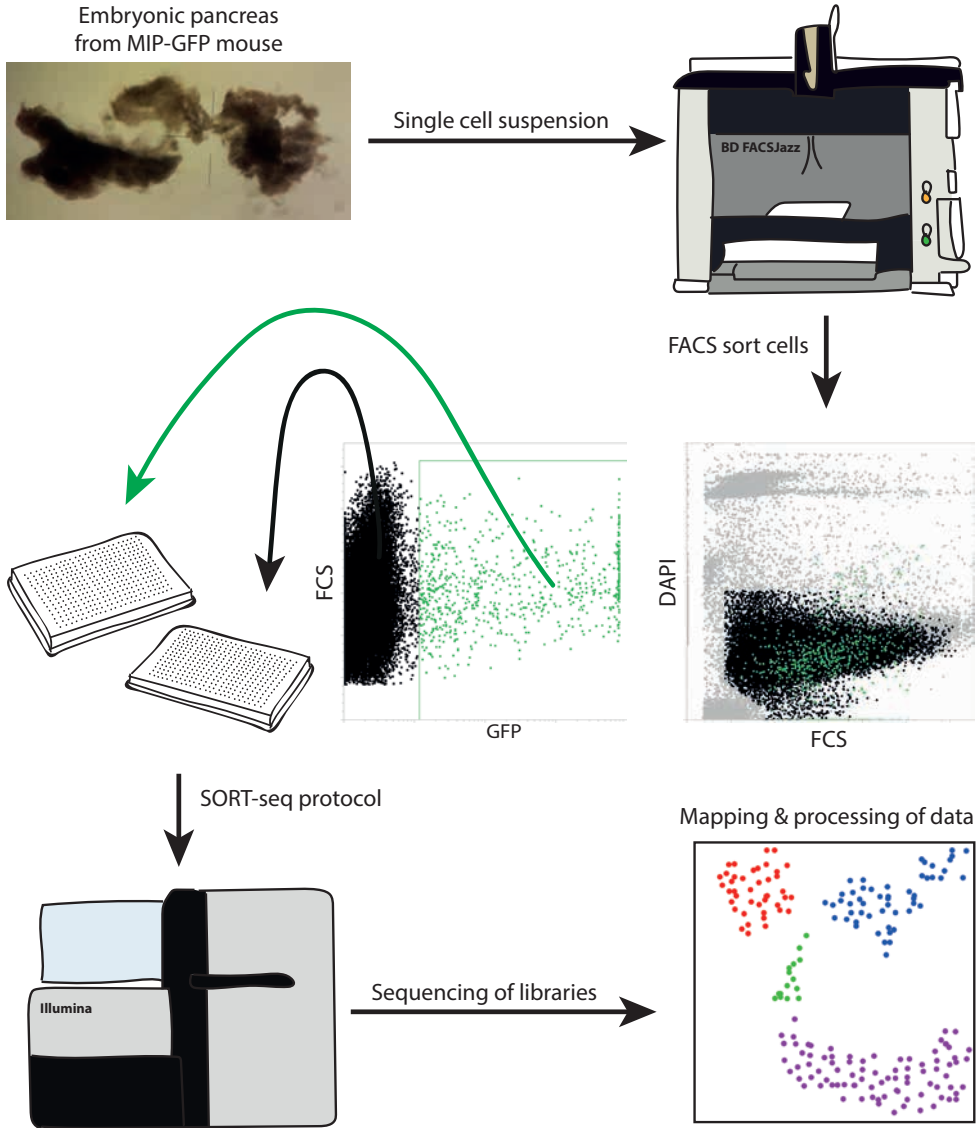
- the Transmitter of Information upon the Cytoplasmic Cancer Stress. *Biomed Res Int* 2016: 7562085
- [34] Anders S, Huber W (2010) Differential expression analysis for sequence count data. *Genome Biol* 11: R106
- [35] Banerji CR, Severini S, Caldas C, Teschendorff AE (2015) Intra-tumour signalling entropy determines clinical outcome in breast and lung cancer. *PLoS Comput Biol* 11: e1004115
- [36] Hara M, Wang X, Kawamura T, et al. (2003) Transgenic mice with green fluorescent protein-labeled pancreatic beta -cells. *Am J Physiol Endocrinol Metab* 284: E177-183
- [37] Katsuta H, Akashi T, Katsuta R, et al. (2010) Single pancreatic beta cells co-express multiple islet hormone genes in mice. *Diabetologia* 53: 128-138
- [38] Serrano-Gomez SJ, Maziveyi M, Alahari SK (2016) Regulation of epithelial-mesenchymal transition through epigenetic and post-translational modifications. *Mol Cancer* 15: 18
- [39] Lin X, Shang X, Manorek G, Howell SB (2013) Regulation of the Epithelial-Mesenchymal Transition by Claudin-3 and Claudin-4. *PLoS One* 8: e67496
- [40] Hu Y, Blair JD, Yuen RK, Robinson WP, von Daddelsen P (2015) Genome-wide DNA methylation identifies trophoblast invasion-related genes: Claudin-4 and Fucosyltransferase IV control mobility via altering matrix metalloproteinase activity. *Mol Hum Reprod* 21: 452-465
- [41] Ma X, Miao H, Jing B, et al. (2015) Claudin-4 controls the proliferation, apoptosis, migration and *in vivo* growth of MCF-7 breast cancer cells. *Oncol Rep* 34: 681-690
- [42] Gage BK, Asadi A, Baker RK, et al. (2015) The Role of ARX in Human Pancreatic Endocrine Specification. *PLoS One* 10: e0144100
- [43] Ahlgren U, Pfaff SL, Jessell TM, Edlund T, Edlund H (1997) Independent requirement for ISL1 in formation of pancreatic mesenchyme and islet cells. *Nature* 385: 257-260
- [44] Du A, Hunter CS, Murray J, et al. (2009) Islet-1 is required for the maturation, proliferation, and survival of the endocrine pancreas. *Diabetes* 58: 2059-2069
- [45] Petri A, Ahnfelt-Ronne J, Frederiksen KS, et al. (2006) The effect of neurogenin3 deficiency on pancreatic gene expression in embryonic mice. *J Mol Endocrinol* 37: 301-316
- [46] Refai E, Dekki N, Yang SN, et al. (2005) Transthyretin constitutes a functional component in pancreatic beta-cell stimulus-secretion coupling. *Proc Natl Acad Sci U S A* 102: 17020-17025
- [47] Su Y, Jono H, Misumi Y, et al. (2012) Novel function of transthyretin in pancreatic alpha cells. *FEBS Lett* 586: 4215-4222
- [48] Benitez CM, Qu K, Sugiyama T, et al. (2014) An integrated cell purification and genomics strategy reveals multiple regulators of pancreas development. *PLoS Genet* 10: e1004645
- [49] Ahmad Z, Rafeeq M, Collombat P, Mansouri A (2015) Pax6 Inactivation in the Adult Pancreas Reveals Ghrelin as Endocrine Cell Maturation Marker. *PLoS One* 10: e0144597
- [50] Itkin-Ansari P, Marcora E, Geron I, et al. (2005) NeuroD1 in the endocrine pancreas: localization and dual function as an activator and repressor. *Dev Dyn* 233: 946-953
- [51] Conrad E, Dai C, Spaeth J, et al. (2016) The MAFB transcription factor impacts islet alpha-cell function in rodents and represents a unique signature of primate islet beta-cells. *Am J Physiol Endocrinol Metab* 310: E91-E102
- [52] Jacovetti C, Matkovich SJ, Rodriguez-Trejo A, Guay C, Regazzi R (2015) Postnatal beta-cell maturation is associated with islet-specific microRNA changes induced by nutrient shifts at weaning. *Nat Commun* 6: 8084

Legends supplemental figures

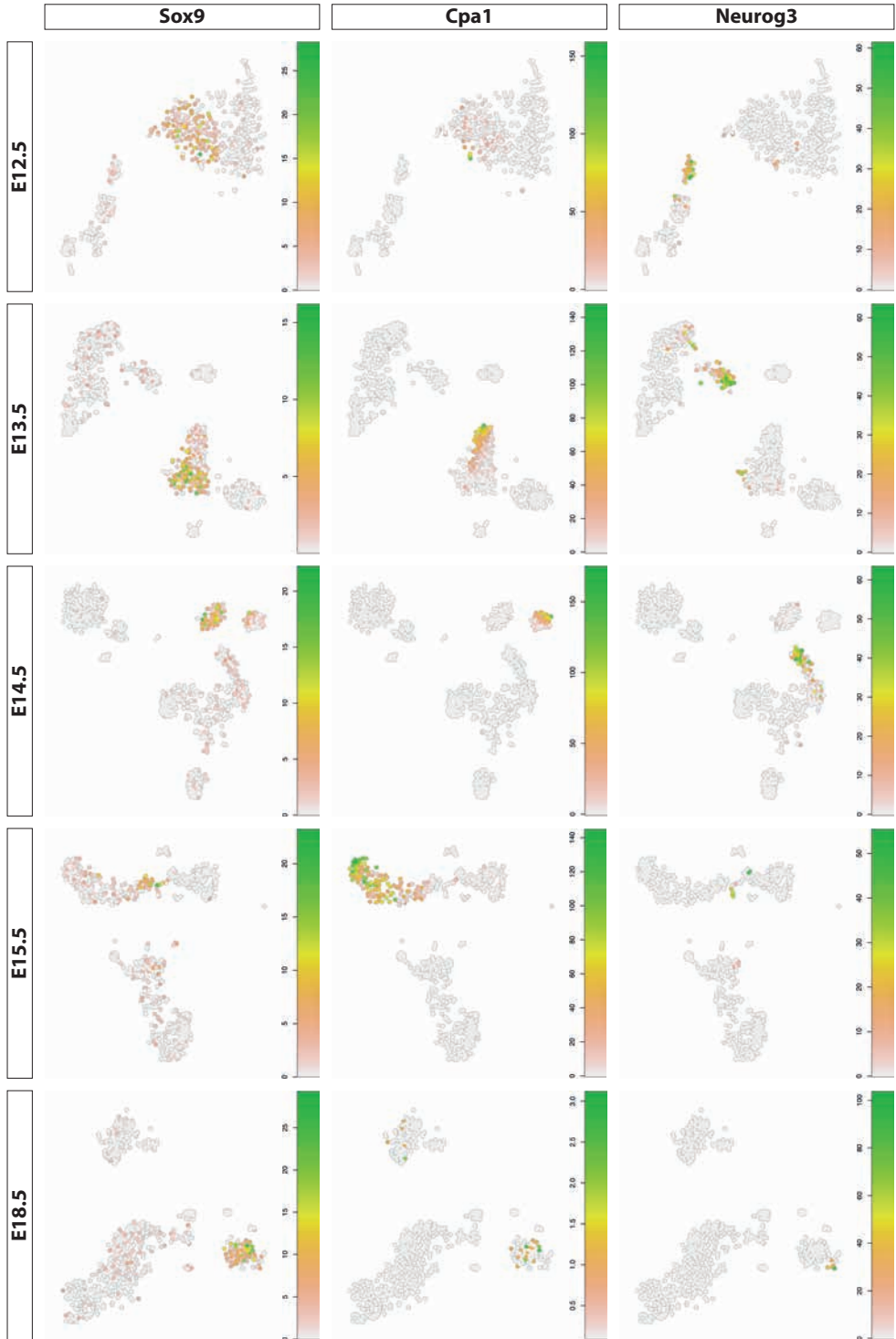
Supplemental Figure 1: Experimental overview of the procedure. Isolation of embryonic pancreas from embryos. Organs were digested into single cells and were then sorted on FACS. Live cells were characterized for GFP intensity. One plate of live cells and one plate of GFP-positive live cells was sorted per time point of development. Cells were processed using the SORT-seq protocol and sent out for sequencing. Sequenced data was mapped and clustered for data analysis.

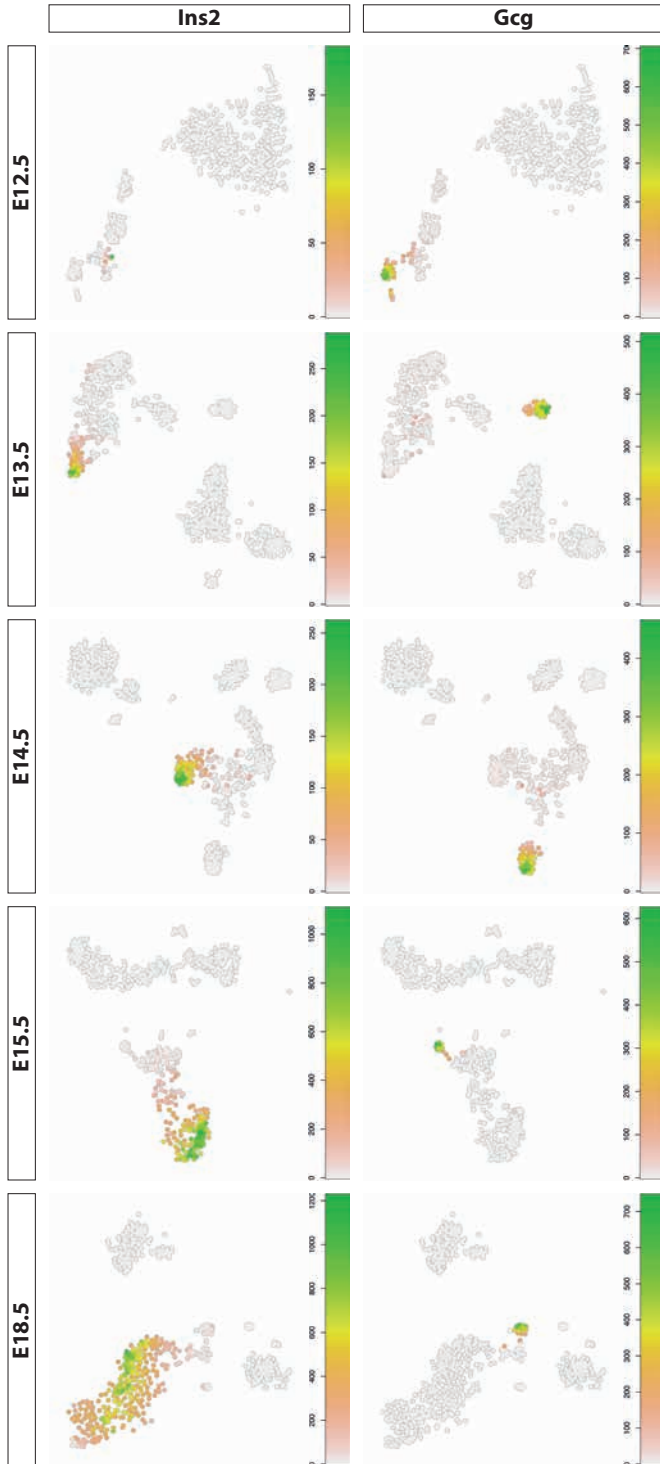
4

Supplemental Figure 2: TSNE mapping of data from individual time points reveals all pancreatic cell types to be present on every time point. Data from individual time points was clustered and TSNE maps that show expression for Sox9, Cpa1, Neurog3, Ins2 and Gcg show where tip cells, trunk cells, endocrine progenitors, beta cells and alpha cells are located in the dataset.



Supplemental figure 1





Supplemental
figure 2

4

Fabrication of three-dimensional bioplotting hydrogel scaffolds for islets of Langerhans transplantation

G. Marchioli^{1,5}, L. van Gorp², P.P. van Krieken², D. Stamatialis⁶, M. Engelse³,
C.A. van Blitterswijk⁵, M.B.J. Karperien¹, E. de Koning^{2,3}, J. Alblas⁴,
L. Moroni⁵ and A.A. van Apeldoorn¹

5

1: Department of Developmental BioEngineering, MIRA Institute for Biomedical Technology and Technical Medicine, Faculty of Science and Technology, University of Twente, Enschede, The Netherlands

2: Hubrecht Institute, Royal Netherlands Academy of Arts and Sciences and University Medical Centre Utrecht, Utrecht, The Netherlands

3: Department of Nephrology, Leiden University Medical Center, Leiden, The Netherlands

4: Department of Orthopedics, University Medical Center Utrecht, Utrecht, The Netherlands

5: Department of Tissue Regeneration, MIRA Institute for Biomedical Technology and Technical Medicine, Faculty of Science and Technology, University of Twente, Enschede, The Netherlands

6: Department of Biomaterials Science and Technology, MIRA institute for Biomedical Technology and Technical Medicine, Faculty of Science and Technology, University of Twente, Enschede, The Netherlands

Published in *Biofabrication*. 2015 May 28;7(2):025009.

Abstract

In clinical islet transplantation, allogeneic islets of Langerhans are transplanted into the portal vein of patients with type 1 diabetes, enabling the restoration of normoglycemia. After intra-hepatic transplantation several factors are involved in the decay in islet mass and function mainly caused by an immediate blood mediated inflammatory response, lack of vascularization, and allo- and autoimmunity. Bioengineered scaffolds can potentially provide an alternative extra-hepatic transplantation site for islets by improving nutrient diffusion and blood supply to the scaffold. This would ultimately result in enhanced islet viability and functionality compared to conventional intra portal transplantation. In this regard, the biomaterial choice, the three-dimensional (3D) shape and scaffold porosity are key parameters for an optimal construct design and, ultimately, transplantation outcome. We used 3D biplotting for the fabrication of a 3D alginate-based porous scaffold as an extra-hepatic islet delivery system. In 3D-plotted alginate scaffolds the surface to volume ratio, and thus oxygen and nutrient transport, is increased compared to conventional bulk hydrogels. Several alginate mixtures have been tested for INS1E β -cell viability. Alginate/gelatin mixtures resulted in high plotting performances, and satisfactory handling properties. INS1E β -cells, human and mouse islets were successfully embedded in 3D-plotted constructs without affecting their morphology and viability, while preventing their aggregation. 3D plotted scaffolds could help in creating an alternative extra-hepatic transplantation site. In contrast to microcapsule embedding, in 3D plotted scaffold islets are confined in one location and blood vessels can grow into the pores of the construct, in closer contact to the embedded tissue. Once revascularization has occurred, the functionality is fully restored upon degradation of the scaffold.

Introduction

Islet transplantation is usually performed in a selected group of patients with type 1 diabetes with unstable glycemia characterized by recurrent low blood glucose levels and hypoglycemia unawareness [1, 2]. However, the efficiency of this procedure is limited: it is estimated that a large proportion of the transplanted islets is destroyed shortly after transplantation [1, 2]. In addition, long term survival is not optimal as less than 50% of the patients remain insulin independent after a 5 years follow-up [3]. Several reasons are relevant for the adverse outcome of islet transplantation, like: (i) the instant blood mediated inflammatory reaction caused by complement activation and innate immune response [4]; (ii) the disruption of cell – extracellular matrix interaction during the isolation phase from the donor pancreas [5–7]; (iii) the loss of islet vasculature, resulting in a reduced nutrient and oxygen supply after transplantation [8, 9]; (iv) toxins and drugs which are commonly processed in the liver and further cause islet mass decay [10, 11]; (v) alloimmune response; and (vi) recurrent autoimmunity. It is likely that a combination of all these factors is responsible for the reduced graft survival in the long term.

The creation of an extra-hepatic transplantation site, aided by the use of bioengineered implants in which islets are combined with scaffolds, could help overcoming the aforementioned disadvantages. Scaffolds can provide a favorable and protective environment for islets of Langerhans, including the possibility of designing the shape of the construct and functionalizing the material to specifically match the requirements of the embedded cells. Recently, a number of polymeric biomaterials have been used for the creation of porous islet-containing implants. Salt leached porous scaffolds of poly(DL-lactide-co-glycolide) acid (PLGA) [12–14], plotted PLGA scaffolds [15], polydimethylsiloxane salt-leached scaffolds [16, 17] and thermoformed microwell scaffolds of

poly(ethylene oxide terephthalate)–poly(butylene terephthalate) (PEOT/PBT) block copolymer [18] are examples of the variety of materials and scaffold shapes used for extra-hepatic islet entrapment and transplantation. Although successful in small animal models, the main disadvantage of such tissue-engineered constructs is the difficulty in scaling them up to a clinically relevant size, containing a therapeutic dosage of islets, without compromising nutrient and oxygen diffusion.

A different approach has been tried by encapsulating islets in hydrogels. Hydrogels are particularly attractive for cell encapsulation and have been used in a variety of applications for soft tissue engineering [19]. Hydrogel encapsulation can be used for immune-protection by preventing contact of the encapsulated cells with the host immune cells. Their mechanical properties and water content closely match the ones of soft tissues in the body [20]. Furthermore, hydrogels can be easily mixed or covalently functionalized with extracellular matrix proteins, peptides and growth factors [21–23]. Among different hydrogel formulations, alginate is a commonly used material for islet encapsulation and has been widely used for immunoprotection of allogeneic transplanted islets from the attack of antibodies and cytokines after transplantation [3, 24, 25]. Islets are either embedded in small alginate beads or mixed in bulk alginate hydrogels, and injected subcutaneously or into the peritoneal cavity [3, 26]. A study by Ludwig et al reports the fabrication of an oxygenated and immunoprotective alginate-based macro-chamber for islets transplantation in a male patient [27]. In all these cases, the mesh size of the surrounding alginate hydrogel has to be carefully tuned to assure optimal insulin and nutrient diffusion to the embedded islet. At the same time, the hydrogel mesh needs to be tight enough to prevent antibodies and cytokines to interact with the embedded islets [24]. The disadvantage of encapsulation is that the embedded islets cannot be regarded as a

single construct but more as a multitude of self-standing micro organs, which are difficult to implant and be retrieved all at once, if needed.

We studied three-dimensional (3D) bioplotting for the fabrication of an alginate-based, islet-laden 3D construct. Islets of Langerhans are mixed in the precursor alginate solution and this is plotted in a predefined 3D fashion. Islets are embedded in the hydrogel strands constituting the construct. Such construct can combine the advantages of a tailor made shape and porosity with the beneficial properties of hydrogels in an innovative construct for islet of Langerhans delivery. In contrast to what happens with other constructs or with islet encapsulation in beads, one of the main advantages of this approach is that this type of construct can host a clinically relevant amount of islets in a defined tridimensional, porous construct. In addition, the fabrication of a cell-laden alginate construct can also combine the advantages of a porous hydrogel scaffold with a defined 3D geometry with the immunoprotection properties provided by alginate embedding.

A variety of different techniques has already been developed to tackle the problem of 3D cell-laden hydrogel constructs for several other tissues. Strategies as 3D plotting and inkjet printing are the most widely used and have been applied to the regeneration of different tissues [28, 29]. 3D deposition of cell-laden hydrogels has been previously investigated for hepatic tissue regeneration [30] and for bone tissue engineering applications [31], showing that a plotted porous structure can be beneficial to enhance cell viability and metabolic activity compared to bulk constructs. 3D hydrogel deposition has been also applied to the fabrication of aortic valves [32], micro-vessels and vascularized tissue fabrication [33], for cell transfection strategies [34] and for cell culture of neural stem cells [35], fibroblasts and keratinocytes [36, 37].

The main advantage of plotting is, therefore, the possibility of fabricating large hydrogel constructs, capable of containing a clinically relevant amount of islets, with a porous structure that might improve oxygen and nutrient supply to the embedded cells. In this study, plotting of cell-laden hydrogels constructs is extended to large cell aggregates of 50–300 μm in diameter, such as islets of Langerhans. We hypothesized that islets embedded in a porous plotted structure could have a better glucose and insulin exchange, compared to bulk hydrogels. We show that the material choice and construct shape are of crucial importance in defining the viability and functionality of the embedded cells.

Materials and methods

INS1E cell culture and islet culture

INS1E β -cell line, derived from rat insulinoma, were kindly provided by Dr Guigas, LUMC, Leiden, The Netherlands and Dr Maechler, University Medical Center, Geneva, Switzerland. Cells were cultured in RPMI 1640 (Gibco) supplemented with 5% (v/v) FBS (Lonza), 1% pen/strep (Gibco), 1% sodium pyruvate (Sigma) and 1% HEPES 1 M (Invitrogen). For cell expansion, β -mercaptoethanol (Invitrogen) was added fresh to the culture to a final concentration of 1 $\mu\text{l ml}^{-1}$ medium. Medium was refreshed every 2–3 days.

Human cadaveric donor pancreata were procured via a multi-organ donation program. Isolated human islets were used in this study if they could not be used for clinical transplantation, according to the national law, and if research consent was present. Human islets were kindly provided by the LUMC Leiden and cultured in CMRL medium (Cellgro) supplemented with 10% FBS and 1% pen/strep according to Fraga et al [38]. Mouse islets were isolated from double heterozygous crossbreed mice between Tg(Ins1-eGFP), Jackson Laboratory strain #006864, and B6(CAG- DsRed*MST),

Jackson Laboratory strain #005441 and kindly provided by Hubrecht Institute Utrecht. Mouse islets were cultured in ultra-low attachment plates with RPMI 1640 (Gibco) supplemented with 10% FBS and 1% pen/strep.

Preparation of alginate mixtures and cell-containing bulk hydrogels

Alginate powder (Sigma) was sterilized by 5 min exposure to UV light (Labino Duo spotlight) with an intensity of 45 mW cm^{-2} at 38 cm and dissolved at a 4% w/v concentration in PBS (PAA). Pre-crosslinked alginate was prepared by mixing a 5.3% w/v alginate solution with a 102 mM CaCl_2 solution (Sigma) in HEPES 10 mM in a 3:1 volume ratio, resulting in a final alginate concentration of 4% w/v. Two syringes connected with a T-shaped connector were used to mix the calcium chloride solution with alginate and after mixing this precursor solution was used for plotting. After scaffold preparation the resulting construct was definitively crosslinked by using 102 mM CaCl_2 solution. Similarly, an alginate 4%/Matrigel 25% w/v mixture was also prepared, by pipetting. Additionally, alginate 4%/gelatin 5% w/v and alginate 4%/hyaluronic acid 0.5% w/v mixtures were prepared by dissolving 0.8 g of alginate in 20 ml of a 5% w/v bovine gelatin solution (gelatin type B, Sigma), or in 0.5% w/v hyaluronic acid solution (Fluka) at 37°. Gelatin and hyaluronic acid solution were filter sterilized using an 0.22 μm filter unit (Millipore) attached to a 10 ml syringe (Norm-Ject HSW). All the different alginate mixtures are summarized in table 1. Ultrapure alginate was kindly provided by De Vos (UMCG Groningen) and used at a concentration of 2% w/v in PBS after purification according to De Vos et al [26].

Viscosity of the different alginate compositions was quantified using an Anton Paar Physica MCR 301 rheometer with flat plate geometry (20 mm diameter, 1 mm gap) (supplemental figure 3). Shear rate ranged from 0.01 to 100 s^{-1} . Given the non-Newtonian behavior

Chapter 5: Fabrication of three-dimensional bioplotted hydrogel scaffolds for islets of Langerhans transplantation

Table 1: Parameters used for plotting different alginate mixtures, number of layers that could be plotted and viscosity values for each alginate composition.

	Needle Ø (mm)	F_{xy} speed (mm min ⁻¹)	Spindle speed (mm min ⁻¹)	Layer thickness (mm)	Layer number	Viscosity (Pa s ⁻¹)
Alginate	0.41	1000	1.75	0.20	10	11.2 ± 0.85
Pre-crosslinked alginate	0.41	500	1.75	0.20	15	2923.33 ± 958.45
Alginate 4%/Gelatin 5%	0.41	1100	1.75	0.10	17	163.67 ± 26.72
Alginate 4%/Hyaluronic acid 0.5%	0.41	1500	1.50	0.10	7	9.13 ± 1.48
Alginate 4%/Matrigel 25%	0.41	1250	2.00	0.10	10	25.8 ± 1.51

of alginate solutions, viscosity measurement at a low shear rate of 0.031 s⁻¹ was selected.

When islets or cells were added to the different gel mixtures, 10 × 10⁶ cells/ml were resuspended in the less viscous component of the mixture (CaCl₂, gelatin, hyaluronic acid solution or in Matrigel) to obtain a homogeneously dispersed cell suspension and mixed with a 5.3% w/v alginate solution, in a 1:3 ratio, to a final 4% w/v alginate concentration. Both plotted and bulk constructs (0.3 ml) were crosslinked with a 102 mM CaCl₂ in 10 mM HEPES solution for 15 min and then washed for 5 min with tris buffered saline (TBS) [31]. Other crosslinking solutions used in this study were 20 mM CaCl₂ in 10 mM HEPES and 20 mM BaCl₂ (Sigma) in 10 mM HEPES to study the effect of crosslinking strength and ion on islet activity.

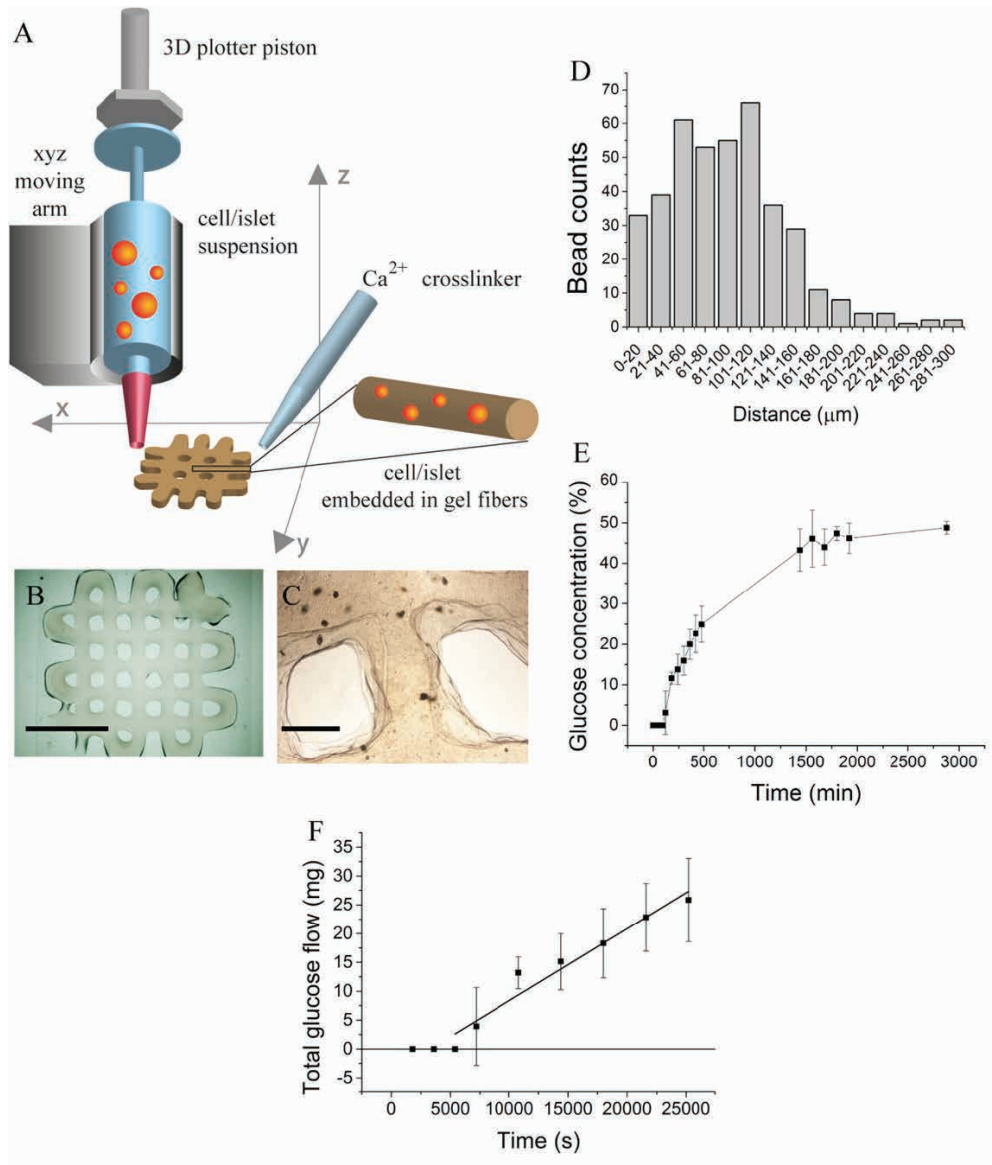
3D hydrogel plotting

Constructs were plotted using a 3D bioplotter (SysENG, Germany). Briefly, a cell

suspension in hydrogel is laden into a syringe. The hydrogel is then extruded from the syringe in a controlled layer by layer fashion by a XYZ moving arm, which deposits the material into a predefined 3D structure according to a computer aided design model (CAD-model).

Plotting settings were set accordingly to the viscosity of the material. Plotting speed ranged from 750 to 1100 mm min⁻¹, needle diameter ranged from 0.41 to 0.2 mm. Alginate 4%/gelatin 5% w/v 2 × 2 cm construct was plotted with a XY speed of 750 mm min⁻¹, a spindle speed of 1.75 mm min⁻¹ and a needle diameter of 0.41 mm for a total of 17 layers. A 0.41 mm needle diameter was selected to be compatible with an islet size, which ranges between 50 and 300 μm. Plotting settings for the other compositions are reported in detail in table 1. The spacing between each individual strand of the porous constructs was set on 3 mm to assure open pores in the constructs, whereas solid constructs were plotted with an offset of 1.16 mm to avoid strand superposition in following layers and create a compact structure. Control bulk samples

Figure 1: (A) 3D printing scheme concept cartoon. (B) alginate 4%/ gelatin 5% 2 × 2 cm plotted scaffold: the pore diameter is 1.88 ± 0.18 mm and the strand thickness 1.55 ± 0.13 mm (scale bar 1 cm). (C) Image of plotted islets in the construct (scale bar 1 mm). (D) Distance islet-pore (μm), polystyrene beads were used as a model for islets distribution in the scaffold. (E) Percentage of glucose diffused through the gel from a 50 ml donor compartment to the acceptor compartment of a custom made diffusion chamber. Equilibrium is reached after circa 24 h (1440 min). (F) Total flow of glucose through the gel layer in time. There is a significant time lag before the system reaches the steady state. Based on the simplified Fick's law of diffusion (see materials and methods) the diffusion coefficient can be estimated.



5

were pre- pared by pipetting the same volume of hydrogel pre- cursor on a petri dish, and they were then immediately crosslinked.

3D plotted construct characterization

Blue colored polystyrene beads of 100 μm diameter (Phosphorex) were used as a model for islets and embedded in a plotted alginate 4%/gelatin 5% w/v construct (referred from now on as alginate/gelatin) in a concentration of 45'000 beads/ml. Constructs were plotted and pictures were taken with a stereomicroscope (Nikon SMZ-10 A, equipped with Qcaputre software). The bead/pore distance of circa 400 beads (20 images) was measured with Image J.

Glucose diffusion measurement

An 80 μl bulk alginate/gelatin hydrogel was prepared as previously described and placed in the rubber insert of a custom made chamber to measure glucose diffusion through the gel. The 80 μl hydrogel volume resulted in a gel thickness of 1 mm. The device is composed of two chambers. One of the compartments has been loaded with 50 ml of 12 mM glucose, 1% pen/strep 102 mM CaCl₂ in 10 mM HEPES; the other compartment was loaded with the same solution, without glucose. Samples were taken from both compartments at defined time points and the concentration of glucose in time was measured using a VITROSS DT60 II chemistry system (Ortho-Clinical diagnostics).

The 'lag time' method was used for the calculation of glucose diffusion coefficient ($\text{cm}^2 \text{s}^{-1}$) in alginate 4%/gelatin 5% (w/v) gel according to the method described by Han-noun and Stephanopoulos [39]. This method is based on Fick's law of diffusion, with constant diffusion coefficient. Total glucose flux through the gel was calculated and plotted as a function of time. A constant flow/time ratio, represented by the linear part of the graph, is reached only after a certain period of time, and this period of time is referred to as the lag time. The lag time

is the time a glucose molecule needs to diffuse through the whole thickness of the gel (l), before the glucose flux becomes constant in time. The lag time is calculated as the intercept of the linear function on the x axis and it is given by $t = l^2 / 6D$, where D is the diffusion coefficient, t the time and l the thickness of the gel layer. The diffusion coefficient can be then calculated as $D = l^2/6t$. The lag time corresponds to the time difference in which the diffusing molecule, glucose in this case, starts penetrating the hydrogel and the time at which the glucose flow rate into the acceptor chamber reaches a steady state [40].

Cell viability and metabolic activity

Cell viability was measured with a live/dead viability assay (Invitrogen) according to the provided protocol and images were taken with a fluorescence microscope (Nikon Eclipse E600). Before imaging, hydrogels were cut in half using a scalpel. The resulting slice had a thickness of about 850 μm , the plotted morphology was maintained and four pictures per scaffold, in a random area, were analyzed to score the percentage of live cells to total cells.

To measure cell metabolism in the three different constructs shapes, medium samples of 3×10^6 cells / construct cultured in bulk, plotted porous or plotted solid hydrogels were taken every second day and glucose and lactate concentrations in the medium were measured with a VITROSS DT60 II chemistry system (Ortho-Clinical diagnostics). After every analysis, medium was refreshed for further culturing.

Lentiviral transduction of human islets

Islets were overnight transduced by incubating them in 3 ml DMEM medium containing 1% pen/strep, 10% FBS, 8 ng mL⁻¹ polybrene (Sigma-Aldrich), and pRRL-CMV-GFP virus (1000 ng ml⁻¹). After transduction, islets were extensively washed in PBS and cultured again in RPMI supplemented with 10% FBS and 1%

pen/strep. Circa 500 of the brightest transduced islets were selected and used for plotting and for bulk hydrogel embedding.

Islet plotting and imaging

1000 IEQ of transduced human islets were mixed with alginate 4%/ gelatin 5% w/v and alginate 4% w/v. Islets were plotted according to the procedure or embedded in bulk hydrogel and imaged at day 1, 4 and 7 with a Leica TCS SP5 AOBS two-photon microscope. The microscope was equipped with a 20x dry objective, NA 0.40. The laser lines used were 488 nm for GFP and the emission filter used was a 495–540 nm. Mouse islets were similarly plotted and imaged using a 488 nm excitation line/495–540 nm emission filter for GFP and a 561 nm excitation line/570–620 nm filter for DsRed. Non-transduced islets were imaged in the bright field mode.

INS1E cell sample preparation for glucose induced insulin secretion test (GIIST)

Glucose responsiveness of INS1E cells embedded in alginate 4%/gelatin 5% w/v bulk hydrogel was compared to INS1E cells cultured on tissue culture plastic. 3×10^6 cells/sample were seeded in a T25 flask and an equal amount of cells was embedded in 0.1 ml of bulk hydrogel. Cells were mixed with alginate 4%/ gelatin 5% w/v solution at a density of 30×10^6 cells/ml and crosslinked with 102 mM CaCl_2 in 10 mM HEPES for 15 min. Cell laden hydrogels were also crosslinked with 20 mM CaCl_2 in 10 mM HEPES for 20 and 30 min, and with 20 mM BaCl_2 in 10 mM HEPES for 10 min. The previous conditions were also compared to INS1E embedded in 1% w/v agarose (Invitrogen).

Islet sample preparation for GIIST Twenty five islets per sample were embedded in 0.1 ml of alginate 4%/ gelatin 5% w/v and crosslinked with 102 mM CaCl_2 in 10 mM HEPES for 5 or 15 min, with CaCl_2 20 mM in 10 mM

HEPES for 20 min or with BaCl_2 20 mM in 10 mM HEPES for 10 min. The same number of islets were also embedded in 2% w/v ultrapure alginate and crosslinked for 15 min with 102 mM CaCl_2 in HEPES. Free floating islets in ultra- low attachment plate were used as control. After gel crosslinking, all the samples were washed with TBS and cultured in CMRL medium. At day one a GIIST was performed. After the function test, the alginate hydrogels (102 mM CaCl_2 crosslinking for 15 min) were solubilized by incubating them in 1ml of dissolving buffer containing 0.15 M NaCl (Merck), 30 mM disodium-ethylenediamine tetra acetic acid (EDTA disodium salt) (Calbiochem) and 55 mM sodium citrate (Sigma-Aldrich) [41] for 40 min. Islets were retrieved from the gel and after 2 days the function test was repeated again comparing free floating untreated islets, free floating islets treated with the dissolving buffer and islets previously embedded in the gel and treated with the dissolving buffer for their retrieval.

For testing islet functionality in the plotted constructs, the plotted scaffold and the bulk samples were prepared with circa 125 islets/sample and crosslinked with a 102 mM CaCl_2 solution in 10 mM HEPES for 15 min, followed by a wash with TBS. Both bulk and plotted constructs final volume was 0.3 μl . Insulin secretion test was performed as following and compared with the same amount of free floating islets.

Islet and INS1E GIIST

Islet functionality was tested as reported elsewhere [18]. The GIIST protocol was slightly modified for testing INS1E functionality. Briefly, islets were pre-incubated in Krebs-Ringer low glucose buffer (1.67 mM glucose) for 1.5 h while INS1E samples were incubated for two hours in RPMI medium without glucose (Invitrogen). Samples were then exposed for 1.5 h in case of islets, or for 45 min in case of INS1E, to a low glucose Krebs-Ringer buffer containing 1.67 mM glucose. Subsequently, samples were incubated for an equal period of

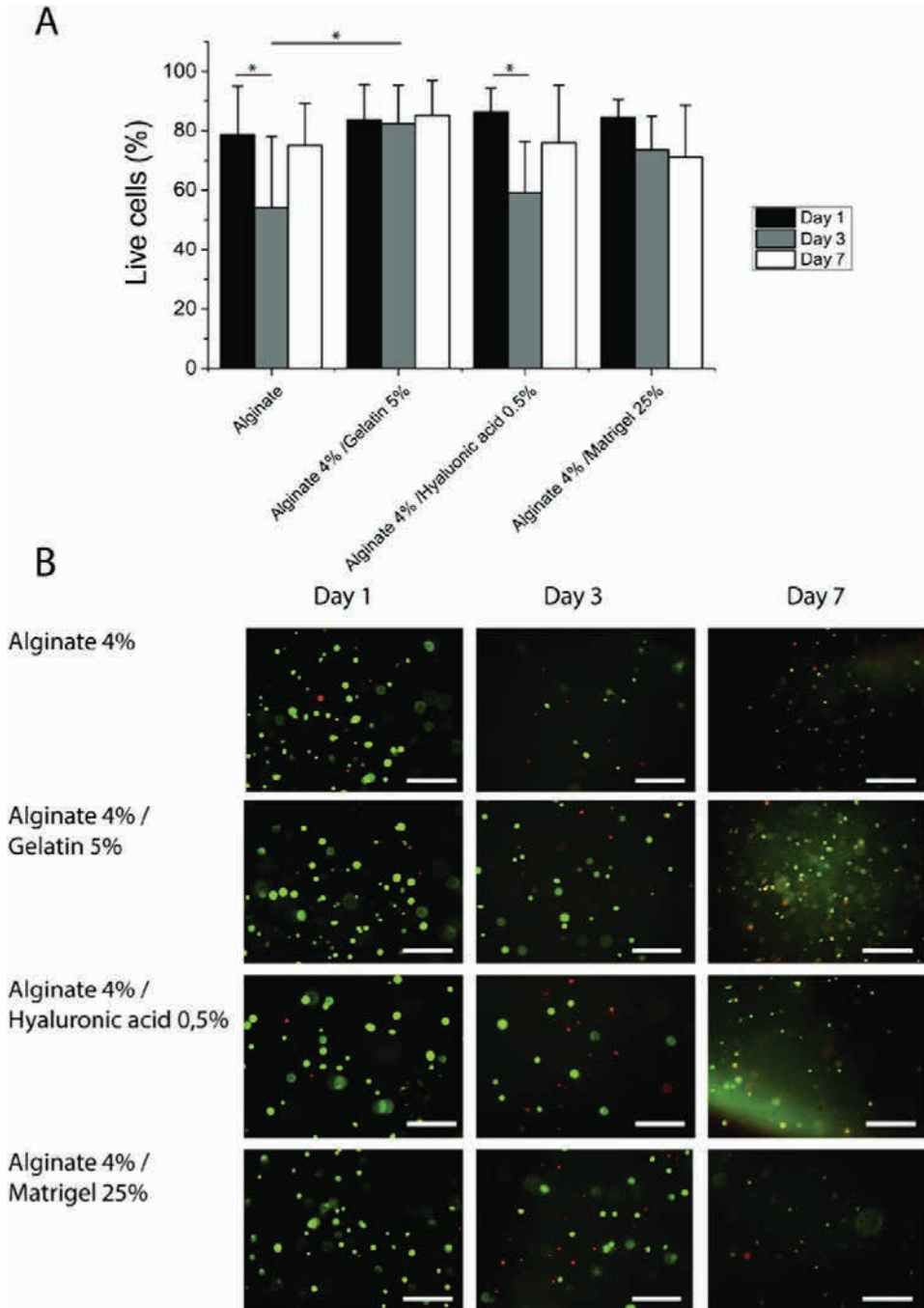


Figure 2: (A) Viability of encapsulated INS1E cells in 4% w/v alginate gel, alginate 4% w/v/gelatin 5% w/v, alginate 4% w/v/hyaluronic acid 0.5% w/v, and alginate 4% w/v /Matrigel 25% w/v. (B) Live/dead pictures of INS1E cells in the different alginate compositions at days 1, 3 and 7 (scale bar 200 μm).

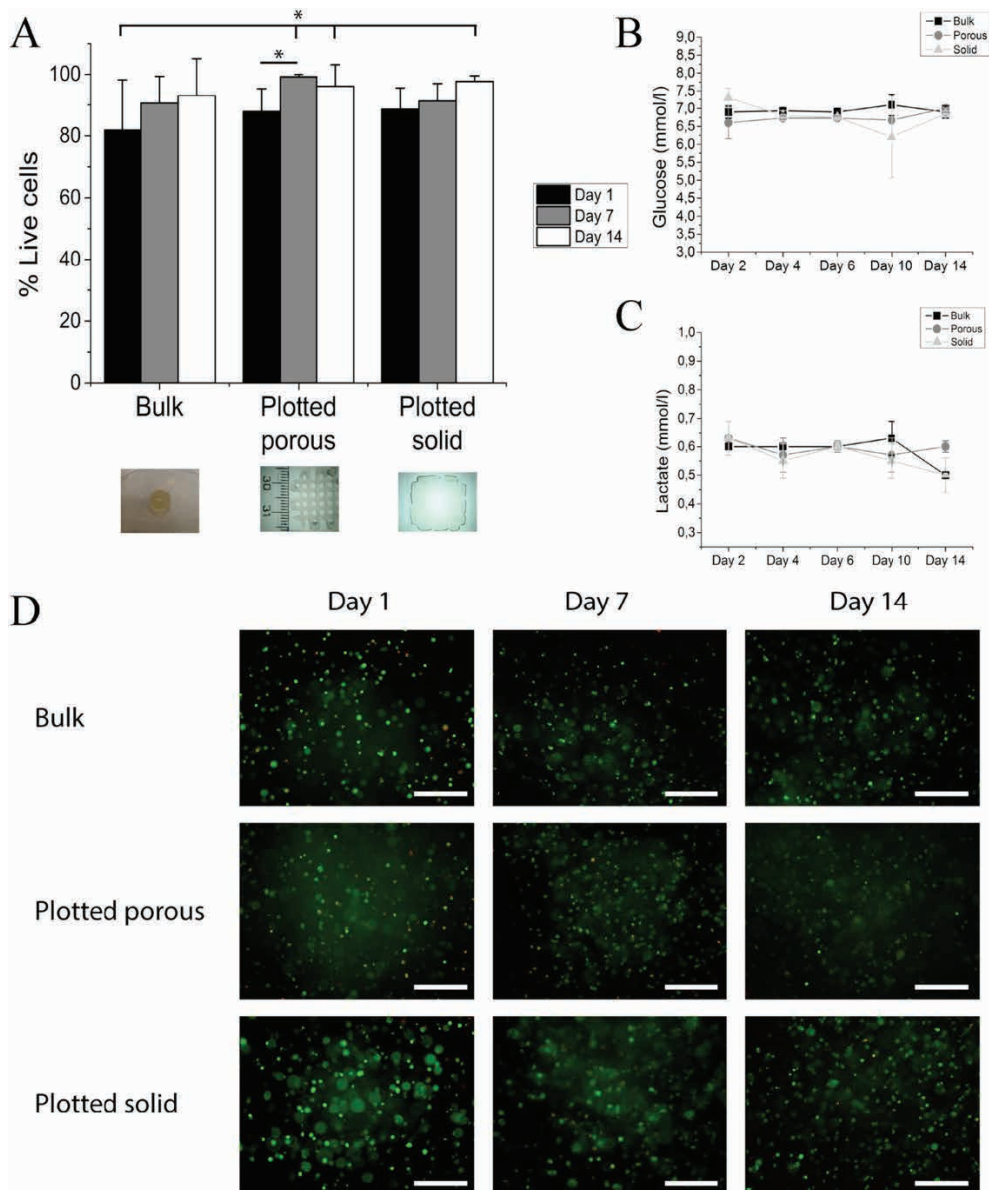


Figure 3: (A) INS1E viability in bulk constructs, plotted porous and plotted solid constructs. (B) and (C) metabolic activity of INS1E cells embedded in constructs with different geometries measured as glucose (B) and lactate (C) concentrations in the culture medium. Viability, glucose consumption and lactate production are not influenced by the plotting process or construct shape. (D) Live/dead images of the INS1E cells in the different constructs at day 1, day 7 and day 14 (scale bar 200 μm).

time respectively in high glucose medium (16.7 mM glucose) followed by a last incubation in low glucose medium (1.67 mM). Samples were collected at the end of each incubation step for further analysis. Released insulin was quantified by using an ELISA kit (Mercodia). Results were presented as low–high–low profiles, both as actual amount of insulin secreted (mU l^{-1}) and as stimulation index, which is the ratio of insulin secretion between the high and low glucose condition.

Statistical analysis

Experiments were performed in triplicate. All the quantitative data are expressed as mean \pm standard deviation. Data were analyzed using a one-way ANOVA, followed by Bonferroni post-hoc test. The analysis was performed using IBM SPSS statistic 20 software. Significant difference between groups is indicated with * ($p < 0.05$).

Implantation and *in vivo* imaging

Circa 500 of the brightest transduced islets were plotted in the scaffold following the usual procedure. A 1 cm circular section of the plotted scaffold was punched out and glued on one side of a pre-sterilized abdominal imaging window by using H-butyl-cyanoacrylate glue. Two other equal sections of the same scaffold were used as a subcutaneously implanted control and as an *in vitro* control, respectively. The window was implanted on the back of NSG mice (Jackson Laboratory), the second part of the scaffold was implanted subcutaneously as a control.

The islet graft was monitored at day 1, 4 and 7 (figure 8). Intravital imaging was performed by placing the mouse in a custom designed imaging box. The imaging window was fixed in a ring-opening on the bottom part of the box. The box was also equipped with a nose cone for anesthesia, air ventilation, and a MouseOx system (Starr Lifescience Corp) to monitor vital signs. The imaging was performed keeping the mouse at a controlled temperature

of 32 °C. A Leica TCS SP5 confocal microscope was used and equipped with a 20x dry, NA 0.40 objective, a 488 nm laser line for GFP and a 495–540 nm emission filter. After seven days the mouse was sacrificed with isoflurane anesthesia and the graft was explanted and processed for histology.

Explants were fixed with 4% w/v paraformaldehyde, dehydrated, and embedded in paraffin. Sections 4–8 μm thick were cut and stained with hematoxylin and eosin. Alternatively, immunostainings for insulin (Dako; 1:200) and glucagon (Vector Laboratories; 1:100) were performed. Images were acquired on a Leica TCS SPE with a 20x oil-immersion objective.

Results

Scaffold fabrication by 3D plotting and characterization

Different alginate-extracellular matrix components blends have been successfully plotted. As shown in table 1, only some of these blends had sufficient mechanical properties to allow plotting and handling of the final construct. The plotting speed and spindle speed were adjusted according to the viscosity of the material, being slower for highly viscous materials (table 1). Among all the other composition tested, alginate 4%/gelatin 5% (w/v) composition was found to be the most suitable for scaffold plotting, because of the high viscosity of the blend compared to all the other materials tested. This assured better plotting performances in terms of handling and stability of multilayered cell-laden constructs (table 1). This mixture was selected for future experimentation. Handling and plotting of the alginate/gelatin mixture was further improved by the partial gelation of gelatin at room temperature, compared to the lower viscosity of its initial state (37 °C, required for solution preparation) because of the gelation of the gelatin component at room temperature,

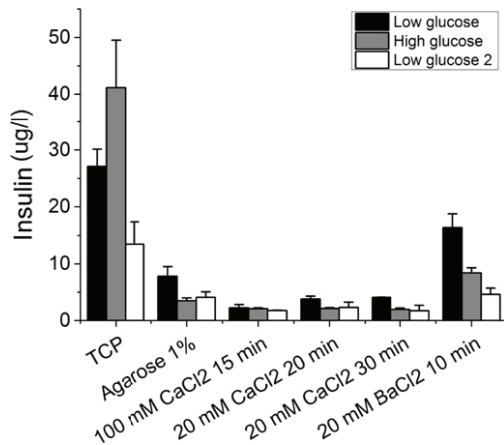


Figure 4: INS1E cells functional response in glucose induced insulin secretion test. Adherent INS1E cells on TCP have been compared to INS1E embedded in bulk agarose gel 1% w/v, bulk alginate 4% w/v /gelatin 5% w/v crosslinked with 102 mM CaCl₂ for 15 min (same crosslinking condition used for plotting) alginate/gelatin crosslinked with 20 mM BaCl₂ for 10 min, or with 20 mM CaCl₂ for 20 or 30 min. In none of the hydrogel composition analyzed, INS1E cells showed a functional response.

which increased the viscosity of the mixture during plotting.

5 Alginate/gelatin blend allowed plotting up to 17 layers, resulting in scaffolds with open pores in the X–Y direction (table 1). The number of layers defines how many times the strand deposition process was repeated on top of each other according to the template (CAD model) to achieve the final construct. In a 2 × 2 cm scaffold, the pore diameter was 1.88 ± 0.18 mm and the strand thickness of the construct 1.55 ± 0.13 mm (figure 1). The diameter of the needle used was 0.41 mm, resulting in a final scaffold 3.7 times thicker because of the superpositioning of 17 layers on top of each other, which showed a partial collapse of the viscous hydrogel precursor before crosslinking. Similarly, the spacing between strands decreased during plotting to 0.5 mm instead of the initial 3 mm programmed into the CAD model. In contrast to conventional thermoplastic polymers extrusion, the hydrogel construct had no pores along the cross-section (z direction). This fact is explained by the low viscosity of the hydrogel precursor compared to molten polymers and also by the fact that the crosslinking procedure was performed after the plotting of the last layer.

Polystyrene beads of 100µm in diameter were used as a model for islets of Langerhans to

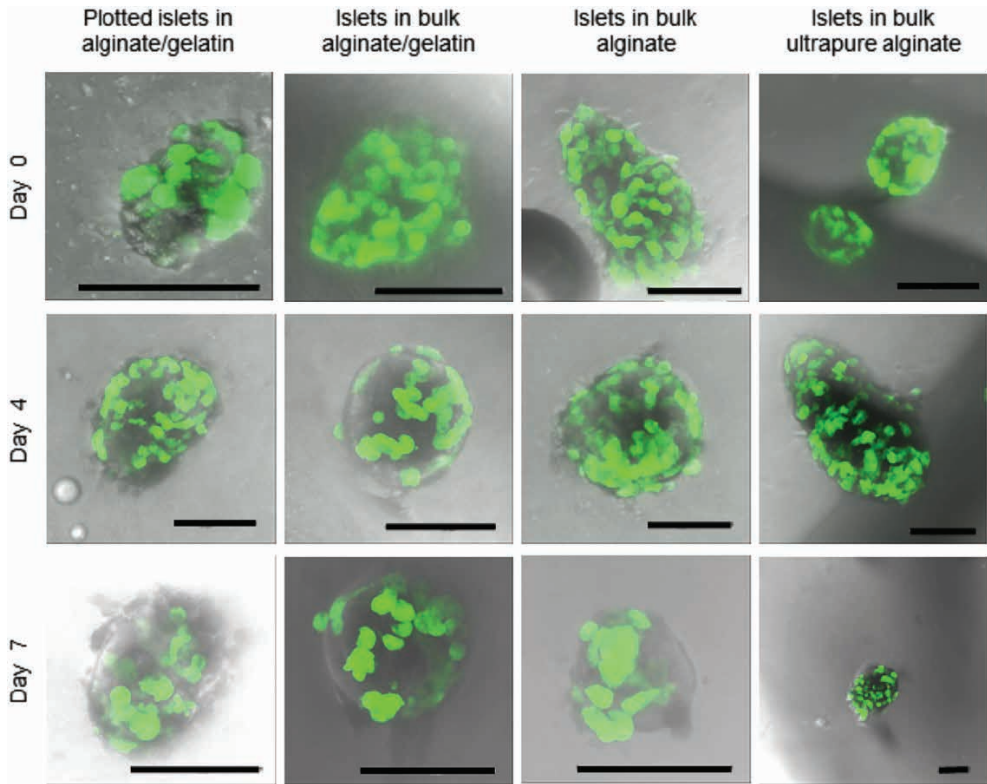
study their distribution in the plotted construct. After plotting, the distance between each bead and the closest pore of the scaffold was measured (figure 1(E)). Beads were homogeneously distributed in the scaffold, in close proximity to the pores. The layer of gel surrounding them had a reduced thickness compared to conventional bulk structures. The great majority of the beads were at less than 200µm from the closest pore (figure 1(E)), which was considered still close enough to the external environment to allow oxygen diffusion to the islets [42].

Glucose diffusion measurements

In order to determine mass transport in this material, a two compartment glucose diffusion assay was performed. Scaffolds were placed in between a compartment containing 12 mM glucose and a compartment containing no glucose. Glucose diffusion through the gel was found to be limited by the alginate/gelatin mesh. Only after 24h the glucose concentration in both 50 ml compartments of the chamber reached the equilibrium, accounting for a delay in glucose diffusion through the gel. The graph in figure 1(F) shows the total flow of glucose in function of time through the gel layer. The graph shows a significant lag time before the glucose flow to time ratio becomes constant (steady state condition). This lag time allows for the calculation of the diffusion coefficient

Chapter 5: Fabrication of three-dimensional bioploted hydrogel scaffolds for islets of Langerhans transplantation

Figure 5: Plotted fluorescent islets in alginate 4% w/v/gelatin 5% w/v, islets in bulk material, islets in bulk alginate and islets in bulk ultrapurified alginate. Images have been taken at days 1, 4 and 7 (scale bar 50 μm).



according to $t = l^2/6D$, as explained in the materials and methods. The resulting glucose diffusion coefficient in alginate 4%/gelatin 5% (w/v) gels was estimated to be $D = 1.13 \times 10^{-6} \text{ cm}^2 \text{ s}^{-1}$. In literature, the diffusion coefficient of glucose in water and in a 4% alginate solution has been reported to be $6.7 \times 10^{-6} \text{ cm}^2 \text{ s}^{-1}$ [43] and $5 \times 10^{-6} \text{ cm}^2 \text{ s}^{-1}$, respectively [39]. Both coefficients are significantly bigger compared to glucose diffusion values in our system.

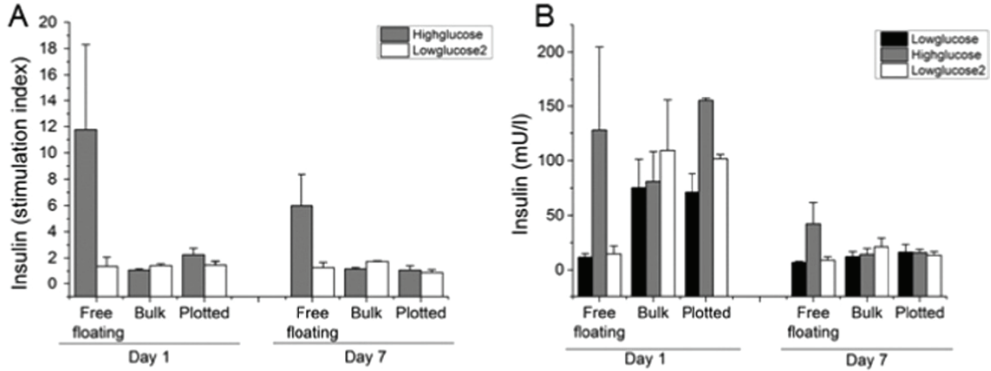
INS1E viability screening in bulk materials

INS1E insulinoma cells were used as a model for islets of Langerhans and encapsulated into the different alginate-ECM blends to study the effect of hydrogel composition on cell viability over 21 days of culture (figure 2 and supplemental table 1). INS1E viability in alginate 4%

w/v was suboptimal, with a mean value of 80% of viable cells 24 h after embedding. Viability dropped to 50% after 3 days of culturing.

In order to further improve hydrogel biocompatibility and cell viability, alginate 4% (w/v) was also mixed with other components such as 5% (w/v) gelatin, 0.5% (w/v) hyaluronic acid or Matrigel 25% (w/v). INS1E cells embedded in alginate 4%/gelatin 5% (w/v) performed the best in terms of cells viability, having a 95% viable cells up to 21 days of culture. Cell viability in alginate 4%/ hyaluronic acid 0.5% (w/v) and alginate 4%/ Matrigel 25% (w/v) also showed improved cell viability, compared to alginate 4% only. However, the handling properties of the alginate/hyaluronic acid and alginate/Matrigel mixtures were less

Figure 6: Glucose induced insulin secretion test on free floating islets, islets embedded in bulk hydrogel and islets in plotted constructs. At day 1, islets are functional in the plotted constructs but not in the bulk hydrogel. (A) Stimulation index normalized to insulin secreted in low glucose 1, (B) actual values of secreted insulin (mU l⁻¹). Islets are considered functional if the stimulation index in high glucose condition is higher than 2 [61].



favorable than alginate/gelatin. Constructs made with these mixtures collapsed easily, were less stiff, and the plotting performances were less consistent to the CAD-model.

5

Construct shape influence on cell viability and metabolic activity

INS1E viability and metabolic activity were not influenced by the shape of the alginate/gelatin construct in which the cells were embedded (figure 3). INS1E cells were embedded in bulk constructs, plotted porous structures and plotted solid hydrogel scaffolds. The volume (0.3ml) and the cell concentration (10×10^6 cells/ml) were kept constant to avoid differences in cell density in the three constructs shapes. Cell viability was assessed by live/dead assay and no difference was observed among the three different construct shapes analyzed (figure 3(A)). The same result was also obtained by analyzing the metabolic activity of the cells. The quantification of glucose and lactate concentrations in the medium resulted in no differences among the three constructs, but in an overall low metabolic activity, suggesting that embedded cells were alive but not functional in the gel (figures 3(B) and (C)), in line with results previously reported by other authors [44].

Responsiveness of hydrogel embedded INS1E cells

In all the conditions tested, INS1E insulin secretion was drastically reduced or totally absent in response to high glucose conditions, when cells were embedded in hydrogel constructs (figure 4). To detect a functional profile, the insulin secreted in the three low–high–low glucose conditions needs to be compared. The only condition in which a functional (low–high–low) insulin profile in response to the correspondent glucose stimulation was detected, are INS1E seeded on tissue culture plastic. In all the hydrogel compositions, no functional response was seen. Irrespectively of the type of hydrogel or the crosslinking conditions (Ca_2+ versus Ba_2+), cells showed limited responsiveness to glucose stimuli. As reported in literature, calcium ion gradients over the cytoplasmic membrane are involved in regulating insulin secretion mechanism. In our experiment, the loss of functionality was independent on the type or on the concentration of the divalent cation used for crosslinking and was also observed when a non-ionic gel, as agarose, was used for embedding. For this reason, we exclude that interfering with Ca_2+ equilibrium during the crosslinking procedure could be responsible for the loss

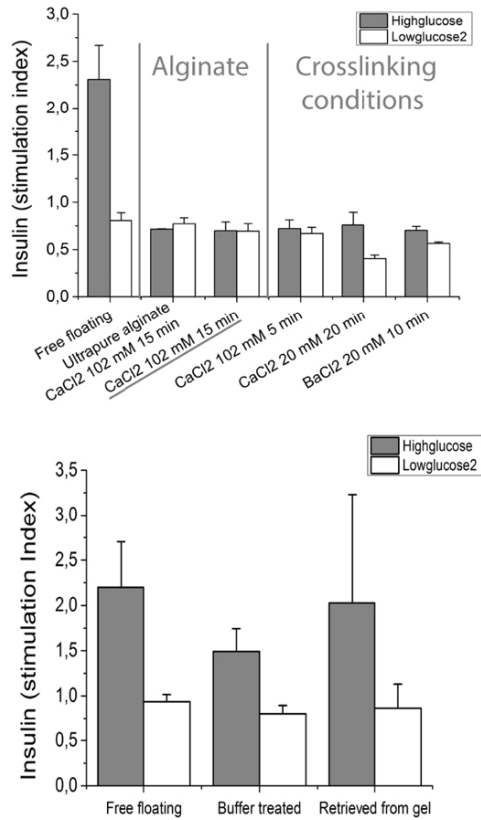
Figure 7: (A) Function test on islets cultured in different hydrogels with various crosslinking conditions. Islets have been embedded in alginate 4%/gelatin 5% or ultrapure alginate and crosslinked with CaCl_2 102 mM for 5 and 15 min, with CaCl_2 20 mM for 20 min and with BaCl_2 for 10 min. None of the conditions tested were functional. (B) Alginate/gelatin gel crosslinked with 102 mM CaCl_2 for 15 min was dissolved and islets were retrieved from the gel. Functionality was tested and compared to free floating islets and free floating islets treated with buffer. After retrieval from the gel, functionality was restored. Statistical test was performed and no significant difference was found among the stimulation indexes of the three conditions.

of insulin secretion [45, 46]. Once the influence of the crosslinker ion was excluded, nutrient diffusion limitations are considered the major reason to explain the loss of functionality when INS1E cells are embedded in bulk hydrogels.

Islet transduction, embedding and functionality in the construct

Human islets were plotted in the construct and their morphology, aggregation, viability and response to glucose challenges were analyzed and compared with bulk constructs. Before plotting, viral transduction was used to induce stable expression of GFP in the islets and allow direct visualization in the plotted construct *in vitro* as well as *in vivo* with intravital imaging techniques.

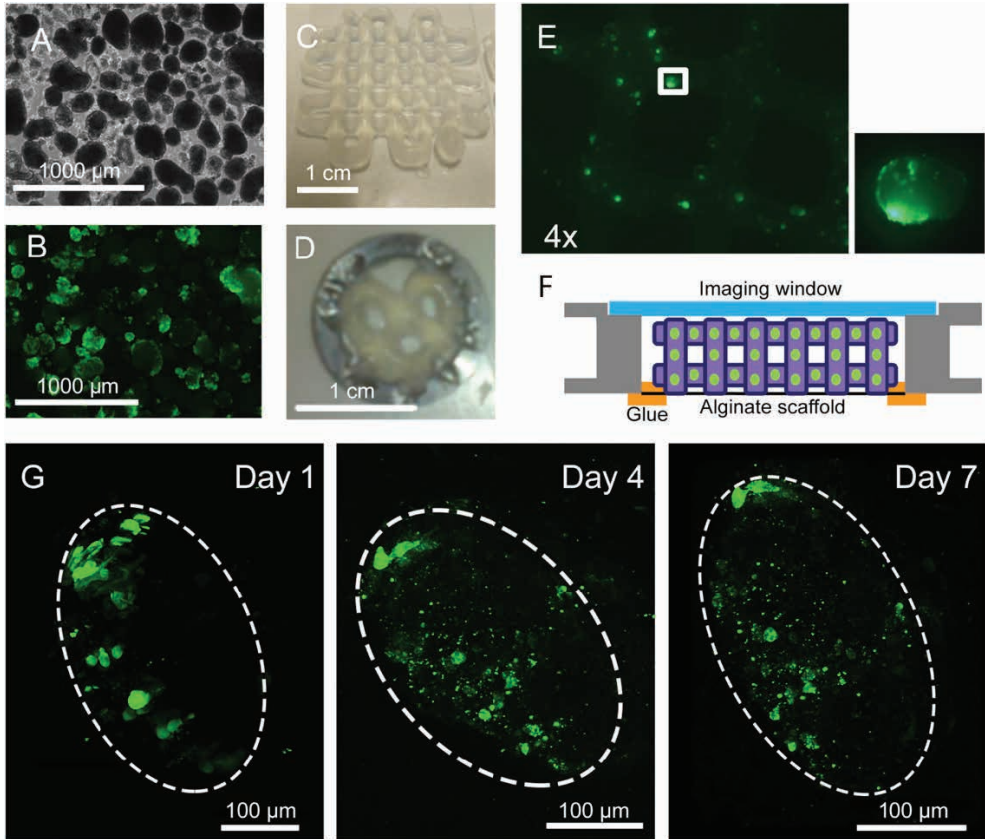
GFP transduced human islets plotted in the alginate/ gelatin constructs showed comparable morphology and GFP expression as the islets embedded in the same alginate/gelatin composition in bulk form, in 4% w/v alginate only, and in ultrapurified alginate [24–26, 47]. Ultrapure alginate was used to compare islet morphology in the new alginate/gelatin mixture to an already used material in the islets encapsulation field (figure 5).



The embedding and the plotting procedure did not induce any change in cell morphology. Islets were still round shaped and the shear stress experienced during plotting did not cause islets to disaggregate or decrease in viability. According to the morphological analysis of the embedded islets, the presence of gelatin in the hydrogel mixture did not induce islet spreading or cell adhesion. Hydrogel embedding also prevented aggregation of individual islets (figure 5 and supplemental figure 2).

The native morphology of the islets was retained after plotting of murine islets (supplemental figure 1). These islets were isolated from double heterozygous crossbreed mice Tg(Ins1-eGFP) and B6(CAG- DsRed*MST). In this mouse strain, all cell types are characterized by the expression of DsRed protein under the control of the ubiquitous chicken β -actin

Figure 8: Human islets (A) were transduced with CMV-GFP virus, handpicked (B), and plotted into a 2×2 alginate construct (C). A 1 cm circular sample was glued to the abdominal imaging window, as shown in (D) and schematically depicted in (F). Figure (E) shows GFP transduced islets in a plotted construct. The same islets could be imaged at days 1, 4 and 7 (G) (scale bar 100 μ m).



5

promoter. Insulin production by β -cells within the plotted islets is visualized by the specific expression of GFP, under the control of the mouse insulin promoter. The GFP signal in β -cells is much stronger than DsRed, allowing for the visualization of the insulin producing β -cells by the green GFP signal.

Islet functionality in plotted constructs was compared to islets in bulk hydrogels and to free floating islets. Islets are regarded as functional when their stimulation index is higher than 2 [61]. As shown in figure 6(A), islets in bulk hydrogels lose their functionality already after one day, being not responsive to glucose stimuli.

In figure 6(B) one can see that the normal low-high-low insulin response to glucose is still present in the plotted construct while it is not visible anymore in the bulk construct. The diffusion of oxygen and insulin is slightly improved in the plotted construct compared to the bulk construct. Functionality in both bulk and plotted constructs is lost after seven days in culture. Interestingly, the reduction in the functional response of plotted islets was not caused by a reduced insulin secretion in high glucose, since this was comparable to the response of the control islets, but was due to an increased insulin secretion in low glucose condition, as

shown in figure 6(B).

Insulin secretion is dependent on the extracellular calcium concentration [44, 45]. In an ionic cross-linked hydrogel such as alginate, the extracellular environment is rich in calcium and this fact could interfere with insulin secretion mechanism and explain the apparent loss of functionality of islets when embedded in the gel. To further investigate if islet loss of functionality is related to the divalent ion used for crosslinking, islets were embedded in different hydrogels, using different crosslinking conditions (figure 7(A)). Irrespectively of the crosslinking ion used (calcium or barium), or the crosslinking time used, for gelation, none of the conditions were able to sustain islet functionality. Islets in ultrapure alginate, that is often used for islet encapsulation [24–26, 47], were crosslinked under the same conditions used for plotting. Also in this case, islets were not responsive to glucose stimulation (characterized by a stimulation index lower than 1).

Since the crosslinking ion appeared not to be the limiting factor for reestablishing islet functionality, we showed that the loss of functionality of embedded islets is caused by a decreased glucose diffusion through the gel. In fact, the glucose diffusion coefficient in these gels ($1.13 \times 10^{-6} \text{ cm}^2 \text{ s}^{-1}$) has been calculated to be significantly smaller than glucose diffusion in water, or in a 4% alginate solution ($6.7 \times 10^{-6} \text{ cm}^2 \text{ s}^{-1}$ [43] and $5 \times 10^{-6} \text{ cm}^2 \text{ s}^{-1}$ [39] respectively). If this hypothesis would be correct, the inhibition of islet response to glucose challenge should be transient and the islets should recover after retrieval from the gel. To further prove this point, embedded islets were retrieved from the gel and their functionality tested again 2 days after retrieval. As shown in figure 7(B), islets functionality was fully restored when retrieved from the hydrogel, statistical test was performed and no significant difference was found among the stimulation indexes of the three conditions. This finding confirmed that islets remained viable in a plotted hydrogel despite losing glucose

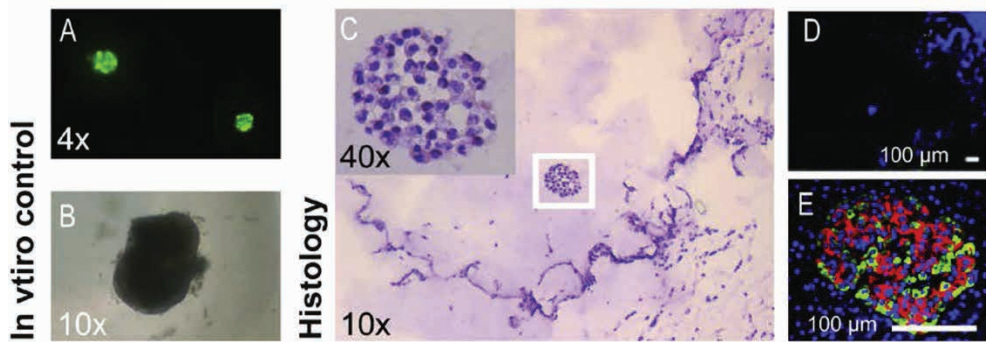
responsiveness. The lack of such responsiveness was likely due to limitations in glucose and nutrient diffusion.

Intravital imaging results

The alginate/gelatin (4%/5% w/v) plotted hydrogel scaffolds containing islets were mounted on the imaging window and transplanted subcutaneously in nude mice. A schematic drawing can be seen in figure 8. With this *in vivo* imaging technique, we were able to non-invasively image the islets in the hydrogel construct up to 7 days after transplantation. This imaging method allowed us to longitudinally monitor a specific islet in consecutive imaging sessions. We were able to detect GFP expression and image the islets in the construct at different time points (figure 8(G)), where single cells within an islet are clearly visible.

At subsequent time points, islets remained visible in the construct and the same islet could be easily traced, although appearance of GFP expression changed and single cells were not as clearly visible as before. This observation can be seen in figure 8(G) by a more speckled appearance as the fluorescent signal of the cells decreased over time. This fact correlates with the diminished metabolic activity and functionality already demonstrated in the *in vitro* experiments. The decreased GFP signal and metabolic activity at day 4 and 7 after transplantation can be again correlated with the fact that nutrient and oxygen diffusion in the construct are limited to the lower layers of the construct, which are in direct contact with the surrounding tissue and blood vessels. The diffusion in the upper layers of the construct is restricted by the presence of the imaging window. Moreover, the intravital technique is limited to 450 μm imaging depth, which allows only for the upper layers of the scaffolds to be studied. These layers are more affected by a lack of nutrients diffusion from the underlying tissues. This hypothesis was confirmed by the fact that islets in the *in vitro* control were still bright fluorescent up to day 7,

Figure 9: *In vitro* islet fluorescence was bright (A), and the morphology of the islets was preserved (B). After explant of the *in vivo* samples, islets were imaged with hematoxylin/eosin staining (C), however no expression of insulin or glucagon was detected by immunostaining (D) compared to pancreas sections (E) (red: insulin, green: glucagon, blue: DAPI. Scale bar 100 μ m).



with no sign of cell death or disaggregation. At day 7 both the mice with a subcutaneous transplant and the mice with window implants were terminated and the alginate/gelatin scaffolds were explanted and processed for histology. Hematoxylin and eosin staining confirmed the presence of islets in the scaffold, which showed no sign of apoptotic nuclei, but no insulin or glucagon was detected by immunostaining (figure 9(D)) which might indicate a reduced metabolism due to the embedding in hydrogel and lack of sufficient nutrient supply.

Discussion

3D bioplotting is a well described technique in the field of tissue engineering, mostly applied for the extrusion of thermoplastic polymers, to create custom engineered scaffolds for the regeneration of bone and cartilage [48, 49]. Printing allows tailoring of shape, porosity and mechanical properties: these parameters can be finely tuned in order to steer cells response to match the properties of the specific tissue to be regenerated. The only application of printing in pancreas tissue engineering is reported in a paper of Daoud et al [15], with islets being seeded in a printed poly (DL-lactide-co-glycolide) construct, a material whose mechanical properties are not comparable with those of the

soft tissues in pancreas.

Combining hydrogels with the 3D bioplotting for the regeneration of soft tissues and in particular for the encapsulation of islets of Langerhans should result in a clinically relevant size construct for islet delivery. This construct will provide a protective environment for the embedded tissue, with mechanical properties better mimicking those of soft tissues, if compared to solid thermoplastic materials. In contrast to conventional embedding in bulk hydrogels, a plotted structure can increase the available surface area for nutrients and catabolites exchange, avoiding the formation of a necrotic core which can affect bulk hydrogels. This would ultimately result in the possibility of up-scaling the construct to a size that can contain a clinically relevant amount of islets.

This study demonstrates that the plotting of large cell aggregates of 50–300 μ m like islets of Langerhans in a hydrogel is feasible, without compromising islet viability, morphology and aggregation.

Material selection was performed using the model cell line INS1E and high viability values were observed for INS1E and islets in the alginate/gelatin composition, but the metabolic activity of cells embedded in the hydrogel is

reduced and these findings are in line with what has been also reported by other authors [44, 50, 51]. Our data suggest that islet plotting per se is not causing the impairment in functionality, but it is caused instead by impaired nutrient diffusion in such a viscous hydrogel precursor. This loss of metabolic activity cannot be rescued only by improving nutrient diffusion by means of a macro-porous structure.

Opposite results in terms of metabolic activity were reported for human mesenchymal stem cells (MSCs) encapsulated in similarly plotted constructs [31]. In this case, embedding the cells in the porous plotted scaffold had a beneficial effect on their viability compared with solid or bulk constructs [31].

The comparison with previously published results highlights that different cell types react oppositely to the embedding in the printed construct and might suggest that INS1E β -cells and islets of Langerhans are more sensitive than MSCs to hydrogel embedding. *In vivo*, islets in the pancreas are extensively vascularized in order to support their high metabolic activity, requiring constant and abundant glucose and oxygen supply for their normal functioning. On the contrary, MSCs normally reside in hypoxic environments in the body and are less metabolically active. This fact could explain why embedding in a porous hydrogel construct is beneficial for MSCs viability and metabolic activity [31], yet not enough for a more sensitive and metabolically requiring cell type as β -cells and islets of Langerhans.

The low INS1E metabolic activity and islet reduced functionality in the gel are indications that their activity is somehow limited by the material in which they are embedded. This is confirmed by the restored islet functionality when retrieved from the gel. According to these data, the major limitations that the plotting of cell-laden constructs still encounters is the availability of a suitable material capable of proper mass transport properties to maintain

cell functionality and having at the same time sufficient mechanical properties for a layer by layer processing.

The optimal material for plotting has to meet various requirements: high viscosity, fast crosslink, bio-compatibility, mechanical properties comparable with soft tissues and, once crosslinked, permeability to metabolites and catabolites. For plotting purposes the material has to be viscous enough to be plotted on subsequent layers on top of each other without collapsing under its own weight: such a highly viscous material restricts mass transport in the material itself, resulting in a limitation for islets functionality. To date, limited materials are available for cell-laden plotting purposes [52–54], and finding a compromise between mechanical properties for plotting, matrix stiffness, nutrient diffusion and functionality of embedded cells is still rather challenging [55]. The main limitations in the hydrogel used for this study are given by nutrient diffusion in such a viscous and highly concentrated gel. This study shows that the viability and functionality of embedded islets could be limitedly improved by a porous construct shape, if compared to solid bulk hydrogels. Islets showed functional response, although reduced, at day one in the porous constructs while no functional behavior was observed in the bulk constructs at this time point (figure 6(B)). This shows that the plotted porous design can offer an improvement, although still limited, for nutrient diffusion in the gel. The reduced mass transport still remains a major limitation to the applicability of this technique to a scaffold of a clinically relevant size.

This is particularly true for islets of Langerhans, since they have very peculiar and demanding metabolic requirements and thus, they are more sensitive to the surrounding environment. In their native state, islets of Langerhans extensive vascularization provides for proper glucose sensing and insulin secretion and this characteristic is essential for their proper functionality.

If this exchange is limited by the tight surrounding matrix, as it happens when islets are embedded in the alginate/gelatin mixture, islet functionality is hampered. Islets are viable in the hydrogel construct, but their ability to detect changes in glucose concentration and respond with proper insulin secretion is reduced by the tight matrix in which they are embedded. Islets are fully functional again when retrieved from the hydrogel construct and this confirms that the apparent loss of functionality is caused by limited mass transport through the gel.

The retrieved islet functionality after dissolution of the gel also excludes that the islets were damaged by the shear stress experienced during printing. It is reported in literature that a mechanical stress could permanently damage islet functionality, but in that case the functionality could not be retrieved simply by dissolving the surrounding gel.

As shown by the bead distribution in the plotted gel, the great majority of the beads is located at less than 200 μm from the interface, less than the oxygen diffusion limit through tissues. Yet, the glucose diffusion coefficient measured in our system ($1.13 \times 10^{-6} \text{ cm}^2 \text{ s}^{-1}$) is significantly lower than glucose diffusion in water ($6.7 \times 10^{-6} \text{ cm}^2 \text{ s}^{-1}$) [43] and in 4% alginate solution only ($5 \times 10^{-6} \text{ cm}^2 \text{ s}^{-1}$) [39].

Such limited glucose diffusion in the construct is explained by a crosslinking obtained in saturation condition and by the presence of gelatin. The mesh size of a 4% w/v alginate solution has been reported to be around 7 nm [56], but the presence of gelatin as an interpenetrating network decreases consistently the number, diameter and length of the pores in an alginate hydrogel. This accounts for a considerable delay in glucose supply to the islets and a corresponding delay in insulin secretion from the hydrogel. Moreover, given the higher molecular weight and bigger hydrodynamic radius of an insulin molecule, the limitations experienced in insulin diffusion through the gel would be

even more severe. Limited diffusion coefficients can explain the low metabolic activity, together with the apparent lack of functionality of the embedded cells. Moreover, the diffusion coefficient D increases with the second power of the gel thickness ($D = l^2/6t$). This means that for a small decrease in the gel thickness, a bigger increase in the diffusion coefficient is expected. This would explain why islets embedded in the plotted construct show some reduced functionality at day one, which is already completely absent in bulk constructs. This emphasizes the importance of construct design for islets functionality.

The effect of calcium ions used for crosslinking on insulin secreting pathways was also investigated as one of the possible reasons to explain INS1E and islet loss of functionality in the construct. As showed by many authors, voltage gated calcium channels, and consequently transmembrane calcium ion gradients are involved in insulin secretion mechanisms [45, 46, 57]. Since the extracellular gel environment is quite rich in calcium ion concentration (102 mM crosslinking), the increased calcium concentration of the extracellular compartment might have caused the increased insulin secretion in low glucose condition. Although no difference in functionality was shown when hydrogels were crosslinked with other divalent cations, different concentrations or with reduced exposure times.

To further study whether encapsulated islets maintained their viability *in vivo*, we implanted plotted constructs subcutaneously in nude mice and monitored their viability by intravital imaging. This is a powerful technique for *in vivo* follow up of transplanted tissue, enabling the imaging of the same transplanted islet in consecutive imaging sessions and study the process of revascularization of the scaffold. Intravital imaging has been applied to transplanted islets implanted under the kidney capsule [58] or in the anterior chamber of the eye [59, 60], which is a highly vascularized location. Here we show for the first time the applicability of this

technique for the imaging of subcutaneously transplanted tissue in an implantable scaffold. In this kind of application, the presence of the window on top of the construct and the poorly vascularized location can furthermore limit oxygen diffusion to the transplanted tissue and islets are not anymore surrounded by tissue and blood vessels from all directions but only from the bottom. Consequently, nutrient diffusion to the islets located in the upper parts of the scaffolds has to rely solely on nutrient supply from the bottom part of the construct. This is even more important if we consider that the imaging depth of this intravital imaging model is also limited to 450 μm , which allow us to monitor only the upper layers of the hydrogel, the ones which suffer the most for lack of oxygen diffusion. Despite these limitations, we were still able to detect GFP expression and image islets for seven days in the construct, although islets showed signs of reduced GFP expression at later time points. This result correlates with our assumption of a reduced metabolic activity of the embedded cells, caused by an increased nutrient diffusion limitation in our model which was even more pronounced when an imaging window was used. Thus, both *in vitro* and *in vivo* results show that the plotting of islets is possible but the material optimization for this application is crucial to allow proper metabolite exchange with the embedded tissue.

In contrast to conventional islet encapsulation, here islets are confined in one location and after transplantation, blood vessels might grow through the pores of the construct, in closer contact with the embedded islets compared to the inner part of a bulk hydrogel scaffold. Potentially, an immunoprotective scaffold could be developed by using a non-degradable hydrogel, with a proper mesh size capable to block antibodies and cells of the immune system and at the same time large enough to allow insulin diffusion.

Conclusions

This study demonstrated that 3D hydrogel plotting can be a valuable technique to couple islet embedding in hydrogel strands with a pre-defined 3D scaffold architecture. 4% alginate/5% gelatin was found to be a suitable hydrogel mixture for plotting of islets and β -cells, without compromising their viability and morphology. However, the high viscosity of the material needed for plotting, resulted in a dense mesh size, which impairs glucose diffusion and limits islet functionality. Since a highly viscous biomaterial is needed for plotting, a compromise has to be established between material properties allowing scaffold plotting and sufficient nutrient diffusion. Plotted hydrogels could effectively increase nutrient diffusion compared to the same bulk hydrogel, but the macroporous structure is not enough to overcome limitations caused by an insufficient diffusion of nutrients in this specific gel composition.

Despite the limitations in islet functionality when embedded in the construct, islets restored full functionality when retrieved from the hydrogel. In conclusion, plotting can be a powerful technique to engineer complex constructs, containing a clinically relevant number of islets. Although promising, the potential of the technique is currently hampered by scarce availability of suitable biomaterials. Further research is needed to develop hydrogels with sufficient viscosity and mechanical properties suitable for plotting but also with the capacity to support sufficient nutrient and secretory product diffusion for a physiologically relevant islet functionality.

References

- [1] Ryan E A et al 2001 Clinical outcomes and insulin secretion after islet transplantation with the edmonton protocol *Diabetes* 50 710–9
- [2] Shapiro A M J et al 2000 Islet transplantation in seven patients with type 1 diabetes mellitus using a glucocorticoid-free immunosuppressive regimen *New England J. Med.* 343 230–8
- [3] Mallett A G and Korbitt G S 2009 Alginate modification improves long-term survival and function of transplanted encapsulated islets *Tissue Eng. A* 15 1301–9
- [4] Bennet W et al 1999 Incompatibility between human blood and isolated islets of Langerhans: a finding with implications for clinical intraportal islet transplantation? *Diabetes* 48 1907–14
- [5] Paraskevas S, Maysinger D, Wang R, Duguid W P and Rosenberg L 2000 Cell loss in isolated human islets occurs by apoptosis *Pancreas* 20 270–6
- [6] Thomas F, Wu J, Contreras J L, Smyth C, Bilbao G, HeJand Thomas J 2001 A tripartite anoikis-like mechanism causes early isolated islet apoptosis *Surgery* 130 333–8
- [7] Thomas F T, Contreras J L, Bilbao G, Ricordi C, Curie I D and Thomas J M 1999 Anoikis, extracellular matrix, and apoptosis factors in isolated cell transplantation *Surgery* 126 299–304
- [8] Lai Y et al 2005 Vascular endothelial growth factor increases functional [beta]-cell mass by improvement of angiogenesis of isolated human and murine pancreatic islets *Transplantation* 79 1530–6
- [9] Pileggi A, Molano R D, Ricordi C, Zahr E, Collins J, Valdes R and Inverardi L 2006 Reversal of diabetes by pancreatic islet transplantation into a subcutaneous, neovascularized device *Transplantation* 81 1318–24
- [10] Shapiro A M J, Gallant H L, Hao E G, Lakey J R T, McCready T, Rajotte R V, Ray V, Yatsciff R W and Kneteman N M 2005 The portal immunosuppressive storm: relevance to islet transplantation? *Therapeutic Drug Monit.* 27 35–7
- [11] Billalud B and Sutter B C J 1982 Immediate in vivo effect of corticosterone on glucose-induced insulin secretion in the rat *J. Endocrinology* 95 315–20
- [12] Blomeier H, Zhang X, Rives C, Brissova M, Hughes E, Baker M, Powers A C, Kaufman D B, Shea L D and Lowe W L 2006 Polymer scaffolds as synthetic microenvironments for extrahepatic islets transplantation *Transplantation* 82 452–9
- [13] Dufour J M, Rajotte R V, Zimmerman M, Rezania A, Kin T, Dixon D E and Korbitt G S 2005 Development of an ectopic site for islet transplantation, using biodegradable scaffolds *Tissue Eng* 11 1323–31
- [14] Mao G H, Chen G A, Bai H Y, Song T R and Wang Y X 2009 The reversal of hyperglycaemia in diabetic mice using PLGA scaffolds seeded with islet-like cells derived from human embryonic stem cells *Biomaterials* 30 1706–14
- [15] Daoud J T, Petropavlovskaja M S, Patapas J M, Degrandpre' C E, DiRaddo R W, Rosenberg L and Tabrizian M 2011 Long-term in vitro human pancreatic islet culture using three-dimensional microfabricated scaffolds *Biomaterials* 32 1536–42
- [16] Brady A C, Martino M M, Pedraza E, Sukert S, Pileggi A, Camillo R, Hubbell J A and Stabler C L 2013 Pro-angiogenic hydrogels within macroporous scaffolds enhances islet engraftment in an extrahepatic site *Tissue Eng. A* 19 2544–52
- [17] Pedraza E, Brady A C, Fraker C A, Molano R D, Sukert S, Berman D M, Kenyon N S, Pileggi A, Ricordi C and Stabler C L 2013 Macroporous three-dimensional PDMS scaffolds for extrahepatic islet transplantation *Cell Transplant* 22 1123–35
- [18] Buitinga M, Truckenmüller R, Engelse M A, Moroni L, Ten Hoopen H W M, van Blitterswijk C A, de Koning E J P, van Apeldoorn A A and Karperien M 2013 Microwell scaffolds for the extrahepatic transplantation of islets of Langerhans *PLoS One* 8 e64772
- [19] Slaughter B V, Khurshid S S, Fisher O Z, Khademhosseini A and Peppas N A 2009 Hydrogels in regenerative medicine *Adv. Mater.* 21 3307–29
- [20] Zhu J and Marchant R E 2011 Design properties of hydrogel tissue-engineering scaffolds *Expert Rev. Med. Devices* 8 607–26
- [21] Lin C C and Anseth K S 2009 Glucagon-like peptide-1 functionalized peg hydrogels promote survival and function of encapsulated pancreatic β -cells *Biomacromolecules* 10 2460–7
- [22] Zieris A, Prokoph S, Levental K R, Welzel P B, Grimmer M, Freudenberg U and Werner C 2010 FGF-2 and VEGF functionalization of starPEG-heparin hydrogels to modulate biomolecular and physical cues of angiogenesis *Biomaterials* 31 7985–94
- [23] Lin C C and Anseth K S 2011 Cell–cell communication mimicry with poly(ethylene glycol) hydrogels for enhancing β -cell function *Proc. Natl Acad. Sci.* 108 6380–5
- [24] de Vos P, Faas M M, Strand B and Calafiore R 2006 Alginate-based microcapsules for immunoisolation of pancreatic islets *Biomaterials* 27 5603–17
- [25] de Vos P, Hamel A F and Tatarkiewicz K 2002

Chapter 5: Fabrication of three-dimensional bioprinted hydrogel scaffolds for islets of Langerhans transplantation

- Considerations for successful transplantation of encapsulated pancreatic islets *Diabetologia* 45 159–73
- [26] De Vos P, De Haan B J, Wolters G H J, Strubbe J H and Van Schilfgaarde R 1997 Improved biocompatibility but limited graft survival after purification of alginate for microencapsulation of pancreatic islets *Diabetologia* 40 262–70
- [27] Ludwig B et al 2013 Transplantation of human islets without immunosuppression *Proc. Natl Acad. Sci.* 110 19054–8
- [28] Cui X, Breitenkamp K, Finn M G, Lotz M and D’Lima D D 2012 Direct human cartilage repair using three-dimensional bioprinting technology *Tissue Eng. A* 18 1304–12
- [29] Roth E A, Xu T, Das M, Gregory C, Hickman J J and Boland T 2004 Inkjet printing for high-throughput cell patterning *Biomaterials* 25 3707–15
- [30] Wang X et al 2006 Generation of three-dimensional hepatocyte/gelatin structures with rapid prototyping system *Tissue Eng.* 12 83–90
- [31] Fedorovich N E, Kuipers E, Gawlitta D, Dhert W J and Alblas J 2011 Scaffold porosity and oxygenation of printed hydrogel constructs affect functionality of embedded osteogenic progenitors *Tissue Eng. A* 17 2473–86
- [32] Hockaday L A et al 2012 Rapid 3D printing of anatomically accurate and mechanically heterogeneous aortic valve hydrogel scaffolds *Biofabrication* 4 1758–5082
- [33] Cui X and Boland T 2009 Human microvasculature fabrication using thermal inkjet printing technology *Biomaterials* 30 6221–7
- [34] Xu T, Rohozinski J, Zhao W, Moorefield E C, Atala A and Yoo J J 2009 Inkjet-mediated gene transfection into living cells combined with targeted delivery *Tissue Eng. A* 15 95–101
- [35] Lee W, Pinckney J, Lee V, Lee J H, Fischer K, Polio S, Park J K and Yoo S S 2009 Three-dimensional bioprinting of rat embryonic neural cells *Neuroreport* 20 798–803
- [36] Lee W, Debasitis J C, Lee V K, Lee J H, Fischer K, Edminster K, Park J K and Yoo S S 2009 Multi-layered culture of human skin fibroblasts and keratinocytes through three-dimensional freeform fabrication *Biomaterials* 30 1587–95
- [37] Saunders R E, Gough J E and Derby B 2008 Delivery of human fibroblast cells by piezoelectric drop-on-demand inkjet printing *Biomaterials* 29 193–203
- [38] Fraga D W, Sabek O, Hathaway D K and Gaber A O 1998 A comparison of media supplement methods for the extended culture of human islet tissue *Transplantation* 65 1060–6
- [39] Hannoun B J and Stephanopoulos G 1986 Diffusion coefficients of glucose and ethanol in cell-free and cell-occupied calcium alginate membranes *Biotechnol. Bioeng.* 28 829–35
- [40] Rutherford S W and Do D D 1997 Review of time lag permeation technique as a method for characterisation of porous media and membranes *Adsorption* 3 283–312
- [41] Masuda K, Takegami K, An H, Kumano F, Chiba K, Andersson G B, Schmid T and Thonar E 2003 Recombinant osteogenic protein-1 upregulates extracellular matrix metabolism by rabbit annulus fibrosus and nucleus pulposus cells cultured in alginate beads *J. Orthopaedic Res.* 21 922–30
- [42] Rouwkema J, Rivron N C and van Blitterswijk C A 2008 Vascularization in tissue engineering *Trends Biotechnol.* 26 434–41
- [43] Longworth L G 1953 Diffusion measurements, at 25°, of aqueous solutions of amino acids, peptides and sugars *J. Am. Chem. Soc.* 75 5705–9
- [44] Simpson N E, Grant S C, Gustavsson L, Peltonen V-M, Blackband S J and Constantinidis I 2006 Biochemical consequences of alginate encapsulation: a NMR study of insulin-secreting cells *Biomaterials* 27 2577–86
- [45] Hales C N and Milner R D 1968 Cations and the secretion of insulin from rabbit pancreas *in vitro* *J. Physiol.* 199 177–87
- [46] Proks P and Ashcroft F M 1995 Effects of divalent cations on exocytosis and endocytosis from single mouse pancreatic beta-cells *J. Physiol.* 487 465–77
- [47] de Vos P, Spasojevic M, de Haan B J and Faas M M 2012 The association between *in vivo* physicochemical changes and inflammatory responses against alginate based microcapsules *Biomaterials* 33 5552–9
- [48] Seyednejad H, Gawlitta D, Dhert W J, van Nostrum C F, Vermonden T and Hennink W E 2011 Preparation and characterization of a three-dimensional printed scaffold based on a functionalized polyester for bone tissue engineering applications *Acta Biomater.* 7 1999–2006 [49] Park S A, Lee S H and Kim W D 2011 Fabrication of porous using a 3D plotting system for bone tissue engineering *Bioprocess Biosyst. Eng.* 34 505–13
- [50] Weber L M, Lopez C G and Anseth K S 2009 Effects of PEG hydrogel crosslinking density on protein diffusion and encapsulated islet survival and function *J. Biomed. Mater. Res. A* 90A 720–9
- [51] Hunt N C, Shelton R M and Grover L M 2009

Reversible mitotic and metabolic inhibition following the encapsulation of fibroblasts in alginate hydrogels *Biomaterials* 30 6435–43

[52] Fedorovich N E, Alblas J, de Wijn J R, Hennink W E, Verbout A J and Dhert W J 2007 Hydrogels as extracellular matrices for skeletal tissue engineering: state-of-the-art and novel application in organ printing *Tissue Eng.* 13 1905–25

[53] Fedorovich N E, De Wijn J R, Verbout A J, Alblas J and Dhert W J 2008 Three-dimensional fiber deposition of cell- laden, viable, patterned constructs for bone tissue printing *Tissue Eng. A* 14 127–33

[54] Fedorovich N E, Swennen I, Girones J, Moroni L, van Blitterswijk C A, Schacht E, Alblas J and Dhert W J 2009 Evaluation of photocrosslinked Lutrol hydrogel for tissue printing applications *Biomacromolecules* 10 1689–96

[55] Brandl F, Sommer F and Goepferich A 2007 Rational design of hydrogels for tissue engineering: impact of physical factors on cell behavior *Biomaterials* 28 134–46

[56] Turco G, Donati I, Grassi M, Marchioli G, Lapasin R and Paoletti S 2001 Mechanical spectroscopy and relaxometry on alginate hydrogels: a comparative analysis for structural characterization and network mesh size determination *Biomacromolecules* 12 1272–82

[57] Merglen A, Theander S, Rubi B, Chaffard G, Wollheim C B and Maechler P 2004 Glucose sensitivity and metabolism-secretion coupling studied during two-year continuous culture in INS-1E insulinoma cells *Endocrinology* 145 667–78

[58] Nyqvist D et al 2011 Donor islet endothelial cells in pancreatic islet revascularization *Diabetes* 60 2571–7

[59] Speier S et al 2008 Noninvasive in vivo imaging of pancreatic islet cell biology *Nat. Med.* 14 574–8

[60] Speier S, Nyqvist D, Kohler M, Caicedo A, Leibiger I B and Berggren P O 2008 Noninvasive high-resolution in vivo imaging of cell biology in the anterior chamber of the mouse eye *Nat. Protocols* 3 1278–86

[61] Benhamou P Y et al 2001 Human islet transplantation network for the treatment of type I diabetes: first data from the Swiss-French GRAGIL consortium (1999–2000) *Diabetologia* 44 859–64

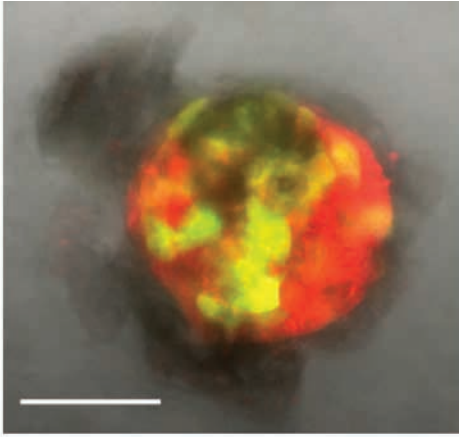
Supplemental legends

Supplemental figure 1: Murine islet isolated from double heterozygous crossbreed mice Tg(Ins1-eGFP) and B6(CAG-DsRed⁺MST). DsRed protein is expressed under the control of the ubiquitous chicken beta-actin promoter. Insulin production by beta cells within the plotted islets is visualized by the specific expression of GFP, under the control of the mouse insulin promoter. Islet maintain their round morphology after plotting in alginate 4% gelatin 5% mixture. Scalebar 100 μ m.

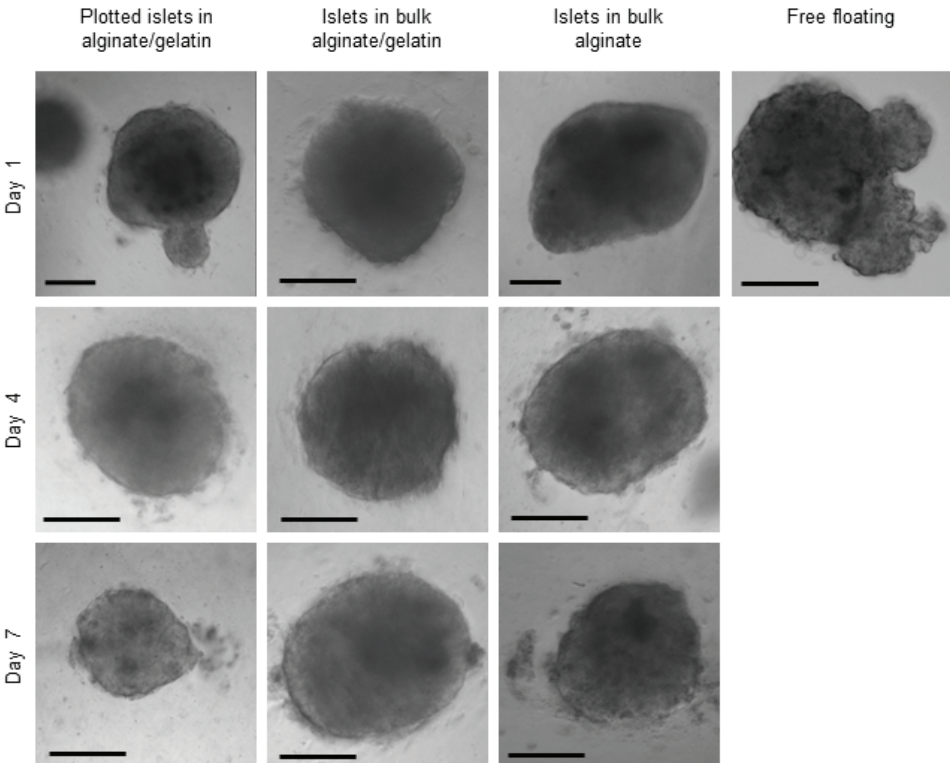
Supplemental figure 2: Human islet plotted in alginate 4% gelatin 5%, embedded in bulk alginate/gelatin, in alginate only and compared to free floating islet. Islets were imaged at 1, 4 and 7 days. Scalebar 100 μ m.

Supplemental figure 3: Viscosity of the different alginate mixtures at different shear rate values. The non-newtonian behavior at different shear rates is evident from the graph.

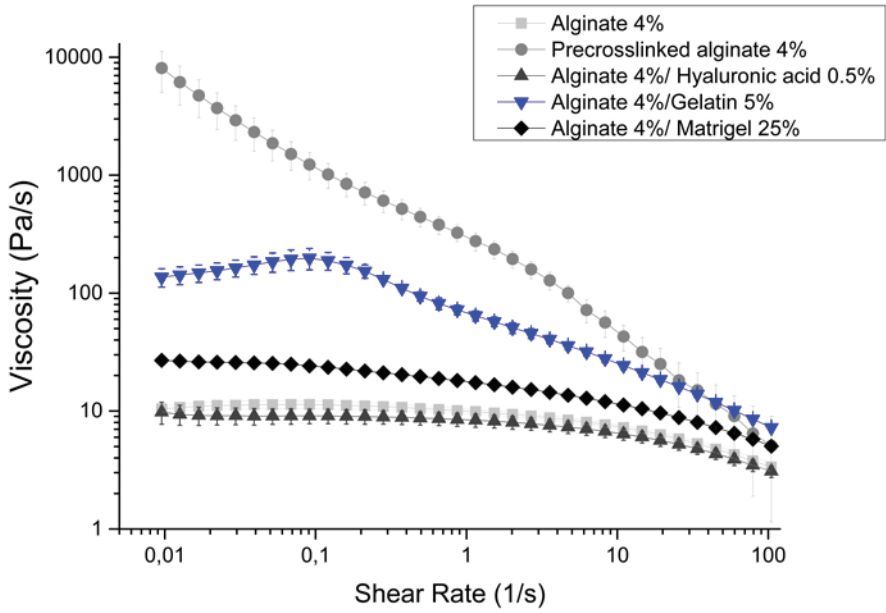
Supplemental table 1: Viability of INS1E in the different hydrogel mixtures at day 14 and 21. Alginate 4% gelatin 5% supports high viability also at later time points



Supplemental figure 1



Supplemental figure 2



Supplemental figure 3

Supplemental table 1

	Day 14	Day 21
Alginate 4%	81.7 ± 21.8	91.7 ± 7.8
Alginate 4% Gelatin %5	91.8 ± 7.8	95.2 ± 5.4
Alginate 4% /Hyaluronic acid 5%	88.5 ± 9.4	87.4 ± 8.8
Alginate 4% /Matrigel 25%	88.0 ± 10.9	86.9 ± 10.6

General Discussion

L. van Gorp

6

Hubrecht Institute, Royal Netherlands Academy of Arts and Sciences and University Medical Centre
Utrecht, Utrecht, The Netherlands

General Discussion

In this thesis, we describe the use of novel techniques with the purpose to better understand the development of pancreatic islet cells, and how islets engraft after transplantation. We developed a new technique that allowed intravital imaging of pancreatic tissue under the kidney capsule. Consequently, we showed that the technique could be applied to study pancreatic islet engraftment, and development of embryonic pancreases into grafts containing mature islets of Langerhans. This way, dynamic processes like cellular migration during islet cell development can be studied *in vivo* for the first time. We also generated a resource of transcriptomic profiles from single cells of the pancreas during the secondary transitional phase of embryonic development. During this phase, progenitor populations are designated in specific domains and islet cells neogenesis peaks. This resource allows the detection of tissue heterogeneity in the embryonic pancreas. Novel genes involved in endocrine differentiation can be detected, and we characterized how genes are dynamically regulated during this developmental process. Finally, we describe a novel technique that allows printing of pancreatic islets into alginate scaffolds. Multiple alginate mixtures were compared, and islets were printed in both bulk and 3D porous scaffolds. Viability of transplanted islets was confirmed, after which the scaffolds were transplanted subcutaneously in mice.

6

Novel insights into pancreatic development

Knowledge of pancreatic development is commonly used as a blueprint for beta cell regeneration studies. Using similar pathways as those involved during development, ES or iPS cells are driven through complex differentiation protocols to generate cells that resemble beta cells *in vitro* [1, 2]. While the majority of these beta-cell-studies focus on the use of specific culturing factors to guide cells towards

a beta-like phenotype, pancreatic development is a much more complex process involving lateral inhibition [3], niche formation [4] and epithelial-to-mesenchymal transition after delamination [5]. Also, many genes may play a role in endocrine development that have yet to be discovered. Because of lacking knowledge in pancreas development the current thesis aimed to enhance the understanding of islet cell differentiation by visualizing pancreatic development (chapter 2) and cellular behavior (chapter 3) *in vivo*, and to characterize pancreatic transcriptional heterogeneity by sequencing the transcriptome of individual cells within the developing pancreas (chapter 4).

Intravital imaging platforms for studying pancreatic islets are already available. In the most commonly accepted protocol so far, pancreatic islets are transplanted to the anterior chamber of the eye [6]. Using such a model, islet cell engraftment can be dynamically studied [7]. Also, embryonic pancreatic tissue can be transplanted for up to a week [8]. Nevertheless, the gold standard location for transplanting pancreatic islets in mice is under the kidney capsule. This site has been very thoroughly used in transplantation studies in mice and can contain greater amounts of transplanted tissue compared to the anterior chamber of the eye. Our novel protocol, allowing intravital microscopy on pancreatic tissue transplanted under the kidney capsule, permits imaging of large grafts of up to 2000 islet equivalents, where the anterior chamber of the eye can contain about 300 islet equivalents [7]. Transplanted embryonic pancreases could be imaged up to two weeks, showing in great detail how the immature tissue differentiates into adult pancreatic tissue.

A critical step in islet cell genesis is the delamination of Neurog3 positive cells from the ductal lining, after which endocrine progenitors undergo a mesenchymal phase before forming islets of Langerhans. Using our novel intravital imaging approach, we were able to perform time-lapse imaging for multiple hours, which

allowed us to identify MIP-GFP positive cells that showed a migratory phenotype in grafts resembling E15.5 embryonic pancreas, the embryonic age where Neurog3 peaks during pancreas development. In grafts resembling E18.5 embryonic pancreas, the amount of migratory cells was found to be diminished. Using the MIP-GFP mouse, we were unable to precisely define which cells express this mesenchymal phenotype. This could be achieved using a different mouse model, based on lineage tracing of Neurog3 positive cells in combination with a mesenchymal marker like vimentin or slug. A more precise characterization of these cells could better explain how pancreatic islets are formed during development, a process that is currently only described as a theoretical model [9].

Single cell transcriptome sequencing has been used to investigate tissue heterogeneity in the adult pancreas [10-15]. In order to look at the genesis of islet cells, we used this technique to characterize cells from embryonic pancreases during various stages of the secondary transition of pancreatic development. During this phase, islet cell genesis is most active, as indicated by Neurog3 expression that starts rising after E12.5 and peaks around E14.5 [16]. This resulted in a resource harboring all cell types present in the developing pancreas, including various stages of endocrine progenitor cells and all islet cell types. The dataset allowed us to take a closer look at endocrine pancreas development, where we identified a cluster of cells that became positive for Neurog3 [5], a cluster of endocrine progenitors that delaminated from the ductal lining [17] and a cluster with the latest common progenitor for the various endocrine cell types. Ordering cells in pseudotime, a principle proven to be an effective and powerful tool to reconstruct temporal signatures in single cell data [18, 19], allowed us to look at how genes were dynamically regulated as cells become more mature over time. Using this tool, we were able to fully reconstruct the developmental pathway of endocrine cells, from bipotent

cells in the ductal epithelium [20] to Neurog3 expressing cells [21] to specific all the endocrine cell fates [22, 23].

Taken together, we have used novel technologies like intravital microscopy and single cell transcriptomics to study cellular behavior and the transcriptional profile to get a better understanding of islet cell development.

Islet cell engraftment after transplantation

Using our intravital imaging platform (chapter 2), we were able to dynamically visualize islet engraftment under the kidney capsule after transplantation. We found that the first blood vessels connect with islets already three days post-transplantation, indicating that islets only have to survive hypoxia for a limited time after transplantation. This time period correlates with previous findings [24]. Over time, the relative beta cell mass deteriorates, indicating a gradual loss of function in transplanted islets. With vascularization of islets gradually increasing over time during the first month [7], one could assume that the decline in islet function will come to a halt after vascularization becomes more complete.

In mice, islets have been virtually transplanted everywhere in the body, whereby every location has its own benefits and drawbacks [25]. Generally speaking, transplanting islets directly *in vivo* always exposes them to the host immune system, unless the immune system is suppressed either by using drugs or genetically [26, 27]. One way of overcoming this problem is by transplanting islets in scaffolds [28]. Commercially available scaffolds are currently being tested in clinical trials, carrying islet-like cells [29, 30]. The advantages of these scaffolds are obvious: immunoprotection from the host immune system, protection of the host from potentially harmful cells and restriction of the graft to a specific location. Scaffolding also presents a specific disadvantage in the form of dead space: molecules have to be transported through

the scaffold in order to supply nutrients to the cells, to sense glucose and to release insulin into the blood stream, decreasing cell viability [31] and most likely insulin action.

Further optimization of scaffolding conditions is crucial for the development of a successful scaffolding platform. In our study, we have tried to optimize these scaffolding conditions for transplantation, using an alginate-based scaffolding system (chapter 5). While alginate does not create a protective barrier for either the graft or the host, it is used as a filler material in both the commercial scaffolds. Alginate, as a natural polymer, has a long history in islet encapsulation [32]. Survival of islets in bulk scaffolds is severely limited [33], due to the distance between islets and the border of the scaffold [34]. Porous scaffolds have an increased ratio between scaffold mass and surface area, decreasing the average diffusion length within the scaffold. Consequently, this should thus result in an increased islet viability and insulin action compared to bulk scaffolds [35]. Porous scaffolds can be created by irregular processes like porogen leaching, but for an optimal average diffusion length, printed (regular) porous scaffolds are a better solution [36]. We tested a porous scaffold setup using 3D-printed alginate scaffolds compared to bulk printed scaffolds and found improved viability in the plotted scaffolds. Unfortunately, insulin action was still impaired in both bulk and printed scaffolds. Also, after transplantation, viability of plotted islets decreased drastically, indicating that nutrient and oxygen delivery to islets was impaired as well. Taken together, these findings indicate that scaffolding as a tool still has room for improvement, as current techniques reduce islet survival and functioning.

Clinical relevance and future perspectives

Curing diabetes mellitus is a puzzle requiring many hands. Research focussed on generating a cell therapy that allows transplantation of differentiated stem cells is a strong method

towards a cure for diabetes patients [1, 2]. Before that strategy is fully functional, pancreas transplantation will be an invaluable tool for helping the lucky few patients that qualify for the procedure. Transplantation of islets is an alternative to whole pancreas transplantation by reducing morbidity and mortality post-surgically, but the efficiency of the procedure is still being improved. Scaffolding is regarded as a useful tool to achieve such improvement. All these strategies profit from the common knowledge obtained in fundamental research involving islet function, development and engraftment. This gain of knowledge cannot be regarded as accomplished, and novel techniques like intravital microscopy and single cell sequencing, as used in this thesis, still allow for a closer and more detailed view of the pancreas in a dynamic fashion.

To develop a cell therapy that has the ability to cure diabetes mellitus patients, cell culture conditions need to be further improved. This can be achieved by learning from embryonic developmental processes which in turn can then be used to, for example, optimize 3D culturing [37, 38] and cellular niches [39] (including co-cultures with other cell types [40-42]), as well as the identification of yet to be discovered growth factors. Using iPS cells from a patient's own body can yield novel islet cells without risk of graft rejection [43]. Ultimately, the ES/iPS approach will yield almost exact copies of beta cells, which can be used for transplantation as replacement for lost beta cells. To do so, these cells will need to be delivered in a device that allows survival of transplanted cells and quick insulin action, combined with a protective system that does not allow cells to cross between the device and the host. Steps in this direction are already underway [44]. If these conditions can be met, a virtually unlimited beta cell replacement strategy can be implemented in a safe and easy delivery system to potentially cure millions of diabetes mellitus patients worldwide.

References

- [1] Pagliuca FW, Millman JR, Gurtler M, et al. (2014) Generation of functional human pancreatic beta cells *in vitro*. *Cell* 159: 428-439
- [2] Reznia A, Bruin JE, Arora P, et al. (2014) Reversal of diabetes with insulin-producing cells derived *in vitro* from human pluripotent stem cells. *Nat Biotechnol* 32: 1121-1133
- [3] Li XY, Zhai WJ, Teng CB (2016) Notch Signaling in Pancreatic Development. *Int J Mol Sci* 17
- [4] Zhou Q, Law AC, Rajagopal J, Anderson WJ, Gray PA, Melton DA (2007) A multipotent progenitor domain guides pancreatic organogenesis. *Dev Cell* 13: 103-114
- [5] Bankaitis ED, Bechard ME, Wright CV (2015) Feedback control of growth, differentiation, and morphogenesis of pancreatic endocrine progenitors in an epithelial plexus niche. *Genes Dev* 29: 2203-2216
- [6] Speier S, Nyqvist D, Kohler M, Caicedo A, Leibiger JB, Berggren PO (2008) Noninvasive high-resolution *in vivo* imaging of cell biology in the anterior chamber of the mouse eye. *Nat Protoc* 3: 1278-1286
- [7] Speier S, Nyqvist D, Cabrera O, et al. (2008) Noninvasive *in vivo* imaging of pancreatic islet cell biology. *Nat Med* 14: 574-578
- [8] Ali Y, Diez J, Selander L, Zheng X, Edlund H, Berggren PO (2016) The anterior chamber of the eye is a transplantation site that supports and enables visualisation of beta cell development in mice. *Diabetologia* 59: 1007-1011
- [9] Jo J, Kilimnik G, Kim A, Guo C, Periwai V, Hara M (2011) Formation of pancreatic islets involves coordinated expansion of small islets and fission of large interconnected islet-like structures. *Biophys J* 101: 565-574
- [10] Muraro MJ, Dharmadhikari G, Grun D, et al. (2016) A Single-Cell Transcriptome Atlas of the Human Pancreas. *Cell Syst*
- [11] Li J, Klughammer J, Farlik M, et al. (2016) Single-cell transcriptomes reveal characteristic features of human pancreatic islet cell types. *EMBO Rep* 17: 178-187
- [12] Segerstolpe A, Palasantza A, Eliasson B, et al. (2016) Single-Cell Transcriptome Profiling of Human Pancreatic Islets in Health and Type 2 Diabetes. *Cell Metab* 24: 593-607
- [13] Wang YJ, Schug J, Won KJ, et al. (2016) Single-Cell Transcriptomics of the Human Endocrine Pancreas. *Diabetes* 65: 3028-3038
- [14] Xin Y, Kim J, Okamoto H, et al. (2016) RNA Sequencing of Single Human Islet Cells Reveals Type 2 Diabetes Genes. *Cell Metab* 24: 608-615
- [15] Baron M, Veres A, Wollock SL, et al. (2016) A Single-Cell Transcriptomic Map of the Human and Mouse Pancreas Reveals Inter- and Intra-cell Population Structure. *Cell Syst*
- [16] White P, May CL, Lamounier RN, Brestelli JE, Kaestner KH (2008) Defining pancreatic endocrine precursors and their descendants. *Diabetes* 57: 654-668
- [17] Gouzi M, Kim YH, Katsumoto K, Johansson K, Grapin-Botton A (2011) Neurogenin3 initiates stepwise delamination of differentiating endocrine cells during pancreas development. *Dev Dyn* 240: 589-604
- [18] Reid JE, Wernisch L (2016) Pseudotime estimation: deconfounding single cell time series. *Bioinformatics* 32: 2973-2980
- [19] Durruthy-Durruthy R, Heller S (2015) Applications for single cell trajectory analysis in inner ear development and regeneration. *Cell Tissue Res* 361: 49-57
- [20] Kim YH, Larsen HL, Rue P, Lemaire LA, Ferrer J, Grapin-Botton A (2015) Cell cycle-dependent differentiation dynamics balances growth and endocrine differentiation in the pancreas. *PLoS Biol* 13: e1002111
- [21] Rukstalis JM, Habener JF (2009) Neurogenin3: a master regulator of pancreatic islet differentiation and regeneration. *Islets* 1: 177-184
- [22] Dassaye R, Naidoo S, Cerf ME (2016) Transcription factor regulation of pancreatic organogenesis, differentiation and maturation. *Islets* 8: 13-34
- [23] Pan FC, Wright C (2011) Pancreas organogenesis: from bud to plexus to gland. *Dev Dyn* 240: 530-565
- [24] Morini S, Brown ML, Cicalese L, et al. (2007) Revascularization and remodelling of pancreatic islets grafted under the kidney capsule. *J Anat* 210: 565-577
- [25] Cantarelli E, Piemonti L (2011) Alternative transplantation sites for pancreatic islet grafts. *Curr Diab Rep* 11: 364-374
- [26] Huurman VA, van der Torren CR, Gillard P, et al. (2012) Immune responses against islet allografts during tapering of immunosuppression - A pilot study in 5 subjects. *Clin Exp Immunol*

- [27] Sandberg JO, Eizirik DL, Sandler S (1997) IL-1 receptor antagonist inhibits recurrence of disease after syngeneic pancreatic islet transplantation to spontaneously diabetic non-obese diabetic (NOD) mice. *Clin Exp Immunol* 108: 314-317
- [28] Coronel MM, Stabler CL (2013) Engineering a local microenvironment for pancreatic islet replacement. *Curr Opin Biotechnol* 24: 900-908
- [29] Barkai U, Weir GC, Colton CK, et al. (2013) Enhanced oxygen supply improves islet viability in a new bioartificial pancreas. *Cell Transplant* 22: 1463-1476
- [30] Agulnick AD, Ambruzs DM, Moorman MA, et al. (2015) Insulin-Producing Endocrine Cells Differentiated *In Vitro* From Human Embryonic Stem Cells Function in Macroencapsulation Devices *In Vivo*. *Stem Cells Transl Med* 4: 1214-1222
- [31] Dunn JC, Chan WY, Cristini V, et al. (2006) Analysis of cell growth in three-dimensional scaffolds. *Tissue Eng* 12: 705-716
- [32] Lim F, Sun AM (1980) Microencapsulated islets as bioartificial endocrine pancreas. *Science* 210: 908-910
- [33] De Vos P, De Haan BJ, Wolters GH, Strubbe JH, Van Schilfhaarde R (1997) Improved biocompatibility but limited graft survival after purification of alginate for microencapsulation of pancreatic islets. *Diabetologia* 40: 262-270
- [34] Marchioli G, van Gurp L, van Krieken PP, et al. (2015) Fabrication of three-dimensional bioplotting hydrogel scaffolds for islets of Langerhans transplantation. *Biofabrication* 7: 025009
- [35] Pedraza E, Brady AC, Fraker CA, et al. (2013) Macroporous three-dimensional PDMS scaffolds for extrahepatic islet transplantation. *Cell Transplant* 22: 1123-1135
- [36] Loh QL, Choong C (2013) Three-dimensional scaffolds for tissue engineering applications: role of porosity and pore size. *Tissue Eng Part B Rev* 19: 485-502
- [37] Huch M, Bonfanti P, Boj SF, et al. (2013) Unlimited *in vitro* expansion of adult bi-potent pancreas progenitors through the Lgr5/R-spondin axis. *EMBO J* 32: 2708-2721
- [38] Greggio C, De Franceschi F, Figueiredo-Larsen M, Grapin-Botton A (2014) *In vitro* pancreas organogenesis from dispersed mouse embryonic progenitors. *J Vis Exp*
- [39] Greggio C, De Franceschi F, Figueiredo-Larsen M, et al. (2013) Artificial three-dimensional niches deconstruct pancreas development *in vitro*. *Development* 140: 4452-4462
- [40] Talavera-Adame D, Wu G, He Y, et al. (2011) Endothelial cells in co-culture enhance embryonic stem cell differentiation to pancreatic progenitors and insulin-producing cells through BMP signaling. *Stem Cell Rev* 7: 532-543
- [41] Buitinga M, Janeczek Portalska K, Cornelissen DJ, et al. (2016) Coculturing Human Islets with Proangiogenic Support Cells to Improve Islet Revascularization at the Subcutaneous Transplantation Site. *Tissue Eng Part A* 22: 375-385
- [42] Zhou Y, Hu Q, Chen F, et al. (2015) Human umbilical cord matrix-derived stem cells exert trophic effects on beta-cell survival in diabetic rats and isolated islets. *Dis Model Mech* 8: 1625-1633
- [43] Millman JR, Xie C, Van Dervort A, Gurtler M, Pagliuca FW, Melton DA (2016) Generation of stem cell-derived beta-cells from patients with type 1 diabetes. *Nat Commun* 7: 11463
- [44] Vegas AJ, Veisoh O, Gurtler M, et al. (2016) Long-term glycemic control using polymer-encapsulated human stem cell-derived beta cells in immune-competent mice. *Nat Med* 22: 306-311

Nederlandse Samenvatting
Dankwoord
Publication List
Curriculum Vitae



Nederlandse samenvatting

Diabetes mellitus is een ziekte waarbij de bloedsuikerspiegel van patiënten niet meer goed wordt gereguleerd in het lichaam. Dit komt doordat de bètacellen in de zogenaamde eilandjes van Langerhans, gespecialiseerde groepjes cellen in de alvleesklier, niet meer goed werken (type 2 diabetes mellitus) of kapot zijn gemaakt door het immuunsysteem (type 1 diabetes mellitus). De bètacellen zijn verantwoordelijk voor de productie van insuline, een hormoon dat ervoor zorgt dat de hoeveelheid beschikbare bloedsuiker, brandstof voor het lichaam, niet te hoog wordt. Als de bètacellen niet meer werken moeten patiënten zichzelf injecteren met insuline om hun bloedsuikerspiegel op peil te houden. Het niet goed reguleren van de bloedsuikerspiegel heeft gevaarlijke korte- en langetermijneffecten, waardoor uiteindelijk de gemiddelde levensverwachting wordt verkort.

Het toedienen van insuline is een symptomatische behandeling. Genezing is momenteel alleen mogelijk door transplantatie van een donoralvleesklier of de geïsoleerde eilandjes van Langerhans uit de alvleesklier. Doordat de hoeveelheid beschikbaar donormateriaal zeer beperkt is, wordt er gezocht naar mogelijkheden om nieuwe bètacellen te maken door gestuurde uitrijping van stamcellen, of door het herprogrammeren van bestaande celtypen. Uitrijping van stamcellen gebeurt door cellen vanuit een stamcelfase gericht te sturen richting endoderm, dan richting alvleesklier endoderm en uiteindelijk naar endocriene voorlopercellen. Van daaruit worden cellen richting de verschillende celtypen in de eilandjes van Langerhans geprogrammeerd, waar de bètacellen een onderdeel van uitmaken. Ook bestaat er de mogelijkheid om bestaande celtypen te herprogrammeren. Hiervoor kunnen bijvoorbeeld de alfa- en deltacellen worden gebruikt, andere celtypen in de eilandjes van Langerhans. Ook de ductale en acinaire cellen van de pancreas kunnen dienen als bron voor het herprogrammeren richting een

bètacel.

Het (her)programmeren van cellen richting bètacellen voltrekt zich grotendeels langs dezelfde route die embryonale stamcellen afdrogen tijdens de ontwikkeling van de pancreas. Betere basale kennis van de ontwikkeling van de alvleesklier kan zodoende bijdragen aan een beter inzicht in het herprogrammeren van cellen tot bètacel. De pancreas ontwikkelt zich in de muis in twee fasen. Tijdens de eerste fase groeit een groep cellen uit de ontwikkelende darm. Deze cellen organiseren zich in steeds kleiner wordende buisjes, waardoor een boomstructuur ontstaat. Tijdens de tweede fase specialiseren cellen zich. De uiteinden van de buisjes bestaan uit stamcellen, terwijl de cellen die de eilandjes van Langerhans vormen zich uit de stammen van de boomstructuur vormen. Dit gebeurt doordat deze cellen uit de buisjes loskomen en in het omringende weefsel clusteren tot groepjes cellen. De keuze welk celtype een cel wordt binnen het eilandje van Langerhans is gebaseerd op een genetische lobsbepaling. In de mens ontwikkelt de alvleesklier zich bijna identiek als in de muis.

In **hoofdstuk 2** beschrijven we een nieuwe techniek waarmee we weefsel herhaaldelijk kunnen meten nadat het is getransplanteerd onder het nierkapsel van muizen. Het nierkapsel is de meest gebruikte locatie om de functie van eilandjes van Langerhans in muizen te testen. Het herhaaldelijk kunnen meten van cellen die daar getransplanteerd zijn geeft meer inzicht in hoe cellen en eilandjes van Langerhans gevasculariseerd worden, of hoe ze zich na transplantatie ontwikkelen. Vascularisatie van deze eilandjes vindt plaats na drie dagen, en de relatieve hoeveelheid bètacellen in de eilandjes neemt gedurende de eerste twee weken na transplantatie af. Hierna hebben we embryonale alvleesklieren met een fluorescent kleurlabel getransplanteerd onder het nierkapsel. Hierbij zien we dat er vlak na transplantatie amper



bètacellen in het alvleesklierweefsel zitten, maar dat deze gedurende twee weken in grote getalen worden gevormd. Ook het alvleesklierweefsel zelf neemt in omvang toe en vormt buizen zoals dat tijdens de embryonale ontwikkeling gebeurt. Twee weken na transplantatie lijkt de alvleesklier uitgerijpt: alle buisstructuren zijn aangelegd en de eilandjes van Langerhans zijn gevormd.

In **hoofdstuk 3** kijken we in meer detail naar de ontwikkeling van de endocriene cellen. Dit zijn alle celtypen die de eilandjes van Langerhans vormen. Eerst laten we zien dat het fluorescente kleurlabel dat specifiek is voor bètacellen in volwassen muizen tijdens de embryonale ontwikkeling van de alvleesklier ook voorlopercellen markeert. Vervolgens maken we een vergelijking tussen embryonaal pancreasweefsel zoals het zich in een embryo ontwikkelt en embryonaal pancreasweefsel dat getransplanteerd is onder het nierkapsel. Hieruit concluderen we dat de ontwikkeling van de endocriene cellen niet anders is in getransplanteerd weefsel dan tijdens de normale ontwikkeling. Tenslotte kijken we naar het gedrag van de endocriene cellen tijdens de ontwikkeling. We later voor het eerst zien dat er een subpopulatie van endocriene cellen is die kunnen migreren. Deze eigenschap is belangrijk voor de vorming van endocriene cellen nadat ze uit de embryonale boomstructuur zijn losgekomen.

In **hoofdstuk 4** bestuderen we wat voor verschillende celtypen er aanwezig zijn tijdens verschillende stadia van ontwikkeling in de embryonale pancreas. Hiervoor kijken we naar het RNA-profiel (transcriptoom) van individuele cellen. We vinden in de embryonale pancreas 17 verschillende celtypen, waarvan de belangrijkste celtypen de cellen van de boomstructuur en de endocriene cellen zijn. Binnen de endocriene celtypen vinden we alle volwassen celtypen en

een aantal celtypen voor endocriene voorlopercellen. Door te kijken hoe groepen cellen met elkaar verbonden zijn, kunnen we een pseudotijdlijn maken voor de ontwikkeling van cellen in de eilandjes van Langerhans. Dit betekent dat we kunnen zien door welke stadia van ontwikkeling cellen heengaan om volwassen te worden, en welke genen daarbij betrokken zijn. Door te kijken naar de veranderingen in genprofielen tussen aan elkaar verbonden celtypen, kunnen we voorspellen welke genen op welk moment betrokken zijn bij de uitrijping van cellen in de eilandjes van Langerhans. Deze resultaten leiden mogelijk tot de identificatie van nieuwe genen die van belang zijn bij het (her)programmeren van cellen richting bètacellen.

In **hoofdstuk 5** testen we het gebruik van verschillende types scaffolds. Scaffolds zijn dragers waarin eilandjes van Langerhans kunnen worden gestopt voor transplantatiedoeleinden. Ze beschermen eilandjes tegen het immuunsysteem van de patiënt, en ze voorkomen dat getransplanteerde cellen kunnen uitzaaien in het lichaam. Het voordeel van scaffolds is dat ze op veel eenvoudigere plaatsen getransplanteerd kunnen worden dan bijvoorbeeld in de lever (tot nu toe de transplantatielocatie). In onze experimenten hebben we scaffolds met verschillende composities en structuren getest op functionaliteit. Scaffolds gemaakt van alginaat met gelatine, geprint in een drie dimensionale structuur, geven eilandjes de beste overlevingskansen. De functionaliteit van de eilandjes was echter verminderd, doordat de scaffolds een dood volume hebben. Hierdoor moeten glucose en insuline eerst door de scaffold trekken voordat ze een effect hebben. Scaffolds met eilandjes werden vervolgens subcutaan getransplanteerd in muizen om te kijken of ze in vivo overleven. Door middel van onze in hoofdstuk 2 beschreven techniek konden we de eilandjes gedurende een week volgen. De overleving van de eilandjes in vivo was echter veel lager dan in vitro.

Samengevat geeft dit proefschrift nieuwe inzichten in de ontwikkeling van eilandjes van Langerhans, en de overleving van eilandjes na transplantatie. Door middel van intravitale microscopie kunnen we de migratie van endocriene voorlopercellen beschrijven, en door naar het transcriptoom te kijken kunnen we zeggen welke genen op welk moment betrokken zijn bij de uitrijping tot volwassen cellen in de eilandjes van Langerhans. Verder kunnen we van getransplanteerde eilandjes zien wanneer deze gevasculariseerd worden, en hoe transplantatie de bètacellen in de eilandjes beïnvloedt. Tot slot testen wat voor effect het gebruik van scaffolds heeft op de overleving en functionaliteit van eilandjes van Langerhans.



Dankwoord

Eindelijk is het zover, na 11 lange jaren is het Hubrecht Instituut van me verlost. De tijd is wat mij betreft voorbijgevoegen en ik kan nog steeds nauwelijks bevatten dat ik weg ben. Wat rest is een lange lijst mensen die een bedankje verdienen.

Ten eerste mijn promotoren. Eelco, jij zag in mij wat niemand anders zag: een potentiële PhD student. Je hebt door de jaren heen altijd vertrouwen in me gehad en ik heb je manier van sturen en begeleiden altijd als erg plezierig beschouwd. Je gaf me de vrijheid om mijn project zelf op poten te zetten en om langzaam te groeien in mijn wetenschappelijke rol. Voor je ligt het resultaat daarvan, en daar ben ik je eeuwig dankbaar voor. Jacco, één van de grappigste momenten op het lab de afgelopen jaren was toen je trots het lab op kwam lopen en “je suis une champignon” tegen me zei. Onze volslagen onkunde om Frans te spreken schepte een band, en ik beschouw je buiten de wetenschap om ook op persoonlijk vlak als een fijn mens. Bedankt dat je mijn promotor wilt zijn, voor je hulp bij de vele microscopie experimenten die we hebben gedaan en voor je oprechte interesse in mij. Succes de aankomende jaren op het NKI!

Voor de mensen in onze werkgroep: ten eerste allemaal bedankt voor de gezelligheid de afgelopen jaren. Het is niet vanzelfsprekend, maar wel heel fijn als het er is. Gita, you just might be a bit too gullible, but I always appreciated your hard work and open way of communicating. Good luck, whatever the future may hold for you and your family. Françoise, thank you for all your feedback and willingness to help, even now that we're in Switzerland. However slowly, my French is improving! Timmie, wat heb jij veel kleuringen gedaan en cellen geteld de laatste maanden. Je was het extra paar handen dat ik broodnodig had, bedankt! Lina, you came to help me with one project, but ended up helping me with all my projects. Your thoroughness and

perseverance will bring you a long way. Thanks for your help and good luck during your PhD. Karin, je deed veel dingen op de achtergrond: de dierenstal, snijden van weefsel, genotyperen. Het wordt vaak ondergewaardeerd, maar het is zo fijn als dit soort dingen geregeld zijn. Groen, altijd goed om te zien dat niet alleen ik, maar ook andere mensen worstelen met hun in silico data. Bedankt voor de gezelligheid, en niet te veel port drinken! Mijn studenten door de afgelopen jaren: Bob, Pim, Paul, Daniëlla en Twan: ik heb echt ontzettend veel geluk gehad met de intelligente, zelfstandige en georganiseerde studenten die jullie waren. Allemaal succes in de toekomst! Van vroeger: Cindy, wat was het leuk om samen met jou deze groep op poten te zetten. Dankzij jou heb ik ieder geval op een basaal niveau leren kweken, for whatever it's worth, waarvoor dank. Erik, we moesten in het begin even aan elkaar wennen, maar uiteindelijk hebben we een goede tijd gehad op het Hubrecht. Succes in Nijmegen. Femke, we hebben nog steeds restjes voorraad die jij hebt aangelegd, kweekmonster dat je bent! We wonen “in de buurt” nu, laten we een keer een biertje gaan drinken. Nathalia, Bernard, Nerys, Marten, Maaïke, Jeetindra, Jason and all the other lab members from the Hubrecht en Leiden: thanks for your ideas and input, and all the best in the future.

Verder natuurlijk Jacco's angels: Lai, Eef, Sas en Nienke, angels van het eerste uur, bedankt voor alle hulp bij het opzetten van mijn microscopie experimenten, warrige gesprekken in de Damberten, kopjes koffie of thee. Also many thanks to the other angels: Daan, Co, Ari, Carrie, Sander, Maria, Pim en Anko. Mauro, bedankt voor alle hulp bij de single cell experimenten, het is een mooi hoofdstuk geworden en uiteindelijk wordt het een mooi manuscript, ik voel het aan m'n water. Giulia, many thanks for your collaboration on the scaffolding paper. May all go well for you in the future. Stefan en Reinier, bedankt voor jullie hulp bij het FACS en mijn cellen. Alles ging altijd soepel met jullie

hulp en de flexibiliteit die jullie boden was heel aangenaam. Stieneke, super bedankt voor al je hulp bij het kweken, voor je gezelligheid en voor het delen van het leed genaamd de Life Tech Supply Center. Ik hoop voor je dat er een moment komt waarop dat soepel loopt. Laat je niet gek maken! Harry en Jeroen, bedankt voor alle gezelligheid in het histologie lab. Sorry voor alle snoepjes die ik (soms stiekem) bij jullie heb gepikt. John, ik maakte vaak grapjes over dat je soms wat lang van stof bent, maar ik heb je hulp altijd enorm gewaardeerd. Getrouwd zijn is trouwens zo gek nog niet.

Het Hubrecht valt en staat bij de ondersteunende diensten. Binnen die diensten zijn altijd een aantal mensen extra bereid om een helpende hand te bieden, wat het leven zoveel makkelijker maakt. Elroy, als ik iets nodig had dat niet binnen het standaard repertoire van de civiele dienst viel (een camera, hulp bij verzending van pakketjes, noem maar op), ik kon altijd bij jou terecht. Je bent een fijn mens! Thea en Anneke, bedankt voor alle gezelligheid, het was altijd leuk binnenkomen of weggaan wanneer jullie er waren. Beste diervverzorgers (eigenlijk geldt dit voor jullie allemaal, maar in het bijzonder natuurlijk voor Miep, Petra en Benaissa), bedankt voor alle goede zorgen voor mijn muisjes de afgelopen jaren. Wat hebben jullie daar een werk aan gehad, en het werd altijd zonder gemor gedaan. Ik wil niet weten hoeveel muizen jullie voor me geplugd hebben op de vroege ochtend, ook in het weekend, en ik ben jullie er heel erg dankbaar voor! Nanneke, zonder jou geen DEC protocollen. Je was altijd bereid om mee te denken met onze aanvragen, wat het proces altijd ten goede kwam. Ik hou van je optimisme en enthousiasme. Rob, Tjeerd en Edwin, jullie waren altijd bereid om iets te knutselen voor het goede doel. Of het nu ging om het bijslijpen van imaging windows of het meten van temperaturen in onze koelkasten, niets was te gek, alles kon en meestal nog dezelfde dag. Heel erg bedankt!

Feestjes op het Hubrecht ben ik in de laatste jaren niet echt meer aan toe gekomen, maar zeker in mijn beginjaren wel. Veel dank voor de gezelligheid aan Anke en Essie (rozen eten en met onbekenden naar de gaybar), Paul (altijd een goed verhaal over porno tijdens de lunch, lekker klauteren op de survivalbaan en sterke drank tijdens werktijd), Flore (3 uur koffietijd, wat hebben wij veel zitten ouwehoeren samen. Ik mis dat!), Petra (liedjes zingen in de slaaptrein naar Sziget, en waarom is er een verband tussen hoeren en honden?), Daniil (winter BBQ will never be the same, and thanks for explaining the many ways to ingest vodka), Maaike (als ik een zweefmolen zie denk ik aan jou), Tamara (dankzij jou weet ik hoe de medische centra van Mallorca er van binnen uitzien), Eirinn (for the many pictures and beers) en Roel (we zijn niet laatste geworden bij Beltrum, dat was al heel wat). En verder: Jarno, Maartje, Pieterjan, Nicolas, AJ, Annabel, Geert, Erica, Jean-Charles, Susanne, Lennart, Kay, Lotte, Laura, Jessica, Saskia, Carla en alle anderen die ik vergeet: bedankt voor de gezelligheid!

Mac en Miranda, ondanks jullie eigen turbulente leventje hebben jullie altijd de tijd om wat leuk te gaan doen (festivalletjes, sportevenementjes, hapje eten) en om te helpen als dat kan. Mac, we kennen elkaar ondertussen bijna 20 jaar en je bent als een broer voor me. Bedankt dat jullie er altijd zijn, en vergeet niet dat wij er altijd voor jullie zijn als jullie ons nodig hebben. Lars en Niké, bedankt voor de vaak bijzonder slechte grappen en jullie belabberde gevoel voor humor. Een mens (in ieder geval dit mens) heeft dat nodig. Nynke, je bent waarschijnlijk degene die m'n boekje helemaal heeft gelezen. Misschien wel de enige die hem helemaal heeft gelezen. Bedankt voor je kritische blik en feedback. Ex-collega's van de Ekko, mijn tijd daar achter de bar en geluidstafels was fantastisch. De uitjes naar Pinkpop en Roskilde waren memorabel. De medewerkersweekenden zijn nog steeds een blur. De naborrels tot drie uur 's middags waren misschien wat overdreven, maar

wel erg leuk. Jullie zijn met teveel om allemaal persoonlijk te bedanken, maar bij deze in ieder geval allemaal collectief bedankt voor een fantastische tijd, ik had het nooit willen missen!

Beste Henk en José, ik kan me geen fijnere schoonouders bedenken dan jullie. Altijd staan jullie klaar om ergens mee te helpen, zelfs als je er helemaal voor uit Almelo moet komen. Jullie zijn de liefste en warmste schoonouders die iemand zich kan wensen! Bart en Nadina, bedankt voor alle gezelligheid, het is altijd leuk om een hapje te doen, wat te drinken, wat te kletsen via whatsapp, etc.

Paps en mams, wat een moment hè? Zoonlief heeft een boek geschreven, en gaat promoveren, wie had dat 20 jaar geleden gedroomd? Wat hebben we een mooi gezin met z'n allen, met twee ouders die zo veel van elkaar houden en zoveel liefde en aandacht hebben voor hun kinderen. Niet alles gaat vanzelfsprekend, maar met elkaar krijgen we alles gedaan. We zitten wat verder weg nu, maar we blijven altijd dichtbij. Ik hou van jullie. Anneke, je bent de sterkste vrouw die ik ken. Je bent de liefste moeder die ik ken. Je bent mijn kleine zusje maar mijn grote voorbeeld. Verander nooit, je bent fantastisch. Mick, kleine dondersteen die je bent, wat is het leuk om jou als neefje te hebben. Laten we snel weer wat leuk gaan doen, zoals sleeën in de bergen!

Anneke en Ester, wat ben ik blij dat jullie mijn paranimfen zijn. Jullie vertegenwoordigen allebei een andere tak van mijn leven, en zijn beiden zo goed in wat jullie doen. Met jullie achter me heb ik het vertrouwen dat mijn promotie goed gaat komen.

Anoek, lieverd. Ik hou zo ontzettend veel van je. Ik ben zo blij dat we samen dit mooie avontuur aan zijn gegaan in Zwitserland. Je motiveert me om meer uit mezelf te halen dan ik beseft dat ik in me had. Je laat me naar het leven kijken op een manier die ik niet kende. Je maakt me beter dan ik ooit was. Ik kan niet uitdrukken hoe belangrijk je voor me bent. Maar het is zo.

Marah, mijn liefde en zaligheid. Ooit als je wat ouder bent zul je dit hopelijk lezen en trots zijn op je vader. Ik ben nu al zo trots op jou. Mijn kleine lachebekje, mijn wondertje. Jouw avontuur is pas net begonnen, ik hoop dat je er een leven lang van kunt genieten. Want het leven is mooi, het is fantastisch. Haal er alles uit wat erin zit en geniet. Dat doet papa ook, met volle teugen.

Het is tijd.

Léon

Publication list

Sequential intravital imaging reveals in vivo dynamics of pancreatic tissue transplanted under the kidney capsule in mice.

van Gorp L, Loomans CJ, van Krieken PP, Dharmadhikari G, Jansen E, Ringnalda FC, Beerling E, van Rheenen J, de Koning EJ.
Diabetologia. 2016 Nov;59(11):2387-92.

A Single-Cell Transcriptome Atlas of the Human Pancreas.

Muraro MJ, Dharmadhikari G, Grün D, Groen N, Dielen T, Jansen E, **van Gorp L**, Engelse MA, Carlotti F, de Koning EJ, van Oudenaarden A.
Cell Syst. 2016 Oct 26;3(4):385-394.e3.

Fabrication of three-dimensional bioprinted hydrogel scaffolds for islets of Langerhans transplantation.

Marchioli G, **van Gorp L**, van Krieken PP, Stamatialis D, Engelse M, van Blitterswijk CA, Karperien MB, de Koning E, Alblas J, Moroni L, van Apeldoorn AA.
Biofabrication. 2015 May 28;7(2):025009.

Intravital microscopy through an abdominal imaging window reveals a pre-micrometastasis stage during liver metastasis.

Ritsma L, Steller EJ, Beerling E, Loomans CJ, Zomer A, Gerlach C, Vriskoop N, Seinstra D, **van Gorp L**, Schäfer R, Raats DA, de Graaff A, Schumacher TN, de Koning EJ, Rinkes IH, Kranenburg O, van Rheenen J.
Sci Transl Med. 2012 Oct 31;4(158):158ra145.

Induced Wnt5a expression perturbs embryonic outgrowth and intestinal elongation, but is well-tolerated in adult mice.

Bakker ER, Raghoebir L, Franken PF, Helvensteijn W, **van Gorp L**, Meijlink F, van der Valk MA, Rottier RJ, Kuipers EJ, van Veelen W, Smits R.
Dev Biol. 2012 Sep 1;369(1):91-100.

Beta-catenin tyrosine 654 phosphorylation increases Wnt signalling and intestinal tumorigenesis.

van Veelen W, Le NH, Helvensteijn W, Blondin L, Theeuwes M, Bakker ER, Franken PF, **van Gorp L**, Meijlink F, van der Valk MA, Kuipers EJ, Fodde R, Smits R.
Gut. 2011 Sep;60(9):1204-12.

An ENU-induced point mutation in the mouse Btfl1 gene causes post-gastrulation embryonic lethality and protein instability.

Wansleeben C, **van Gorp L**, de Graaf P, Mousson F, Marc Timmers HT, Meijlink F.
Mech Dev. 2011 May-Jun;128(5-6):279-88.

An ENU-mutagenesis screen in the mouse: identification of novel developmental gene functions.

Wansleeben C, **van Gorp L**, Feitsma H, Kroon C, Rieter E, Verberne M, Guryev V, Cuppen E, Meijlink F.
PLoS One. 2011 Apr 29;6(4):e19357.

Duodenal pain and spinal morphine induce conditioned taste aversion in rats.

Geerse GJ, **van Gorp L**, van Wijk DC, Wiegant VM, Stam R.

Physiol Behav. 2007 Jun 8;91(2-3):310-7.

Individual reactivity to the open-field predicts the expression of cardiovascular and behavioural sensitisation to novel stress.

Geerse GJ, **van Gorp L**, Wiegant VM, Stam R.

Behav Brain Res. 2006 Nov 25;175(1):9-17.

Individual reactivity to the open-field predicts the expression of stress-induced behavioural and somatic pain sensitisation.

Geerse GJ, **van Gorp L**, Wiegant VM, Stam R.

Behav Brain Res. 2006 Nov 1;174(1):112-8.

Curriculum Vitae

Leon van Gurp werd geboren op 13 september 1978 te Gorinchem. In 1996 behaalde hij zijn Havo diploma aan de christelijke scholengemeenschap Oude Hoven in Gorinchem. In 1997 begon hij aan de bacheloropleiding biotechniek op de Hogeschool Utrecht, die hij in 2002 afrondde. Na zijn opleiding begon hij als analist in het Rudolf Magnus Instituut voor neurowetenschappen, in de groep van Dr. Stam. In 2005 maakte hij de overstap naar het Hubrecht Instituut, waar hij als analist ging werken binnen de onderzoeksgroep van Dr. Meijlink. In 2009 volgde de overstap binnen het Hubrecht Instituut naar de onderzoeksgroep van Prof. Dr. de Koning. In eerste instantie was Leon ook hier werkzaam als analist, maar gedurende de tijd ging hij zich richten op zijn eigen onderzoek, wat uitmondde in het promotieonderzoek zoals beschreven in dit proefschrift. Momenteel is hij werkzaam als postdoctoraal onderzoeker in de groep van Prof. Dr. Herrera aan de Universiteit van Geneve.

